Aus dem

Lübecker Institut für Experimentelle Dermatologie

Direktoren: Prof. Dr. Ralf Ludwig, Prof. Dr. Dr. Enno Schmidt,

Prof. Dr. Hauke Busch

Einfluss der Glykosylierung auf die IgG2-induzierte Signalgebung in Neutrophilen

Inauguraldissertation zur

Erlangung der Doktorwürde

der Universität zu Lübeck

– Aus der Sektion Medizin –

vorgelegt von

Cristian Păpară, aus Mediaș, Rumänien

Lübeck 2025

1. Berichterstatter*in: PD Dr. rer. physiol. Katja Bieber

Ko-Betreuer*in: Prof. Dr. rer. nat. Kathrin Kalies

2. Berichterstatter*in: Prof. Dr. med. Malte Ziemann

Tag der mündlichen Prüfung: 14.01.2025

Zum Druck genehmigt. Lübeck, den 17.01.2025

-Promotionskommission der Sektion Medizin-

Table of Contents

Abbreviations

ABB	Annexin binding buffer
ADCC	Antibody-dependent cell-mediated cytotoxicity
AKT	Ak strain transforming
ALK	Anaplastic lymphoma kinase
ANOVA	Analysis of variance
APC	Allophycocyanin
ARAF	Serine/threonine-protein kinase A-Raf
Arg	Abelson-related gene protein
Asn	Asparagine
ATP	Adenosine triphosphate
ATR	Phosphoinositide 3-kinase-related protein kinase
AUC	Area under the curve
Axl	Axl receptor tyrosine kinase
BLK	B lymphocyte kinase
BRAF	V-raf murine sarcoma viral oncogene homolog B1 kinase
BSA	Bovine serum albumin
Btk	Bruton's tyrosine kinase
C3	Complement component 3
C5	Complement component 5
CaMK4	Calcium/calmodulin dependent protein kinase IV
CARD	Caspase recruitment domain-containing protein
CCD	Charge-coupled device
CCK/PTK	Cholecystokinin receptor/protein-tyrosine kinase
CD	Cluster of differentiation
CDK	Cyclin-dependent kinases
CHUK	Conserved helix-loop-helix ubiquitous kinase
CK1ε	Casein kinase 1 isoform epsilon
CK2	Casein kinase 2
CL	Chemiluminescence
CO2	Carbon dioxide
COL7	Type VII collagen
CTK	C-terminal Src kinase (Csk)-type kinase

CXCL	C-X-C motif chemokine ligand
CXCR	C-X-C chemokine receptor
Cy	Cyanine
DAG	Diacylglycerol
DAPK3	Death associated protein kinase 3
DMSO	Dimethyl sulfoxide
DTT	Dithiothreitol
EBA	Epidermolysis bullosa acquisita
EDTA	Ethylenediaminetetraacetic acid
EphA	Ephrin type-A receptor
ERBB3	Receptor tyrosine-protein kinase erbB-3
ERK	Extracellular signal-regulated kinase
Etk/BMX	Epithelial and endothelial tyrosine kinase/bone marrow tyrosine kinase gene in chromosome X protein
FACS	Fluorescence-activated cell sorting
FAK	Focal adhesion kinase
FcR	Fragment crystallizable receptors
FCS	Fetal calf serum
FITC	Fluorescein isothiocyanate
FLT	Fms-related receptor tyrosine kinase
FRAP	FKBP12-rapamycin-associated protein
FRK	FYN-related kinase
FSC-A	Forward scatter area
FSC-H	Forward scatter height
G-CSF	Granulocyte-colony stimulating factor
GlcNAc	N-acetylglucosamine
GPI	Glycosylphosphatidylinositol
GSK3	Glycogen synthase kinase-3
GTP	Guanosine triphosphate
HC	Heavy chaines
HCK	Hematopoietic cell kinase
hCOL7	Human collagen VII
HEK	Human EPH/ELK-like kinase

HEPES	4-(2-hydroxyethyl)-1-piperazineethanesulfonic acid
HER	Human epidermal growth factor receptor
HPLC	High-performance liquid chromatography
IC	Immune complexes
ICAM	Intracellular adhesion molecule
IFG1R	Insulin-like growth factor 1 receptor
IFN-γ	Interferon γ
Ig	Immunoglobulin
IKK	Ikappab kinase
IL	Interleukin
InSR	Insulin receptor
IP3	Inositol triphosphate
IRR	Insulin receptor-related receptor
ITAM	Immunoreceptor tyrosine-based activation motif
ITIM	Immunoreceptor tyrosine-based inhibition motif
ITK	Interleukin-2-Inducible T-cell Kinase
JAK	Janus kinase
JNK	C-Jun N-terminal kinase
KDR	Kinase insert domain receptor
Lck	Leukocyte C-terminal Src kinase
Lmr	Lemur tyrosine kinase 1
LTK	Leukocyte receptor tyrosine kinase
MAPK	Mitogen-activated protein kinase(s)
MAPKAPK3	MAP kinase-activated protein kinase 3
MBL	Mannose-binding lectin
Met	Hepatocyte growth factor receptor
mTOR	Mammalian target of rapamycin
Na_2CO_3	Sodium carbonate
$Na_2H_2PO_4$ x 2 H_2O	Disodium phosphate dihydrate
Na_2HCO_3	Sodium bicarbonate
NaCl	Sodium chloride
NADPH	Nicotinamide adenine dinucleotide phosphate
NaOH	Sodium hydroxide

NC1	Non-collagenous 1
NET	Neutrophil extracellular trap
NF-κB	Nuclear factor kappa-light-chain-enhancer of activated B-cells
NTRK	Neurotrophic receptor tyrosine kinase
Nuak1	NUAK family SNF1-like kinase 1
p38Δ	Mitogen-activated protein kinase p38 delta
p70S6K	70-kda ribosomal protein S6 kinase
PAK1	P21-Activated kinase 1
PBMC	Peripheral blood mononuclear cell
PBS	Phosphate-buffered saline
PBS	Phosphate-buffered saline
PCR	Polymerase chain reaction
PCTAIRE2	PCTAIRE-motif Protein Kinase 2
PDGFR	Platelet-derived growth factor
PE	Phycoerythrin
PerCP	Peridinin-chlorophyll-protein complex
PFTAIRE1	Cyclin dependent kinase 14
PI	Propidium iodide
PI3K	Phosphoinositide 3-kinase
PIP2	Phosphatidylinositol (4,5)-bisphosphate
PIP_3	Phosphatidylinositol [3-5]-triphosphate
PKA	Protein kinase A
PKC	Protein kinase C
PKD1	Protein kinase D1
PKG1	Protein kinase G1
PKG2	Protein kinase G2
PKN1/PRK1	Protein Kinase C-Related Kinase
PLC	Phospholipase C
PMA	Phorbol 12-myristate 13-acetate
PMN	Polymorphonuclear neutrophil(s)
PMP	Polymorphprep®
PRKACA	Protein kinase cAMP-activated catalytic subunit alpha

PRKD1	Protein kinase D1
PRKG	Protein kinase cGMP-dependent
PRKX	Protein kinase X
PTK	Protein tyrosine kinases
PY20	Monoclonal antiphosphotyrosine FITC conjugate
RA	Rheumatoid arthritis
RAF1	Raf-1 serine/threonine kinase
RBC	Red blood cell(s)
RPS6KB2	Ribosomal protein S6 kinase B2
Ret	Retinol-binding protein
ROCK1	Rho-associated coiled-coil kinase 1
ROS	Reactive oxygen species
RSKL2	Ribosomal protein S6 kinase like 1
RT	Room temperature
SH	Src homology
SHIP	SH2-domain containing inositol phosphatase(s)
SHP	SH2-domain containing phosphatase(s)
SLP-76	SH2 domain-containing leukocyte protein of 76 kda
Src	Proto-oncogene tyrosine-protein kinase Src
Srm	Spermidine synthase
SSC-A	Side scatter area
STAT	Signal transducer and activator of transcription
STK	Serine-threonine kinase
Syk	Spleen tyrosine kinase
TAK1	Transforming growth factor-β-activated kinase 1
TEC	Tec protein tyrosine kinase
Th	T-helper lymphocytes
TRKA	Tropomyosin-related kinase A
TRKB	Tropomyosin-related kinase B
TRKC	Tropomyosin-related kinase C
TXK	Tyrosine-protein kinase TXK
Yes	Tyrosine-protein kinase Yes
ZAP70	Zeta chain of T cell receptor-associated protein kinase 70

Table descriptions

Figure descriptions

1 INTRODUCTION

1.1. Autoimmunity

Autoimmunity primarily denotes the inability of the immune system to distinguish self from non-self, otherwise known as loss of tolerance, resulting in the development of autoimmune diseases (1).

Autoimmune diseases are chronic, highly heterogeneous disorders that affect approximately 5% of the general population (2). Even though the etiopathogenesis is not fully understood, it is considered to be driven by an interplay between genetic and environmental factors, causing important dysregulation of innate and adaptive immune responses (3). As a result, pathogenic autoantibodies and dysregulated immune effector cells are produced, promoting a proinflammatory state and significant tissue damage. Autoimmune diseases are difficult to treat, they are associated with significant morbidity and economic burden, and their prevalence has continuously increased over the past years (1,3,4).

Taken all together, there is a considerable need for novel and, ultimately, curative therapies in autoimmune disorders, which can be developed by further deciphering their complex pathogenesis.

1.2 Neutrophil granulocytes

Neutrophil granulocytes or polymorphonuclear neutrophils (PMNs), shortly neutrophils, represent the most abundant immune cell type in human blood, comprising up to 70% of the total circulating leukocytes (5). They establish the first line of defense against invading microorganisms by deploying their antimicrobial enzymes, cytokines and reactive oxygen species (ROS) through processes such as phagocytosis, degranulation and NETosis (6). While a reduced number of neutrophils is associated with severe infections, inappropriate recruitment and activation can damage the host, contributing to the development of atherosclerosis, autoimmune diseases and cancer (7–9).

For several years, neutrophils were considered as primitive innate immune cells exclusively killing invading pathogens (6). However, recent evidence showed that their functions extend far beyond their antimicrobial activity. Neutrophils are complex cells with transcriptional activity, capable of actively migrating to lymphoid organs, facilitating antigen uptake by macrophages, interacting with dendritic cells as well as modulating T and B lymphocyte responses through secretion of various cytokines

and chemokines (10–19). Moreover, they also play a role in innate immune memory (20).

Recent findings demonstrated the existence of heterogenous neutrophil subpopulations with different transcription, functions and phenotypes in health and disease, in both human and mice (21–25). In homeostasis, neutrophils can reside beside the circulation in marginated pools within the liver, spleen and lungs (22). If an infection or injury is present, these marginated neutrophils can be rapidly released along with immature, banded neutrophils (25,26). In addition, activated neutrophils can further extend their production by the bone marrow as well as their lifespan (27,28). If, however, the number of recruited neutrophils is too low, an emergency granulopoiesis can be prompted (29). Of note, a distinct subset, so called B cell-helper neutrophils, was found in the marginal zone of the spleen, where it promotes antibody production and immunoglobulin class switching via B cells activation (16). Interestingly, circulating neutrophils also change their phenotype in a circadian manner under homeostatic conditions by expressing surface receptors that correlate with neutrophil maturation and aging (30,31). In disease, two distinct populations of low-density neutrophils were described: one with immunosuppressive effects, typically seen in cancer, and a proinflammatory subset characteristic for autoimmune diseases (32,33). Nevertheless, since there are no specific markers to distinguish between these phenotypes, it is not clear whether neutrophils switch their phenotype based on the stimulus and local microenvironment respectively, or if they are produced as distinct subsets with separate functions (6,24). Overall, neutrophils can either prevent or promote diseases.

1.3 Neutrophil life cycle and effector functions

The production of neutrophils takes place in the bone marrow and begins with a self-renewing hematopoietic stem cell that, ultimately, differentiates into myeloblasts (34). Next, they progress sequentially from the promyelocyte stage to finally, the segmented, mature neutrophil (PMN) (35). During this maturation process, neutrophils change the shape of their nucleus and acquire the characteristic four types of granules that are released as follows: secretory vesicles, containing albumin, cytokines, parts of the nicotinamide adenine dinucleotide phosphate (NADPH) oxidase complex, and membrane receptors; tertiary (gelatinase),

containing gelatinase, arginase 1 and lysozyme; secondary (specific), containing metalloproteinases, lactoferrin and cathelicidin, and lastly, primary (azurophilic), containing neutrophil elastase, myeloperoxidase, lysozyme and defensins (6,36).

In humans, approximately 1 to 2 x 10^{11} neutrophils are produced in the bone marrow daily, yet only 1-2% are released into the bloodstream under homeostatic conditions (37,38). This is ensured by a complex interplay between receptors and their corresponding ligands, chemokines and cytokines.

In the bone marrow, granulocyte-colony stimulating factor (G-CSF) regulates both granulopoiesis and release of neutrophils into the bloodstream (39). Neutrophils express the C-X-C chemokine receptor 4 (CXCR4) that interacts with the C-X-C motif chemokine ligand 12 (CXCL12) produced by the bone marrow cells and osteoblasts (40). As a result, mature neutrophils are homed in the bone marrow (28,41). By interfering with this interaction, G-CSF enables the release of neutrophils into the circulation (27). Likewise, it reduces the expression of CXCL12 by stromal cells and of CXCR4 by neutrophils, while upregulating CXCR2 expression on megakaryocytes (42–44). Correspondingly, endothelial cells express various ligands for CXCR2 in response to the recruited neutrophils, including CXCL1, CXCL2, CXCL5 and CXCL8 (44).

Regarding circulating neutrophils, the interleukin (IL)-23/IL-17/G-CSF axis is the major homeostatic regulator (45). IL-17-producing T-helper (Th) lymphocytes 17 secrete IL-17, which in turn stimulates granulopoiesis and neutrophil secretion by upregulating G-CSF (45–47). Remarkably, neutrophils themselves can produce IL-17, thus attracting more Th17 cells by increasing the expression of their corresponding chemokine ligands (47,48). Ultimately, neutrophils are removed by macrophages and dendritic cells resulting in reduced IL-23 production. This leads to a negative feedback loop affecting the IL-23/IL-17/G-CSF axis (46,49).

After being released from the bone marrow, neutrophils can stay up to 5 days in the circulation or reside in marginated pools (22,50,51). Meanwhile, they change morphologies, switch phenotypes and exert different functions by expressing various surface markers (23,24,31). For instance, aged neutrophils shed cluster of differentiation (CD) 62L and express CXCR4 in order to be removed from circulation via CXCL12 interaction in the bone marrow, spleen or liver and subsequently cleared by resident macrophages (23,52,53).

In response to inflammatory signals, neutrophils are rapidly mobilized into the affected sites through a process called leukocyte adhesion cascade (54). Here, endothelial cells get activated and express adhesion receptors such as E- and P-selectins that will be recognized by neutrophils from the bloodstream, thus allowing them to initially roll and ultimately adhere to their surface (55). The latter is ensured by the interaction between neutrophils activated integrins and their corresponding ligands on endothelial cells, such as intracellular adhesion molecule 1 (ICAM-1) or ICAM-2 (56). Afterwards they transmigrate into the tissues following chemoattractant gradients, including IL-8, anaphylatoxins complement component 3 (C3) a and complement component 5 (C5) a, and bacterial component, formyl-methionyl-leucyl-phenylalanine (57).

At the site of the insult, activated neutrophils kill pathogens by deploying various strategies. First, they ingest incriminating pathogens and destroy them by phagocytosis in the intracellular phagolysosome (6). Second, neutrophils release their granules with antimicrobial substances and ROS generated by the NADPH oxidase complex, either intracellularly into the phagolysosome or directly into the extracellular space (58,59). Last, if the microorganisms are too large for phagocytosis, neutrophils commit a specific type of programmed cell death known as NETosis to trap pathogens. Therefore, characteristic neutrophil extracellular traps (NET) are formed from decondensed chromatin fibers, histones and granules (60,61). Besides the putative antimicrobial role, NET formation can also occur in various autoimmune diseases (62).

After fulfilling their functions, neutrophils can undergo various mechanisms of cell death, including apoptosis, autophagy, necroptosis, necrosis, NETosis and pyroptosis, the latter being an inflammatory type of death driven by microbes and mediated by the inflammasome. This step is crucial for the prompt resolution of inflammation and thus, prevention of tissue damage and further disease development (63,64).

However, when neutrophils exhibit dysregulated recruitment and activation, altered ROS production and NET formation, as well as faulty clearance mechanisms, their destructive activity can be directed towards host cells. This can contribute to the development of cardiovascular disease, cancer, and autoimmune diseases. Despite their significant role, the precise contribution of neutrophils to these pathological conditions remains not fully understood (9,57,62,64).

1.4 Fcγ receptors signaling in neutrophils

Antibodies recognize pathogens with great specificity based on their antigen-binding region (Fab), and eliminate them by relying primarily on the effector functions of innate immune cells, including neutrophils (65). This is facilitated by immune cells expressing receptors that recognize the fragment crystallizable (Fc) portion of the immunoglobulins (Ig) (66). The main Fc receptors in neutrophils are the Fc gamma receptors (FcγR) that specifically bind to IgG.

In humans, six classical FcγR have been described so far: FcγRI, FcγRIIA, FcγRIIB, FcγRIIC, FcγRIIIA and FcγRIIIB (67). They can be either activating (FcγRI, FcγRIIA, FcγRIIIA and FcγRIIIB) or inhibitory (FcγRIIB) receptors, and exhibit high (FcγRI) or low affinity (FcγRIIA, FcγRIIB, FcγRIIIA and FcγRIIIB) towards antibodies (65,68). FcγRI binds monomeric IgG, whereas low-affinity FcγR bind mainly antigen-antibody aggregates, so-called immune complexes (IC) (68). The affinity of antibodies for specific FcγR is influenced by several factors, including IgG subclass type. Thus, it was shown that IgG1, IgG3 and, to a lesser extent, IgG4 bind to all FcγR, whereas IgG2 binds to FcγRIIA and FcγRIIIA, but not to FcγRIIIB (67).

Circulating neutrophils express mainly FcγRIIIB but also FcγRIIA and FcγRI and, to a lesser extent, FcγRIIB (69). To be activated by IC, neutrophils require both FcγRIIA and FcγRIIIB (70). In infections as well as in chronic inflammation, interferon-γ (IFN-γ) or G-CSF upregulate the expression of FcγRI on neutrophils, thus enabling them to phagocytose IgG-opsonized bacteria, release ROS and trigger antibody-dependent cytotoxicity (ADCC) (69,71,72).

Accumulating evidence showed that each FcγR leads to the activation of a particular signaling pathway that renders distinct neutrophilic functions (73). For instance, FcγRIIIB which is only expressed in neutrophils is involved in NET formation, but not FcγRIIa (74,75).

FcγR consist of at least two Ig-like extracellular domains and a tyrosine-based motif located in the intracellular part (65). Activating FcγR use immunoreceptor tyrosine-based activation motifs (ITAM) for signal transduction, except for FcγRIIIB, which is a glycosylphosphatidylinositol (GPI)-linked receptor that lacks an intracellular domain (65,76). In contrast, FcγRIIB is the only inhibitory receptor and contains an immunoreceptor tyrosine-based inhibition motif (ITIM) (Figure 1) (77).

Following cross-linking of all receptors, tyrosine residues of the ITAM are phosphorylated by kinases of the Src family and thus become the binding site for

the Spleen tyrosine kinase (Syk) (78). Consequently, activated Syk phosphorylates the Src homology (SH) 2 domain-containing leukocyte protein of 76 kDa (SLP-76) protein complex containing SLP-76, Bruton's tyrosine kinase (C), Vav, phosphoinositide 3-kinase (PI3K) and phospholipase C gamma (PLCγ), with all of them being activated in neutrophils (73). The activation of PI3K generates phosphatidylinositol 3,4,5-triphosphate (PIP_3), which in turn activates guanosine triphosphate (GTP)ases, such as Rho and Rac that are associated with cytoskeleton realignment for phagocytosis as well as NADPH oxidase activation (79,80). In addition, Rac modulates the activation of mitogen-activated protein kinases (MAPK) and c-Jun N-terminal kinases (JNK), which will activate nuclear factors and thus produce inflammatory cytokines (81). Activated PLCγ generates inositol triphosphate (IP_3) and diacylglycerol (DAG) (73). IP3 releases calcium from the endoplasmic reticulum to favor cytoskeletal remodeling for intracellular granule release or chemotaxis (82). On the other hand, DAG further activates protein kinase C (PKC), which regulates NADPH oxidase system and results in the downstream activation of MAPK and nuclear factor kappa-light-chain-enhancer of activated B-cells (NF-κB), the latter being involved in transcriptional activity (Figure 1) (73,83).

With respect to activating FcγRIIIB, it is a GPI-linked receptor that is associated with the activation of Syk, transforming growth factor-β-activated kinase 1 (TAK1) and MAPK/ extracellular signal regulated kinases (ERK) signaling pathway (74). Therefore, it was shown to be involved in various neutrophil functions, including activation of integrins, ROS release, and NETosis (75,84,85).

In contrast, FcγRIIB counteracts the activating signaling pathways through Src-mediated phosphorylation of ITIM, which will engage two groups of neutrophil-associated phosphatases, the SH2 domain-containing phosphatases (SHP)-1 and SHP-2, and the SH2- domain containing inositol phosphatases (SHIP)-1 and SHIP-2 (86,87). SHP-1 promotes dephosphorylation of SLP-76 complex and Syk, whereas SHIP-1 and SHIP-2 converts PIP_3 into PIP_2 (73).

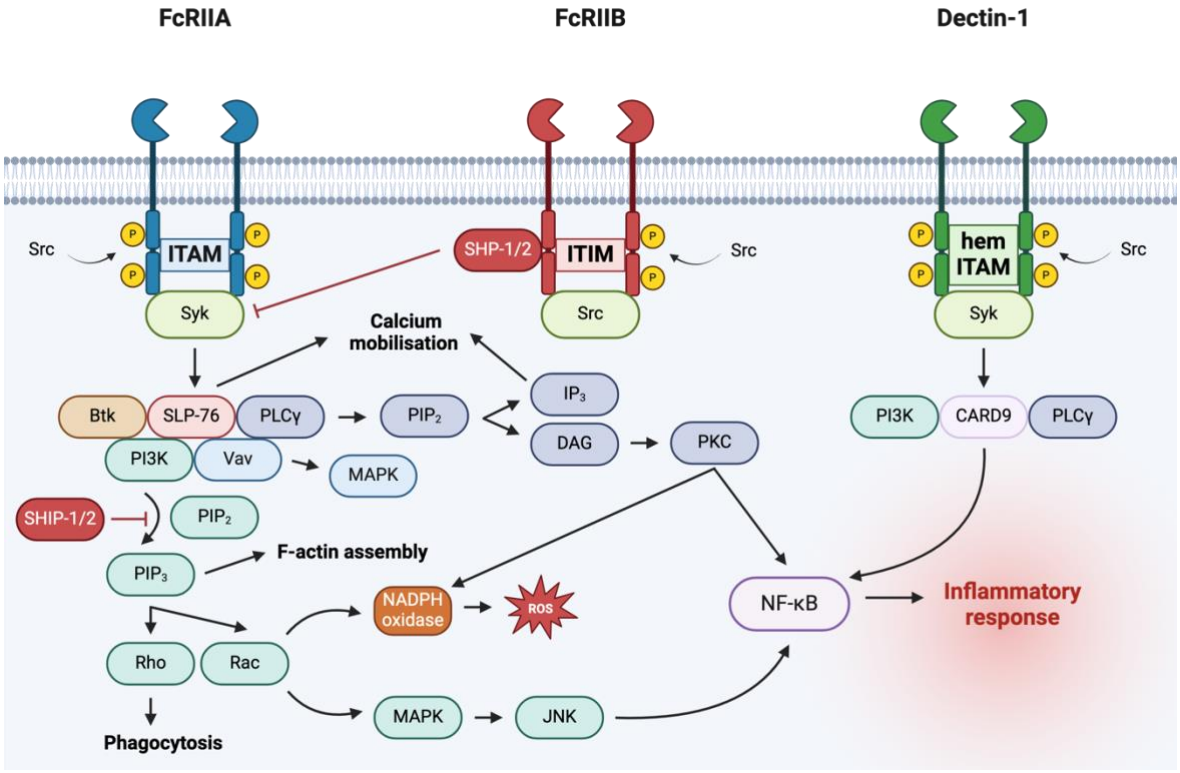

Figure 1. Signaling pathways via activating and inhibitory Fc receptors (FcR) as well as Dectin-1 in neutrophils. Activating FcR, such as FcRIIA contain the immunoreceptor tyrosine-based activation motif (ITAM). Src kinases phosphorylate the tyrosine residues of ITAM, leading to the recruitment and activation of Spleen tyrosine kinase (Syk). In turn, this activates the Src homology 2 (SH2) domain-containing leukocyte protein of 76 kDa (SLP-76) protein complex, which includes SLP-76, Bruton's tyrosine kinase (Btk), Vav, phosphatidylinositol-4,5-bisphosphate 3-kinase (PI3K), and phospholipase C gamma (PLCγ). The activation of PI3K converts phosphatidylinositol (4,5)-bisphosphate (PIP_2) to phosphatidylinositol 3,4,5-triphosphate (PIP_3), which in turn activates guanosine triphosphate (GTP)ases, such as Rho and Rac, which are associated with cytoskeleton realignment for phagocytosis. Additionally, Rac modulates the activation of mitogen-activated protein kinases (MAPK) and c-Jun N-terminal kinases (JNK), which in turn activate nuclear factor kappa-light-chain-enhancer of activated B-cells (NF-κB) and thus promote the production of inflammatory cytokines. Moreover, Rac activates NADPH oxidase, leading to the production of reactive oxygen species (ROS). Activated PLCγ generates inositol triphosphate (IP3) and diacylglycerol (DAG). SLP-76 and IP3 release calcium from the endoplasmic reticulum to facilitate chemotaxis. DAG further activates protein kinase C (PKC), which regulates the NADPH oxidase system and results in the downstream activation of MAPK and NF-κB. Similar activating pathways are involved downstream of Dectin-1, including caspase recruitment domain-containing protein 9 (CARD9), all leading to the activation of NF-κB. The exception is that Dectin-1 contains only one copy of the ITAM, known as hemITAM. Inhibitory FcR, such as FcRIIB, contain an immunoreceptor tyrosine-based inhibition motif (ITIM), which engages the SH2 domain-containing phosphatase (SHP)-1/2, thus inhibiting the SLP-76 complex and Syk. Additionally, ITIM recruits the SH2 domain-containing inositol phosphatase (SHIP)-1/2 phosphatases, which convert PIP3 to PIP2, further dampening the signaling cascade.

Figure modified after Futosi *et al.* (56), Mata-Martinez *et al.* (88), and van Rees *et al.* (73). Figure created with BioRender.com.

Overall, both activating and inhibitory FcγR may be engaged at once in neutrophils, suggesting that their different expression levels and combinations render the functional outcome of this binding (67). In pemphigoid diseases, animal studies have demonstrated that complement activation is a prerequisite for blister formation. Autoantibodies binding to the hemidesmosome in the skin lead to complement deposition, which subsequently recruits neutrophils. These neutrophils then bind IC in an Fc-dependent manner, thus activating them and ultimately resulting in characteristic split formation (89).

1.5 Role of IgG glycosylation in autoimmunity

In addition to the different types of IgG subclasses, the affinity of IgG antibodies for FcγR can also be influenced by their glycosylation status (65).

IgG consists of four polypeptides, two heavy chains (HC) each linked to a light chain (LC) through disulfide bonds, forming together two functional domains: the Fab fragment that specifically recognize the antigen, and the Fc part that allows IgG to bind FcγR on innate immune cells and complement (68). Human IgG contains a conserved N-linked glycosylation site attached to each of the asparagine 297 (Asn297) residues of the two HC (CH2 domain) (90). The core of this sugar moiety is composed of two sequential N-acetylglucosamine (GlcNAc) attached to Asn297, followed by mannose and additional GlcNAc (90). Post-translational IgG glycosylation starts in the endoplasmic reticulum but predominantly takes place in the Golgi apparatus (91). The core glycan can be further modified by adding fucose to the primary GlcNAc or galactose topped with sialic acid to the terminal GlcNAc, generating up to 36 glycan variants (91). Since 70% of human IgG are asymmetrically glycosylated and considering the four IgG subclasses, there are up to 144 functional glycoforms that may elicit different antibody-driven effector functions (92).

Antibody glycosylation is shaped by various factors, including age, sex, pregnancy, body mass index and smoking (92). Typically, in humans 16% of IgG is galactosylated on both terminal GlcNAc branches (G2), 35% on only one (G1), and 35% on none (G0). The remaining 14% possess sialic acid at one (S1) or both terminal galactose residues (S2) (93). In addition, the majority of circulating IgG

glycoforms contain a branching fucose residue (F) attached to the primary GlcNAc. Interestingly, the heptasaccharide glycan core can be completely removed by hydrolysis with the Streptococcus pyogenes-derived endoglycosidase EndoS leaving only one GlcNAc at Asn297 (94). Thus, it will result in a significant reduction in IgG binding to activating FcγR, which explains the anti-inflammatory effects of EndoS in various autoimmune disease models (95).

Consistent data showed that different autoimmune diseases are associated with altered glycosylation patterns (96). Indeed, changes in glycan form may exert pro- or anti-inflammatory effects by changing the affinity of IgG for FcγR, thereby modulating antibody-driven responses (92). For instance, agalactosylated IgG glycoforms (G0F) are increased in various autoimmune diseases, such as rheumatoid arthritis (RA), systemic lupus erythematosus, inflammatory bowel disease and vasculitis (96). In patients with RA, they were also associated with disease activity and treatment with methotrexate (97,98). Correspondingly, highly galactosylated IgG exert anti-inflammatory effects when present as IC (99). Absence of fucose residues stimulates ADCC activity by significantly increasing IgG affinity for FcγRIIIA and FcγRIIIB (100).

In contrast, sialylation exerts anti-inflammatory effects (101). In fact, patients with autoimmune diseases exhibit low levels of sialylated antibodies that could also predict disease relapse, while effective treatment recovered antibody's sialylation status (96,102,103). Furthermore, the therapeutic effect of intravenous immunoglobulin that is used in the treatment of various immune-mediated and autoimmune diseases was shown to be related to antibodies carrying α2,6 sialylation (101). In addition, the synthetic sialylation of intravenous immunoglobulin boosted its anti-inflammatory effect up to 10-fold (104). Regarding the underlying mechanisms, sialylation changes IgG structure so that FcγR binding is hindered, thus decreasing antibody-driven inflammatory effector functions (101).

Furthermore, changes in antibody glycosylation patterns determine which FcRs can attach to them, thus influencing the recruitment of immune cells and resulting in different effector functions. Immune cells detect these differences in glycosylation patterns through specific glycan-binding proteins, including C-type lectin receptors, siglecs (sialic acid-binding immunoglobulin-like lectins), and galectins (105). These complementary glycoreceptors further modulate this interaction, either activating or inhibiting inflammatory responses. For instance, murine studies have shown that the

anti-inflammatory effects of highly galactosylated IgG are mediated by the association between FcγRIIb and galectin-3, as well as the C-type lectin receptor Dectin-1, which inhibits C5a-mediated inflammatory responses (99,106). Conversely, the pro-inflammatory effect of agalactosylated IgG could be due to the activation of mannose-binding lectin (MBL)-dependent complement pathway, leading to activation of the lectin complement pathway, but findings are contradictory (107,108). In addition to altered glycosylation patterns observed in autoimmune diseases, levels of galectin-1 and galectin-3 are decreased in RA and systemic lupus erythematosus (105). Galectin-1 was shown to dampen the inflammatory process by blocking neutrophil recruitment and promoting their clearance through apoptosis, while galectin-3-mediated ligand clustering triggers neutrophil activation (109,110).

Apart from the Fc glycosylation, growing evidence showed that up to 25% of circulating IgG contain N-linked glycans also in the Fab fragments that consist mainly of sialylated residues (111). Despite its exact role is not fully understood, Fab glycosylation may play a role in pregnancy as well as RA (111).

1.6 Epidermolysis bullosa acquisita

Epidermolysis bullosa acquisita (EBA) is a typical example of an organ-specific autoimmune disease, where binding of innate immune cells, in particular neutrophils, to skin-bound IC via FcγR, represents the key pathogenetic event in the characteristic autoantibody-induced tissue destruction (112).

EBA is a rare autoimmune blistering disease, with a reported prevalence of 2.8 cases per million people. Although it can occur at any age, two peaks of disease onset were observed: in the second and seventh decades (113).

Despite the wide range of clinical presentations, EBA can be classified into two major types, namely mechano-bullous (non-inflammatory) and non-mechano-bullous (inflammatory) (114). The classic presentation, which mimics hereditary dystrophic epidermolysis bullosa, includes significant skin fragility, trauma-induced blisters and erosions localized on the extensor surfaces, which heal with scars and milia (112). In contrast, inflammatory EBA can resemble other autoimmune blistering diseases, including bullous pemphigoid, mucous membrane pemphigoid, in particular the Brunsting-Perry entity, and linear IgA disease (112,114).

EBA is linked to various systemic diseases, including lichen planus, cutaneous and systemic lupus erythematosus, which also pose a higher risk for future development of EBA (115). Additionally, it is associated with metabolic and cardiovascular disease, as well as thrombosis. The notable association with inflammatory bowel disease is debatable (115,116).

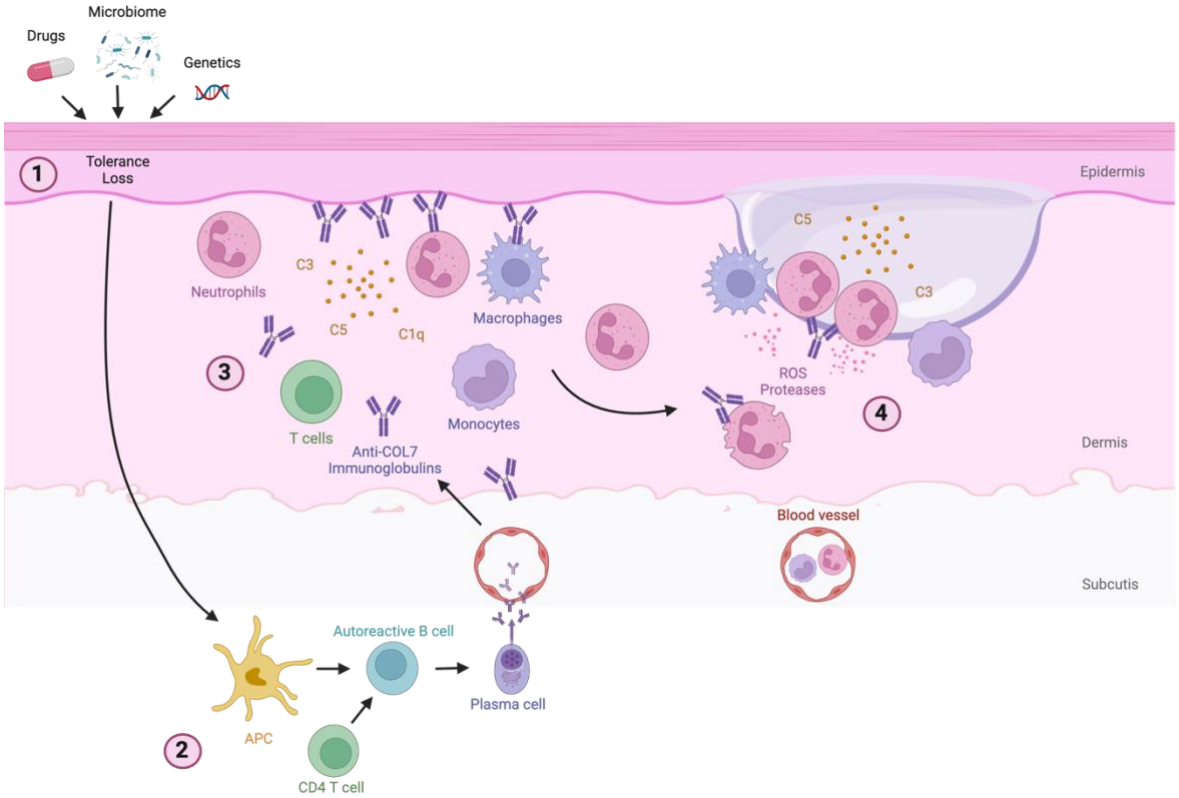

Figure 2. Epidermolysis bullosa acquisita (EBA) pathogenesis overview. (1) Genetic factors, diverse medications, and the skin microbiome all contribute to a breakdown in tolerance. (2) This process entails interactions between APC and autoreactive B and T cells, leading to their clonal expansion and differentiation into plasma cells. Autoantibodies directed against COL7 are generated and dispersed throughout the bloodstream and various tissues. (3) Pathogenic IgG autoantibodies targeting COL7 bind to the dermal-epidermal junction, triggering complement activation, the release of pro-inflammatory cytokines and mediators, and subsequent recruitment of leukocytes, primarily neutrophils. (4) Immune complexes engage neutrophils in an Fc-dependent manner, initiating a signaling cascade that includes the release of ROS and proteases, ultimately resulting in the characteristic formation of subepidermal blisters. APC, antigen-presenting cells; C, complement; CD4, cluster of differentiation 4; COL7, type VII collagen; ROS, reactive oxygen species. Figure modified after Koga *et al.* (112). Figure created with BioRender.com.

In the presence of characteristic clinical features, the diagnosis of EBA is confirmed by demonstrating linear Ig (predominantly IgG) in a u-serrated pattern and/or C3 deposits along the basement membrane by direct immunofluorescence microscopy

or by circulating IgG binding to the dermal site on human salt-split skin by indirect immunofluorescence microscopy (112). In addition, the presence of pathogenic autoantibodies against type VII collagen (COL7) can be demonstrated by immunoblotting, fluorescent overlay antigen mapping, immunoelectron microscopy and serology (112).

Considering that EBA is a rare disease, most data regarding its pathogenesis originate from experimental murine models that resemble human disease, and that also serve as models for the study of the effector phase of autoimmune blistering diseases (117). EBA is characterized by pathogenic autoantibodies targeting the carboxyl terminus of COL7 in the dermal-epidermal junction (Figure 2) (118). COL7 is a major component of the anchoring fibrils produced by keratinocytes and fibroblasts. It provides mechanical stability for the skin by connecting the basement membrane to the underlying connective tissue. COL7 is characterized by a triple-helical structure consisting of a central collagenous domain flanked by two non-collagenous (NC) domains (119). The large NC1 domain interacts with extracellular proteins and contains the second von Willebrand factor type A subdomain. This subdomain modulates various interactions and is also utilized for the immunization of mice to induce skin blistering in certain strains (117,119).

In the afferent phase, it has been demonstrated that the interaction between autoreactive T cells and antigen-presenting cells such as monocytes and B cells leads to the formation of antigen-specific CD4+ T cells (112). This interaction results in clonal expansion, differentiation into plasma cells, and the production of specific anti-COL7 autoantibodies. While most of these data are derived from murine studies, COL7-specific T cells have also been detected in humans (120,121). Next, circulating autoantibodies bind to COL7 at the skin basement membrane, predominantly targeting epitopes within the NC1 domain (122). These autoantibodies are primarily of the IgG isotype, with some also belonging to IgA (123,124). Notably, complement-fixing IgG1 and IgG3 autoantibodies against COL7, but not IgG2 and IgG4, induced skin blistering *ex vivo* (125). Activation of complement consequently releases pro-inflammatory cytokines, leading to leukocyte recruitment (89). Mainly neutrophils bind to the skin-bound IC in an FcγR-dependent manner, initiating downstream signaling pathways to release ROS and proteases, the latter being responsible for the characteristic subepidermal blister formation (Figure 2) (126,127). Cumulating evidence demonstrated that neutrophils

are the major culprit in blistering in experimental EBA(128). The variability in blister locations over time in most autoimmune blistering diseases suggests an inadequate cutaneous healing process (112). Factors such as flightless I, an actin remodeling protein, IL-10-positive plasma cells and integrin CD11b, have been shown to modulate the resolution phase of experimental EBA (112,129–131).

Since EBA is not steroid responsive and there are currently no randomized clinical trials available, treatment is often challenging. Current approaches include various systemic agents such as colchicine, dapsone, cyclosporine, azathioprine, intravenous immunoglobulin, rituximab, plasmapheresis and immunoadsorption (112). Among these, only intravenous immunoglobulin and rituximab have demonstrated complete remission (124). Thus, there is an urgent need to develop disease-specific and curative treatment strategies for EBA.

1.7 Aim of this thesis

Antibody glycosylation is critical for the modulation of pro- and anti-inflammatory effector functions of antibodies (96). While antibody-mediated immune responses are mainly neutrophil-driven, they are further influenced by specific FcγR interactions and characteristic subsequent signaling pathways (65,67,69). Even though complement-fixing, IgG1 and IgG3 antibodies are primarily involved in EBA induction, the role of IgG2 remains largely unknown (125).

IgG2 is the second most abundant Ig, accounting for 32% of serum IgG (92). It is characterized by low FcγR- and complement-binding, hence diminished functionality. Antibody responses to bacterial capsular polysaccharide antigens typically involve IgG2 subclass (68). Consequently, a deficiency in IgG2 has been associated with increased susceptibility to bacterial infections (132). In addition, low IgG2 levels have also been linked to decreased IgG4 and/or IgA levels (133).

The traditional understanding is that the IgG2 subclass primarily comprises low-functioning carbohydrate-specific antibodies induced via T-independent mechanisms (92). While IgG2 was once thought to be unable to fix complement, it has been observed that at high epitope densities, IgG2 can enhance its affinity for C1q, thereby enabling activation of the complement cascade (134). Nevertheless, this could also explain why recent data showed that carbohydrate-specific antibodies may contribute to the development of autoimmune diseases (135). Interestingly, bullous pemphigoid patients showed decreased levels of IgG2, thus

implying its potential protective role in autoimmune blistering diseases including EBA (136). Conversely, a deficiency in IgG2 may be compensated for by elevated levels of IgG1 and IgG3 antibodies, which have been shown to induce skin separation *ex vivo* and contribute to disease development (125,137).

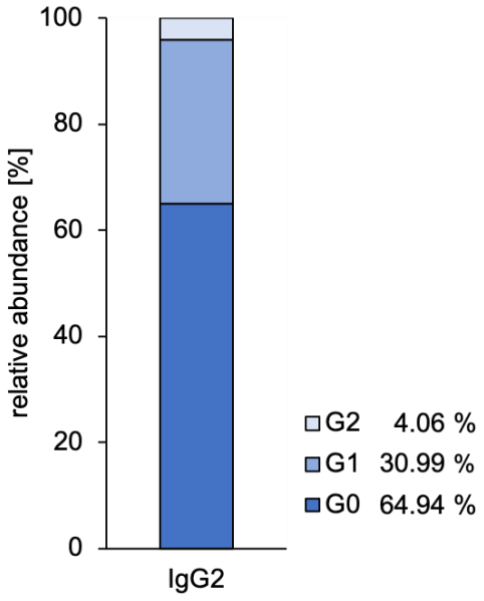

Figure 3. Glycan analysis of reference IgG2. The reference IgG2 is composed of the G0, the G1 and the G2 glycoforms. The relative abundance in % is indicated next to the legend. The data were obtained by chromatographic analysis by Prof. Manfred Wuhrer (Center of Proteomics and Metabolomics, Leiden University Medical Center, Leiden, The Netherlands) in cooperation with Prof. Marc Ehlers (Laboratories of Immunology and Antibody Glycan Analysis, Institute of Nutritional Medicine, University Medical Center Schleswig-Holstein, Lübeck, Germany).

In view of this, the aim of current work was to test the impact of differentially glycosylated anti-human collagen VII (hCOL7) IgG2-based IC on human neutrophils. Five different IgG2-based glycoforms were used in this thesis, i.e., EndoS, degalactosylated (G0), galactosylated (G1/G2), and sialylated (G1S1/G2S1/G2S2). They were compared to reference IgG2 (Figure 3). Antibodies were recombinantly produced in HEK-293T cells in cooperation with Prof. Gestur Vidarsson and Dr. Remco Visser (Utrecht University Department of Pharmaceutical Sciences, The Netherlands and Sanquin Research and Landsteiner Laboratory, Amsterdam) then analyzed by high performance liquid chromatography (HPLC) in cooperation with Prof. Marc Ehlers (Laboratories of Immunology and Antibody Glycan Analysis, Institute of Nutritional Medicine, University Medical Center Schleswig-Holstein, Lübeck, Germany) and Prof. Manfred Wuhrer (Center of Proteomics and Metabolomics, Leiden University Medical Center, Leiden, The Netherlands) (125).

Human neutrophils were stimulated by the immobilized IC to assess their activation, adhesion, ROS release, kinase activity and toxicity. The purpose of this

experimental work is to shed light on the intricate pathomechanisms of EBA by deciphering the IgG2-induced signaling pathway in neutrophils, and thus, identify potential therapeutic targets or develop novel glyco-based treatment strategies for EBA.

2 MATERIALS AND METHODS

2.1 Materials

2.1.1 Chemicals and biochemicals

Name	Manufacturer
4-(2-hydroxyethyl)-1-piperazineethanesulfonic acid (HEPES)	Sigma-Aldrich, Taufkirchen, Germany
ammonium persulfate (APS)	Sigma-Aldrich, Taufkirchen, Germany
bovine serum albumin (fraction V, biotin-free; BSA)	Roth, Karlsruhe, Germany
dimethyl sulfoxide (DMSO)	Geyer, Renningen, Germany
disodium phosphate dihydrate ($Na_2H_2PO_4$ x 2 H_2O)	Roth, Karlsruhe, Germany
distilled water	Fresenius Kabi, Bad Homburg vor der Höhe, Germany
ethanol	Roth, Karlsruhe, Germany
HALT™ Phosphatase-Inhibitor-Cocktail	Thermo scientific, Rockford, USA
HALT™ Protease-Inhibitor-Cocktail, EDTA-free	Thermo scientific, Rockford, USA
human collagen VII E-F (hCOL7 E-F)	produced at Lübecker Institut für experimentelle Dermatologie, Universität zu Lübeck, Lübeck, Germany according to Recke *et al.* (2014)
ion-free water (Ampuwa® Plastipur®)	Fresenius Kabi, Bad Homburg, Germany
liquid nitrogen	Air Liquide, Düsseldorf, Germany
luminol	Sigma-Aldrich, Taufkirchen, Germany
phorbol 12-myristate 13-acetate (PMA)	Sigma-Aldrich, Taufkirchen, Germany

propidium iodide (PI)	Miltenyi Biotec, Bergisch Gladbach, Germany
sodium bicarbonate (Na_2HCO_3)	Roth, Karlsruhe, Germany
sodium carbonate (Na_2CO_3)	Merck, Darmstadt, Germany
sodium chloride (NaCl)	Merck, Darmstadt, Germany
sodium hydroxide (NaOH)	Merck, Darmstadt, Germany
trypan blue	Sigma-Aldrich, Taufkirchen, Germany
Tween® 20	Roth, Karlsruhe, Germany

2.1.2 Buffers, media and solutions

Name	**Manufacturer/Composition**
annexin binding buffer (ABB)	BioLegend, San Diego, USA
blocking buffer	0.05 % (v/v) Tween® 20, 1 % (w/v) BSA in PBS, pH 7.2-7.4
bovine serum albumin (BSA) 100x	1 g powdered BSA dissolved in 10 mL of distilled H_2O
carbonate buffer	0.05 M Na_2CO_3, 0.05 M $NaHCO_3$ in distilled water, pH 9.6
chemiluminescence (CL) medium	1 % FCS, 25 mM HEPES, 2 g/L glucose in RPMI-1640 without phenol red
D (+) glucose solution	Sigma-Aldrich, Taufkirchen, Germany
dithiothreitol (DTT) solution 1 mol/L	Sigma-Aldrich, Taufkirchen, Germany
fetal calf serum (FCS)	Sigma-Aldrich, Taufkirchen, Germany
fixation buffer	BioLegend, San Diego, USA
fluorescence-activated cell sorting (FACS) buffer	0.5 % (w/v) BSA in PBS
luminol solution	1.82 g/L luminol, 0.72 % (v/v) NaOH in distilled water
MACSQuant® running buffer	Miltenyi Biotec, Bergisch Gladbach, Germany

MACSQuant® storage solution	Miltenyi Biotec, Bergisch Gladbach, Germany
MACSQuant® washing solution	Miltenyi Biotec, Bergisch Gladbach, Germany
M-PER™ cocktail	HALT™ Phosphatase-Inhibitor-Cocktail and HALT™ Protease-Inhibitor-Cocktail, EDTA-free diluted 1:100, respectively, in M-PER™
PBS-T	0.05 % (v/v) Tween® 20 in PBS, pH 7.2-7.4
phosphate-buffered saline (PBS)	0.01 M NaH_2PO_4 x H_2O, 0.15 M NaCl in distilled water, pH 7.2-7.4
PTK reaction buffer (PK) wash buffer	300 µL of 10x PK buffer with ultrapure water to a final volume of 3.0 mL
Polymorphprep™ (PMP)	Alere technologies, Oslo, Norway
red blood cell (RBC) lysis solution	Miltenyi Biotec, Bergisch Gladbach, Germany
RPMI-1640 with phenol red (with L-glutamine and sodium bicarbonate)	Sigma-Aldrich, Taufkirchen, Germany
RPMI-1640 without phenol red (with L-glutamine and sodium bicarbonate)	Sigma-Aldrich, Taufkirchen, Germany
trypan blue solution	0.4 % (w/v) in PBS

2.1.3 Antibodies

Name	**Host**	**Source**	**Manufacturer**
native anti-human COL7 IgG2	human	*recombinant*	produced at Lübeck Institute of Experimental Dermatology, University of Lübeck, Lübeck, Germany; according to Recke *et al.* (2014)
anti-human COL7 IgG2/EndoS	human	*recombinant*	based on native anti-human COL7 IgG2, modification of glycosylation in cooperation

			with Prof. Marc Ehlers and Prof. Manfred Wuhrer
anti-human COL7 IgG2/degalactosylated	human	*recombinant*	based on native anti-human COL7 IgG2, modification of glycosylation in cooperation with Prof. Marc Ehlers (Laboratories of Immunology and Antibody Glycan Analysis, Institute of Nutritional Medicine, University Medical Center Schleswig-Holstein, Lübeck, Germany) and Prof. Manfred (Center of Proteomics and Metabolomics, Leiden University Medical Center, Leiden, The Netherlands)
anti-human COL7 IgG2/galactosylated	human	*recombinant*	based on native anti-human COL7 IgG2, modification of glycosylation in cooperation with Prof. Marc Ehlers and Prof. Manfred Wuhrer
anti-human COL7 IgG2/sialylated	human	*recombinant*	based on native anti-human COL7 IgG1, modification of glycosylation in cooperation with Prof. Marc Ehlers and Prof. Manfred Wuhrer

2.1.4 Fluorescent dyes

Name	**Clone**	**Manufacturer**
APC-conjugated mouse anti-human CD14 antibody	63D3	BioLegend, San Diego, USA
APC-conjugated mouse anti-human CD18 antibody	1B4	BioLegend, San Diego, USA

Brilliant violet 510-conjugated mouse anti-human CD45 antibody	HI30	BioLegend, San Diego, USA
FITC-conjugated Annexin V	-	BioLegend, San Diego, USA
Pacific Blue-conjugated mouse anti-human CD16 antibody	3G8	BioLegend, San Diego, USA
PE-conjugated mouse anti-human CD193 antibody	5E8	BioLegend, San Diego, USA
PE-Cy7-conjugated mouse anti-human CD14 antibody	M5E2	BioLegend, San Diego, USA
PerCP-Cy 5.5-conjugated mouse anti-human CD62L antibody	DREG-56	BioLegend, San Diego, USA
Zombie NIR™	-	BioLegend, San Diego, USA

2.1.5 Kits

Name	**Manufacturer**
Pierce™ BCA Protein Assay Kit	Thermo scientific, Rockford, USA
PTK Reagent Kit	PamGene, BJ ‘s-Hertogenbosch, The Netherlands
STK Reagent Kit	PamGene, BJ ‘s-Hertogenbosch, The Netherlands

2.1.6 Consumables

Name	**Manufacturer**
6-well plates (clear, for suspension culture)	Greiner, Kremsmünster, Austria
96-well filter plates (AcroPrep™ Advance)	Pall, Dreieich, Germany
96-well plate (F-bottom, clear)	Greiner, Kremsmünster, Austria
96-well plates (F-bottom, clear, high-binding)	Thermo scientific, Schwerte, Germany
96-well plates (F-bottom, white, high-binding)	Greiner, Kremsmünster, Austria
96-well plates (V-bottom, clear)	Greiner, Kremsmünster, Austria

96-well plates, gold-coated (E-Plate 96 PET)	Agilent, Santa Clara, CA, USA
adhesive foil seal	Sarstedt, Nümbrecht, Germany
FACS tubes	Corning™ Falcon™, Kaiserslautern, Germany
hypodermic needle (Safety-Multifly®)	Sarstedt, Nümbrecht, Germany
PamChip® PTK	PamGene, BJ 's-Hertogenbosch, The Netherlands
PamChip® STK	PamGene, BJ 's-Hertogenbosch, The Netherlands
pipette tips	Sarstedt, Nümbrecht, Germany
polymerase chain reaction (PCR) tubes	Sarstedt, Nümbrecht, Germany
serological pipettes	Sarstedt, Nümbrecht, Germany
S-Monovette® K3 (EDTA)	Sarstedt, Nümbrecht, Germany
transparent 6-well plates, suspension cells	Greiner, Kremsmünster, Austria
tubes (1.5, 2 and 5, 15 and 50 mL)	Sarstedt, Nümbrecht, Germany
vacuum filtration unit (Filtropur V50, 500 mL, 0.45 µm)	Sarstedt, Nümbrecht, Germany

2.1.7 Equipment and devices

Name	**Manufacturer**
autoclave (DX-65)	Systec, Linden, Germany
centrifuge (for 0.2-mL tubes)	neolab, Heidelberg, Germany
centrifuge (for 1.5- and 2-mL tubes; Heraeus Fresco 17)	Thermo scientific, Schwerte, Germany
centrifuge (for 50- and 15-mL tubes; 5810 R)	Eppendorf, Hamburg, Germany
flow cytometer (MACS Quant® Analyzer 10)	Miltenyi Biotec, Bergisch Gladbach, Germany
freezers	Liebherr, Biberach an der Riß, Germany
ice machine (AF103)	Scotsman, Milano, Italy
incubator with CO_2 supply (Hera cell)	Heraeus, Hanau, Germany

incubator without CO_2 supply	Binder, Tuttlingen, Germany
laminar flow hood (NU440-401)	Nuaire, Plymouth, USA
light microscope (Dmi1)	Leica, Wetzlar, Germany
microplate reader (GloMax® Discover)	Miltenyi Biotec, Bergisch Gladbach, Germany
microplate shaker (PMS-1000i)	Grant Instruments, Shepreth, UK
Neubauer chamber	Marienfeld, Lauda-Königshofen, Germany
PamStation® 12	PamGene, BJ 's-Hertogenbosch, The Netherlands
pH metre (WTW™ inoLab™ pH7110)	Xylem, Weilheim, Germany
pipette controller	Geyer, Renningen, Germany
pipettes (single- and multi-channel)	Eppendorf, Hamburg, Germany; Brand, Wertheim, Germany
precision scale (ATB 1005-NM)	Kern, Balingen-Frommern, Germany
refrigerators	Liebherr, Biberach an der Riß, Germany
scale (EMB 1000-2)	Kern, Balingen-Frommern, Germany
tubes (50 and 15 mL)	Sarstedt, Nümbrecht, Germany
Vortex mixer (Analog vortex mixer)	VWR, Darmstadt, Germany
xCELLigence RTCA device	Agilent, Santa Clara, CA, USA

2.1.8 Software

Name	**Manufacturer**
BioRender.com	BioRender, Toronto, Ontario, Canada
Coral - Clear and customizable visualization of human kinome data	Phanstiel Lab, UNC, USA
GloMax® Discover System Software	Promega, Walldorf, Germany
MACSQuantify™ Version 2.13	Miltenyi Biotec, Bergisch Gladbach, Germany

Office 365	Microsoft Corporation, Redmond, WA, USA
PamGene® Annotator	PamGene, BJ ‘s-Hertogenbosch, The Netherlands
PamGene® BioNavigator63	PamGene, BJ ‘s-Hertogenbosch, The Netherlands
Prism 9.3.1	GraphPad Software, San Diego, CA, USA
Proteomaps/Bionic Visualization Version 2.0	DFG Research Initiative SFB Transregio34 Z1, Germany
R studio Version 2023.06.1+524	Posit PBC, Boston, USA
RTCA Software 2.0	Agilent, Santa Clara, CA, USA
STRING Database Version 12.0	Global Biodata Coalition and ELIXIR, UK
Venny 2.1	Juan Carlos Oliveros (Spanish National Centre for Biotechnology, Marid, Spain)

2.2 Methods

2.2.1 Isolation of human neutrophils from whole blood

The current study was approved by the local ethics committee of the University of Lübeck (file number 20-338, issued on November 17th, 2020, see Appendix 9.1) and all experiments were carried out in accordance with the Declaration of Helsinki. Fresh blood was first obtained from healthy volunteers for the purpose of isolating PMNs. All donors signed prior a written consent and blood was collected in 9 mL S-Monovettes K3 containing EDTA to prevent coagulation. Depending on the nature of experiment and the number of required cells, between 27 and 162 mL venous blood was drawn from each donor. 25 mL blood was then transferred from monovettes to a 50 mL tube by cautiously pipetting it onto 25 mL Polymorphprep™ (PMP) in a 1:1 proportion. PMP is a hyperosmotic solution causing erythrocytes to lose water, increase their density, and thus sink to the bottom of the tube(138). To obtain PMNs, we carried out a density gradient centrifugation at 560 x g for 35 min

at room temperature (RT) without break and with the lowest acceleration. Thus, PMNs can be visualised as a distinct density-based fraction (Figure 4). Of note, all subsequent centrifugations were performed at 4 °C, excepting the ones for the multiplex kinase activity profiling, which were performed at 23 °C. After discarding the plasma and peripheral blood mononuclear cells (PBMC), neutrophils were transferred into a new 50 mL tube, which was then topped with cold (4 °C) RPMI 1640 with phenol red and centrifuged at 460 x g for 10 min at 4 °C with maximum acceleration and deceleration.

The obtained pellet containing PMNs was then resuspended in 10 mL RBC lysis solution, incubated for 5 min at RT and then centrifuged at 460 x g for 10 min at 4 °C. The lysis step was repeated until the pellet was not reddish anymore. Next, the supernatant was discarded, the cells were resuspended in 10 mL chemiluminescence (CL) medium and centrifuged at 460 x g for 10 min at 4 °C. The cells were then resuspended in 2 mL CL medium. To determine the number of cells, 10 µL of the cell suspension were withdrawn and added to 80 µL CL medium and 10 µL trypan blue solution. Of this, 10 µL were added to a Neubauer chamber and cells were counted under the microscope taking into account the chamber (10^4) and the dilution (1:10) factors. Finally, the cell suspension was diluted with CL medium to bring it to the desired concentration of 2 x 10^6 cells/mL.

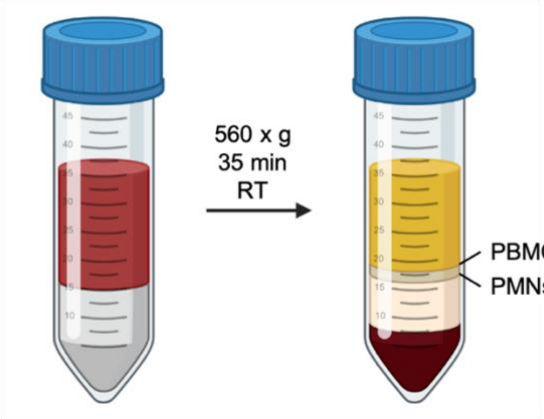

Figure 4. Isolation of human neutrophils using Polymorphprep™-based density gradient. Left tube depicts whole blood layered on top of Polymorphprep™ before centrifugation. Right tube depicts the different fractions resulted after density gradient centrifugation. PBMCs, peripheral blood mononuclear cells; PMNs, polymorphonuclear cells; RT, room temperature. Figure created with BioRender.com

2.2.2 Neutrophil purity testing by flow cytometry

After each isolation, neutrophil purity was tested by flow cytometry. This method is used to distinguish different cell subpopulations in a cell suspension based on their size, granularity and antibody-bound fluorophores by means of specific lasers of varying wavelengths. Thus, cells were first gated according to cell size (FSC-A), granularity (SSC-A), presence of singlets, exclusion of dead cells by staining with propidium iodide (PI), and of macrophages and monocytes by using anti-CD14 antibody. PMNs were identified based on the anti-CD16 antibody staining (Figure 5). Measurements were carried out at the Miltenyi MacsQuant10® Analyzer, and data were analyzed with the MACSQuantify™ Software (Version 2.13).

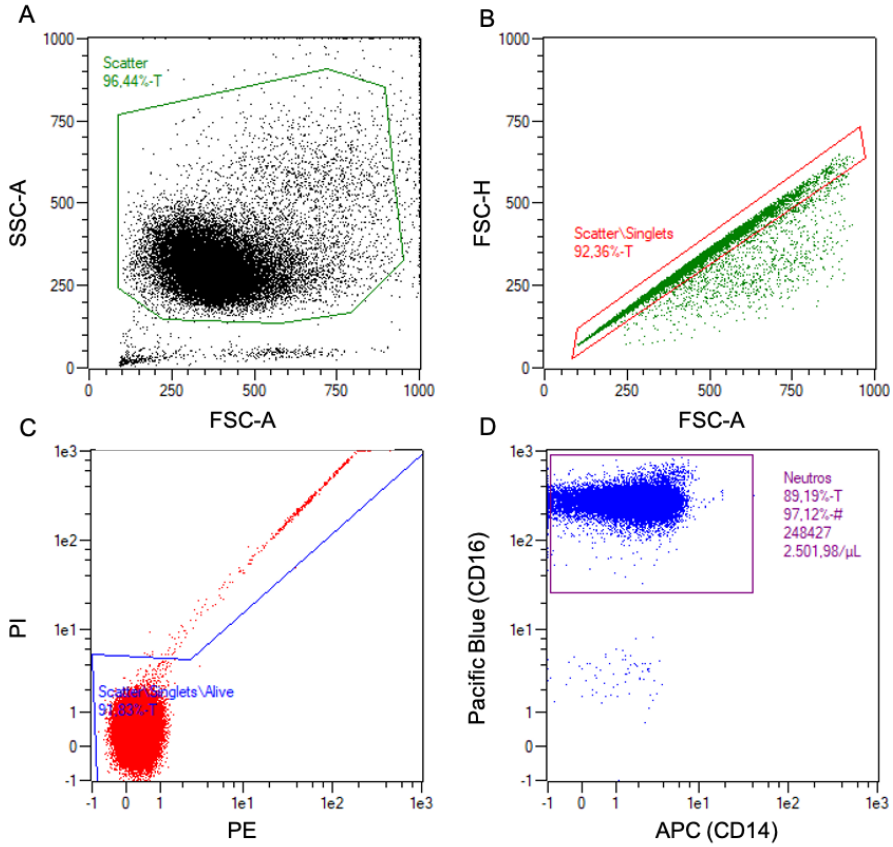

Figure 5. Representative flow cytometric gating strategy for neutrophil purity testing. A. Cells were gated based on their size (FSC-A) and granularity (SSC-A) to exclude debris. **B.** Only single cells were included (FSC-H/FSC-A). **C.** Dead cells were excluded by PI staining. **D.** Macrophages and monocytes were excluded by staining with PE-Cy7-conjugated mouse anti-human CD14 antibody, and neutrophils were detected by Pacific Blue-conjugated mouse anti-human CD16 antibody staining. APC, allophycocyanin; CD, cluster of differentiation; Cy7, cyanine 7; FSC-A, forward scatter area; FSC-H, forward scatter height; PE, phycoerythrin; PI, propidium iodide; SSC-A, side scatter area.

For this purpose, 1 mL cell suspension containing 1,000,000 purified PMNs were centrifuged at 400 x g for 5 min at 4 °C. After the supernatant was discarded, 1 µL of PE-Cy7-conjugated mouse anti-human CD14 antibody and 1 µL of Pacific Blue-conjugated mouse anti-human CD16 antibody were added, followed by the addition of 98 µL FACS buffer. The cell suspension was then incubated for 20 min at 4 °C in the dark. Next, 400 µL of FACS buffer and 5 µL of PI were added to stop the reaction and stain dead cells, respectively. After the sample was filtered into a FACS tube, measurement at the flow cytometer was carried out. Only isolates containing at least 85% neutrophils had been included in further experiments.

2.2.3 Adhesion assay

The adhesion of neutrophils was determined by quantitatively measuring the electrical impedance after binding onto a surface (139). When cells are added to a gold-coated plate and an electric current is applied, the measured impedance reflects the surface area covered by cells. The xCELLigence RTCA system converts these measurements into a unitless cell index that reflects the adhesion of IC-stimulated neutrophils (140).

	1	2	3	4	5	6	7	8	9	10	11	12
A												
B		reference IgG2	reference IgG2	reference IgG2	reference IgG2	reference IgG2	reference IgG2	reference IgG2	reference IgG2	cells	cells	
C		EndoS	EndoS	EndoS	EndoS	EndoS	EndoS	ab EndoS	ab EndoS	ag	ag	
D		degal	degal	degal	degal	degal	degal	ab degal	ab degal	PMA	PMA	
E		gal	gal	gal	gal	gal	gal	ab gal	ab gal			
F		sial	sial	sial	sial	sial	sial	ab sial	ab sial			
G												
H												

Figure 6. Plate layout for adhesion assay. Differentially glycosylated immune complexes (IC) were added on a gold-coated 96-well plate. The IC had following glycosylation patterns: reference IgG2, EndoS, degalactosylated (degal), galactosylated (gal), and sialylated (sial) at three different concentrations, respectively. First (light green) refers to 5 µg/mL antigen and 1 µg/mL antibody, second (green) refers to 10 µg/mL antigen and 2 µg/mL antibody, and last (dark green) refers to 20 µg/mL antigen and 4 µg/mL antibody concentrations. Controls are shown in yellow. Phorbol 12-myristate 13-acetate (PMA) at 0.1 µg/mL added to uncoated wells was used as a positive control. Only antibodies (ab) meaning reference IgG2 and each of all 4 glycoforms, only antigen (ag), and unstimulated cells (cells) served as negative controls.

First, we coated a 96-well E plate with 50 µL of 5, 10 or 20 µg/mL hCOL7 E-F produced as described previously(125) and diluted in carbonate buffer, except for the unstimulated cells, antibody and PMA control wells that contained only 50 µL

carbonate buffer (Figure 6 and Table 1). After the plate was incubated overnight at 4 °C, following steps were carried out: four-times washing with 200 µL PBS-T, blocking with blocking buffer for 1 h on shaker, followed by another four-times washing step.

Next, 100 µL of 1, 2 or 4 µg/mL of the antibody diluted in blocking buffer (reference IgG2, EndoS, degalactosylated, galactosylated or sialylated) were added to the corresponding wells (Figure 6), while 100 µL blocking buffer were added to the unstimulated cells, antigen and PMA control wells. During the 1.5 h shake-incubation of the immobilised IC, human PMNs were isolated from whole blood as described in chapter 2.2.1. Thereafter, the plate was washed three times with 200 µL PBS-T and once with 200 µL CL medium, followed by the addition of 50 µL CL medium. PMA was added last to the corresponding well in a concentration of 0.1 µg/mL. While the neutrophils were warmed up in the water bath for 15 min at 37 °C, the xCELLigence RTCA device was calibrated with the plate. Then, 50 µL of the 2 x 10^6/ml cell suspension was added to each well and the impedance measurements were carried out every minute for 1 h at 37 °C. Results expressed as cell indices were first analysed with the RTCA Software 2.0, then represented as area under the curve (AUC) using GraphPad Prism (Version 9.3.1), and finally normalised to the corresponding concentrations of reference IgG2, namely to 5 µg/mL antigen and 1 µg/mL antibody, 10 µg/mL antigen and 2 µg/mL antibody, and 20 µg/mL antigen and 4 µg/mL antibody, respectively.

Table 1. Concentration and composition of the used IC.

IC concentration	**Antigen concentration [µg/mL]**	**Antibody concentration [µg/mL]**
0.5 x	5	1
1 x	10	2
2 x	20	4

For the visual representation of adhesion, a transparent 96-well plate (F-bottom, high-binding) was coated as described above, excepting the last steps: wells were coated with 100 µL CL medium and incubated for 10 min at 37 °C and 5 % CO_2, while cells were heated at 37 °C in the water bath. Next, 100 µL of the 2 x 10^6 cell suspension were added and incubated for another 45 min under same conditions.

The cells were visualised under light microscopy, and images were taken by the inbuilt camera and further processed using ImageJ 2.1.0.

2.2.4 Neutrophil activity and toxicity testing by flow cytometry

Apart from the general features, we also evaluated the activity and survival of IC-stimulated neutrophils by flow cytometry. To ensure that these measurements are made only for neutrophils, we used following markers: antibodies directed against CD16 (FcγRII) and CD45 (protein tyrosine phosphatase receptor type C) to include only leukocytes and thus neutrophils, antibodies targeting CD14 to exclude monocytes and macrophages, and antibodies against CD193 to exclude eosinophils (Figure 7).

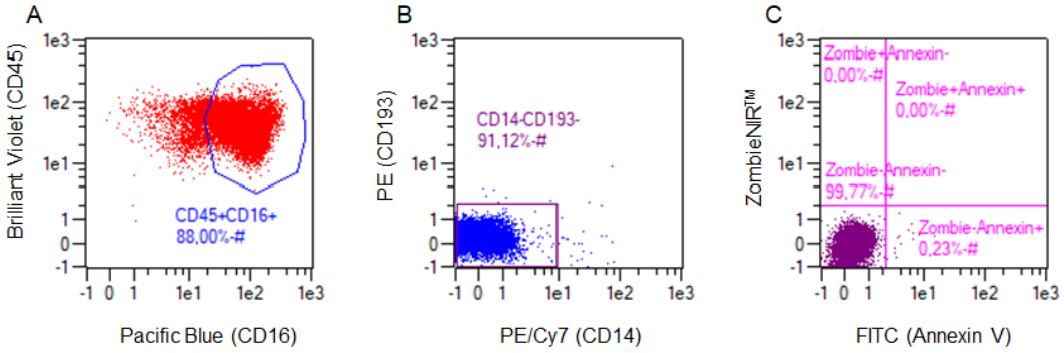

Figure 7. Representative gating strategy used to identify viable neutrophils. A. Leukocytes were included by staining with anti-CD45 and anti-CD16 antibodies. **B.** Monocytes and eosinophils were excluded by staining with anti-CD14 and anti-CD193, respectively. **C.** Necrotic and apoptotic cells were stained with Zombie NIR™ and Annexin V, respectively. Cells negative for both markers were identified as viable neutrophils. CD, cluster of differentiation; Cy7, cyanine 7; FITC, fluorescein isothiocyanate; PE, phycoerythrin.

To analyse the impact of the differentially glycosylated IC on neutrophils vitality, we used Annexin V and Zombie NIR™ stainings as markers of apoptosis and necrosis, respectively (Figure 7). Annexin V binds to phosphatidylserine, which in apoptosis changes its location from the inner to the extracellular side of the cell membrane, thus enabling the detection of apoptotic cells in the flow cytometer due to the bound fluorescein isothiocyanate (FITC) dye (141). Zombie NIR™ is an amine-reactive fluorophore that is able to permeate only cells with disrupted cellular membranes, such as during necrosis or late apoptosis (142). Based on the emitted fluorescence, it can thus distinguish vital cells from necroptotic and late apoptotic cells.

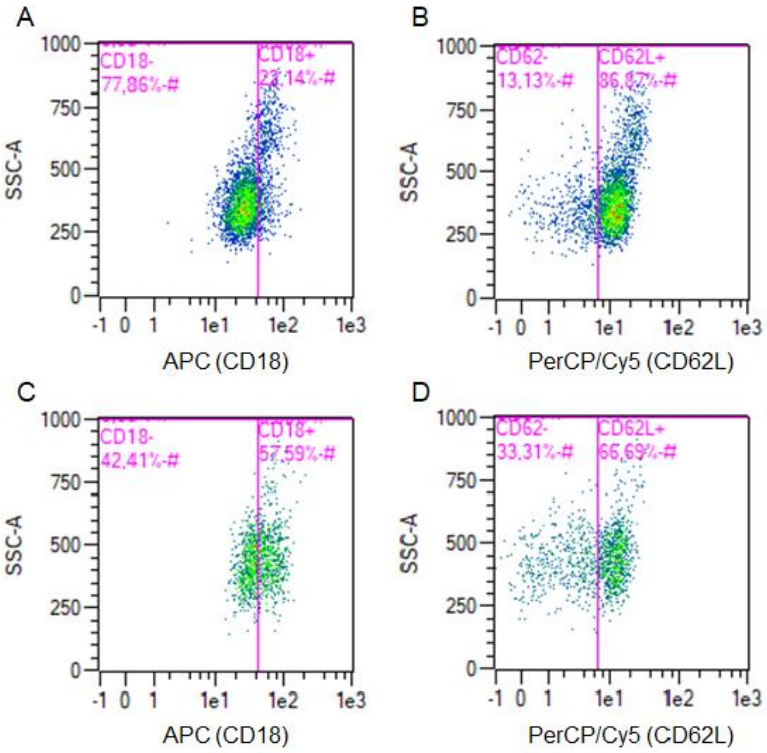

Figure 8. Representative gating strategy used to identify activated neutrophils. Differentiating between activated and inactivated neutrophils was accomplished by staining with anti-CD18 and anti-CD62L antibodies. Unstimulated (**A, B**) and immune complex-stimulated (**C, D**) neutrophils were stained for CD18 (**A, C**) or CD62L (**B, D**). APC, allophycocyanin; CD, cluster of differentiation; Cy5, cyanine 5; PerCP, peridinin-chlorophyll-protein complex; SSC-A, side scatter area.

Activation of neutrophils was assessed by using two surface markers, CD18 (integrin β chain-2) and CD62L (L-selectin). CD18 is highly expressed on activated neutrophils and is linked to adhesion and transmigration processes, while L-selectin is shed upon activation of neutrophils to enable migration through the endothelium (143,144). Thus, CD62L expression inversely correlates with CD18 expression in neutrophil activation (Figure 8).

For this experiment, human neutrophils were isolated as described in chapter 2.2.1, and a high-binding 96-well plate was prepared as presented previously in chapter 2.2.3, with following modifications: in the last step, instead of CL measurement with luminol, the plate was incubated for 2 h at 37 °C and 5 % CO_2. In the meantime, a 96-well filter plate was calibrated by adding 200 µL DPBS per well and centrifuging it at 500 x g for 10 min at RT. After the eluate was discarded, cell suspension from the previous 96-well incubated plate was resuspended and added to the filter, followed by a centrifugation at 450 x g for 6 min at RT. Next, the supernatant was

discarded, the pellets were washed with 100 µL FACS buffer per well and then centrifuged at 450 x g for 6 min at RT. After the removal of the supernatant, 50 µL Zombie NIR™ (diluted 1:1000 in ABB) were added to each well and the plate was incubated for 15 min at 4 °C in the dark. Meanwhile, the anti-CD mix solution containing all the above-mentioned fluorochrome-labelled antibodies was prepared (Table 2). After incubation, 10 µL of the anti-CD mix were added to each well and the plate was incubated for another 15 min at RT in the dark. This was succeeded by a centrifugation at 450 x g for 6 min at RT, and after discarding the supernatant and resuspension of pellet in 200 µL FACS buffer each, the centrifugation step was repeated. After the supernatant was removed, the cells were fixed by using 100 µL fixation buffer per well and incubating them for 15 min at RT in the dark. Next, 100 µL FACS buffer were added to each well and the plate underwent another centrifugation (450 x g, 6 min, RT). Finally, after discarding the supernatant, the pellets were resuspended in 100 µL FACS buffer. The plates were stored overnight in the dark at 4 °C and analyzed next day at the flow cytometer. Measurements were carried out at the Miltenyi MacsQuant10® Analyzer, and data were analyzed with the MACSQuantify™ Software (Version 2.11).

Table 2. Composition of the anti-CD mix solution.

Marker	Volume per well [µL]	Volume per 46 wells [µL]
anti-CD14-PE-Cy7	0.38	19
anti-CD16-Pacific blue	0.38	19
anti-CD18-APC	0.38	19
anti-CD45-Brilliant violet	0.8	40
anti-CD62L-PerCP/Cy 5.5	0.38	19
anti-CD193-PE	0.38	10
Annexin V-FITC	0.31	15.5
Annexin V binding buffer	6.99	358.5

APC, allophycocyanin; CD, cluster of differentiation; Cy 5.5, cyanine 5.5; Cy7, cyanine 7; FITC, fluorescein isothiocyanate; PE, phycoerythrin; PerCP, peridinin-chlorophyll-protein complex.

2.2.5 ROS release assay

To investigate the release of ROS from differentially glycosylated IC-stimulated neutrophils, a high-binding 96-well plate (F-bottom, white) was first coated with antigen according to the respective layout (Figure 9 and Table 1), blocked for

unspecific binding, and then incubated with corresponding antibodies to form immobilised IC by the method described extensively in chapter 2.2.3. Before adding 100 µL of the 2 x 10^6 cell suspension to each well, the GloMax® Discover device was preheated to 37 °C and the injector of the microplate reader was primed with 550 µL luminol solution to subsequently inject 10 µL of luminol solution into each well. The chemiluminescence resulting from the ROS production was measured by the device for every minute for a total of approximately 2 hours.

	1	2	3	4	5	6	7	8	9	10	11	12
A	reference IgG2	reference IgG2		reference IgG2	reference IgG2		reference IgG2	reference IgG2		cells	cells	
B	EndoS	EndoS		EndoS	EndoS		EndoS	EndoS		ag	ag	
C	degal	degal		degal	degal		degal	degal		reference IgG2	reference IgG2	
D	gal	gal		gal	gal		gal	gal		ab EndoS	ab EndoS	
E	sial	sial		sial	sial		sial	sial		ab degal	ab degal	
F										ab gal	ab gal	
G										ab sial	ab sial	
H										PMA	PMA	

Figure 9. Plate layout for ROS release assay. Differentially glycosylated immune complexes (IC) were coated onto a 96-well plate. The IC had following glycosylation patterns: reference IgG2, EndoS, degalactosylated (degal), galactosylated (gal), and sialylated (sial) at three different concentrations, respectively. First (light green) refers to 5 µg/mL antigen and 1 µg/mL antibody, second (green) refers to 10 µg/mL antigen and 2 µg/mL antibody, and last (dark green) refers to 20 µg/mL antigen and 4 µg/mL antibody concentrations. Controls are shown in yellow. Phorbol 12-myristate 13-acetate (PMA) at 0.1 µg/mL added to uncoated wells was used as a positive control. Only antibodies (ab) meaning reference IgG2 and each of all 4 glycoforms, only antigen (ag), and unstimulated cells (cells) served as negative controls.

The obtained results, which were determined in duplicates for each glycoform, control and concentration, were used to calculate AUC using GraphPad Prism (Version 9.3.1), and then normalized to the corresponding concentrations of reference IgG2: 5 µg/mL antigen with 1 µg/mL antibody, 10 µg/mL antigen with 2 µg/mL antibody, and 20 µg/mL antigen with 4 µg/mL antibody, respectively.

2.2.6 Multiplex kinase activity assay

2.2.6.1 PamGene® technology

Multiplex kinase activity profiling by PamGene® technology (BJ's-Hertogenbosch, The Netherlands) allows the direct examination of the activity of kinases in cell lysates by using the PamChips®. Each chip consists of four identical arrays, each array containing 144 serine/threonine kinases (STK) or 196 protein tyrosine kinases

(PTK) peptide sequences immobilized on their surface. These peptides contain phosphorylation sites derived from literature or computational predictions and are linked to one or various PTK or STK kinases (145).

Once the chip with the dispensed sample is introduced into the PamStation®12 instrument, the kinases present in the lysates rapidly phosphorylate the immobilised peptides in the presence of adenosine triphosphate (ATP). Meanwhile, FITC-conjugated anti-phosphotyrosine antibodies detect the phosphorylation activity of the kinases, and the emitted fluorescence is then captured by an inbuilt charge-coupled device (CCD) camera at several exposure times. The resulting images of each array are used by the BioNavigator® software to create kinetic data curves of each peptide. Eventually, all further steps of this analysis consisting of image quantification, quality control, statistical analysis, visualization and interpretation is performed using this software.

2.2.6.2 Preparation of samples

To analyse the kinase activity profiles of the differentially glycosylated IC-stimulated neutrophils, six flat bottom 6-well plates (clear, for suspension culture) were coated with 1200 µL hCOL7 E-F at a concentration of 10 µg/mL and then incubated overnight at 4 °C. On the following day, the plates were washed three times with 2 mL PBS-T per well, blocked with 1500 µL blocking buffer for 1 h on shaker, and washed again for three times. Next, 1500 µL of antibody (reference IgG2, EndoS, degalactosylated, galactosylated, or sialylated) at a final concentration of 2 µg/mL were added to corresponding wells according to the plate layout (Figure 10) and shake-incubated for 1.5 h. Meanwhile, PMNs were isolated as described in chapter 2.2.1, and all required centrifugations were carried out at 23 °C. To ensure correct implementation, each multiplex kinase activity assay was accompanied by a ROS release assay. After plates were washed three times with 2 mL PBS-T and once with 2 mL CL medium, 1.5 mL of the 6.6 x 10^6 cells/mL cell suspension were added to each well, excepting the control well that contained 4.5 mL cell suspension, without stimulating antigen, antibodies or IC. The corresponding wells were then incubated at 37 °C and 5 % CO_2 for 2, 8 or 15 min, respectively. After incubation, the plates were placed immediately on ice, cell solutions were transferred to separate 15 mL tubes, and each well was washed with 1 mL cold PBS to detach remnant cells. With the rest volume being added to the corresponding tubes, the cell solutions were centrifuged at 1000 x g for 5 min at 4 °C. After the resulting

supernatant was removed, the pellet was resuspended in 100 µL M-PER™ lysis cocktail, pipetted up and down and incubated for 15 min on ice, followed by a centrifugation at 16,000 x g for 15 min at 4 °C. The supernatants were then aliquoted (12 µL) into iced PCR tubes, snap frozen in liquid nitrogen and stored at -80 °C. The samples were further used to run the PTK and STK microarray protocols according to the manufacturer's instructions using the PamStation®12 instrument. To allow valid comparisons, samples originating from the same donor were dispensed on the same chip.

reference IgG2	reference IgG2	EndoS	cells	ag	ab reference IgG2
degal	gal	sial			

Figure 10. Plate layout for multiplex kinase activity profiling. Two 6-well plates (clear, for suspension culture) per condition were coated with immune complexes consisting of human collagen VII E-F and the antibody with the indicated glycosylation pattern: reference IgG2, EndoS, degalactosylated (degal), galactosylated (gal), or sialylated (sial). Unstimulated cells (cells), antigen only (ag) and reference IgG2 only (ab IgG2) were used as negative controls.

2.2.6.3 Tyrosine kinase protocol

To prepare a lysate mix for the PTK assay, 5.5 µg protein sample were added to 11 µL volume containing 1.1 µL M-PER™ cocktail and M-PER™. In the following step, the basic mix was prepared by using 249 µL distilled water, 60 µL PK buffer, 6 µL of 100x BSA and 1 M DTT solution, 60 µL PTK additive, 9 µL PY20 and 60 µL 4 mM ATP from the PTK Reagent Kit. Before blocking each array with 30 µL 2 % BSA, the PamChips® PTK were warmed up for 10 min at RT. Afterwards, the total mixes were prepared by mixing each lysate mix with 33 µL basic mix, with 40 µL of the total mix applied then to each array. To allow the kinase reaction to occur, the reaction mix was pumped for 60 cycles at 30 °C through the three-dimensional surface of the PamChips® PTK, while images were taken every fifth cycle over the course of the reaction.

2.2.6.4 Serine/Threonine kinase protocol

The lysate samples for a STK assay were first diluted 1:5 in M-PER™, and then 1.1 µg protein lysate were added to 11 µL volume consisting of 1.1 µL M-PER™ cocktail and the rest M-PER™. The basic mix was prepared by using 317 µL distilled

water, 60 µL PK buffer, 6 µL 100x BSA, 6.9 µL STK antibody, and 60 µL 4 mM ATP from the STK Reagent Kit. Next, the PamChips® STK were warmed up for 10 min at RT before blocking them with 30 µL 2 % BSA added into each array. Afterwards, the total mixes were prepared by mixing each lysate mix with 33 µL basic mix, with 40 µL of the total mix applied then to each array. To allow the kinase reaction to occur, the reaction mix was pumped for 60 cycles at 30 °C through the PamChips® STK. Next, a detection mix with a secondary antibody containing 351 µL distilled water, 39.6 µL AB buffer and 5.3 µL STK antibody, was added to each array. The detection mix was then pumped for 30 cycles at 30 °C through the PamChips® STK, while images were taken every fifth cycle over the course of the reaction.

2.2.6.5 Image analysis

The captured images were analysed using the PamGene® BioNavigator63 software tool. This programme allows the interpretation of data in a comprehensive pre-defined or customized modular manner. First, all kinetic images of each array were evaluated and analysed to check that the assay ran without complications using software application Image analysis, respectively. Subsequently, the fluorescence signal intensity of each spot on the chip was automatically normalised to the local background signal, thus rendering each kinase peptide substrate per array. Next, the data were $\log_2$-transformed to normalize the distribution of the signal intensities. First, the impact of each glycoform or reference IgG2 IC on neutrophil activation was tested by comparing data from each glycoform or reference IgG2 IC to the unstimulated cell control. Second, the impact of neutrophils stimulation itself was tested by comparing each glycoform at 2, 8 or 15 min versus cell control. Next, PTK or STK Upstream Kinase analysis was conducted to identify impaired kinases between each of the compared groups. Therefore, using the normalized peptide signal intensities, the normalized kinase statistic was calculated by analysing the change in phosphorylation between the two samples to be compared. The specificity and the significance of the resulting kinase statistic was determined by a permutation test. While for the significance the samples were randomly permuted between the groups, for the specificity the permutation of the peptides between the peptide sets of each kinase was carried out. A kinase was considered impaired (activated or inhibited) if its mean specificity score and mean significance score were higher than 1 and 0.5, respectively. The specificity score warrants that the association between assigned peptides and corresponding kinase is specific and

not random, while the significance score indicates whether the change represented by the mean kinase statistic is higher than for random allocation of peptides to kinases. The mean kinase statistic score was calculated as the mean difference between the signal intensity of a sample and its corresponding control, of each peptide assigned to a specific kinase, overall implying the total change of the peptide substrates that constitute a kinase. Positive values indicate increased kinase activity, while negative values indicate decreased activity compared to the control group. The final score for ranking kinases is determined by combining the mean specificity score and the mean significance score. This summation ranks and predicts the top kinase hits that show differential regulation between the compared groups. The method for calculating this final score is automatically determined by the application based on the number of samples provided as input. These scores were utilized to generate heatmaps using R Studio (Version 2023.06.1+524) with the heatmap package ("pheatmap"), while kinome trees were constructed using Coral.

2.2.7 BCA assay

Accurate determination of protein concentration in the cell lysates is a prerequisite for the multiplex kinase activity profiling (recommended level > 0.5 µg/µL). The bicinchoninic acid (BCA) assay quantifies proteins in biological samples based on the reduction of Cu^{2+} to Cu^{+} under alkaline conditions by proteins, followed by the subsequent spectrophotometrically detection of the purple chelate complex formed between Cu^{+} and two molecules of BCA (146). In the conducted experiments, the Pierce™ BCA Protein Assay Kit was used in accordance with the manufacturer's instructions. First, a serial dilution of BSA (standards) in M-PER™ was carried out for the following concentrations: 2000, 1500, 1000, 750, 500, 250, 125, 25 and 0 µg/mL. Meanwhile, the lysate samples from the multiplex kinase activity profiling experiments were diluted 1:10 in M-PER™. In the following step, a transparent, F-bottom TC 96-well plate was coated with 25 µL of either standards or diluted samples in duplicates, followed by the addition of 200 µL working reagent (containing reagents A:B in a 50:1 dilution) to each well. Next, a shake-incubation of 30 s followed by an incubation for 30 min at 37 °C of the plate was carried out. After the plate was cooled at RT, the absorbance at 562 nm was measured by the GloMax® Discover microplate reader. The protein concentrations of the samples

were subsequently calculated via linear regression in GraphPad Prism (Version 9.3.1).

2.2.8 Statistical analysis

For all obtained data from the carried-out experiments, each of the three concentration of the differentially glycosylated IC (1, 2 or 4 µg/mL) were normalised to the reference IgG2 IC at 10 µg/mL antigen and 2 µg/mL antibody concentration, the latter being set at 100%. All statistical analyses were performed using GraphPad Prism (Version 9.3.1). The results were displayed as bar graphs denoting the mean ± standard deviation with the individual values represented as dots. The ordinary one-way analysis of variance (ANOVA) with Turkey post-test compared for each concentration group corresponding reference IgG2 and all glycoforms between themselves. Thus, the impact of each glycoform on the various functions of IC-stimulated neutrophils was examined. Statistical significance was defined as p-value < 0.05.

3 RESULTS

3.1 Adhesion of IC-stimulated neutrophils

The adhesion of neutrophils to the endothelial cells is crucial for the subsequent detrimental release of ROS and proteases (139). Thus, blocking this step could protect from neutrophil-mediated tissue injury, the latter being a major culprit in the pathogenesis of EBA (126,128). An adhesion assay (n=5) was carried out to test the impact of the differentially glycosylated (reference IgG2, EndoS, degalactosylated, galactosylated, or sialylated) IgG2 IC at various concentrations (0.5x, 1x, and 2x) on the adhesion of neutrophils *in vitro*. Unstimulated cells, antigens or antibodies alone served as negative controls, while PMA was used as a positive control (data not shown for clarity).

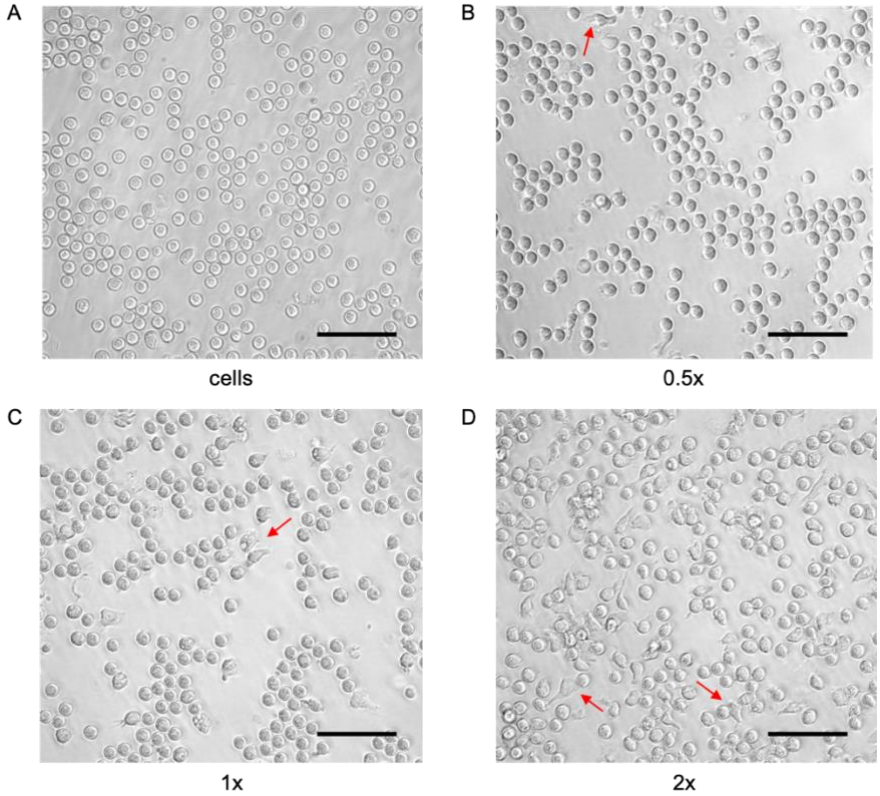

Figure 11. Microscopic appearance of IC-stimulated neutrophils. Freshly isolated human neutrophils were stimulated with IC consisting of reference IgG2 and compared to unstimulated cells after an incubation of 45 min at 37 °C and 5 % CO_2. Light microscopic images were taken afterwards with an 80x/0.3 objective (scale bar: 75 µm). (**A**) Unstimulated neutrophils retained their morphology, while IC-stimulated neutrophils at three different concentrations of (**B**) 0.5x (5 µg/mL antigen and 1 µg/mL antibody), (**C**) 1x (10 µg/mL antigen and 2 µg/mL antibody), and (**D**) 2x (20 µg/mL antigen and 4 µg/mL), showed clear spreading on surface (red arrows), with their number increasing with IC concentration. Representative data (n=1) from independent experiments (n=5). IC, immune complexes; IgG2, immunoglobulin γ 2.

The spreading of neutrophils on the IC-coated surfaces was quantified by impedance measurement every minute for 1 hour, and the AUC was calculated using GraphPad Prism. ANOVA with Turkey post-test was used for comparisons between the different antibodies (Figures 11-14). In addition, microscopic images were taken of the IC-induced spreading of neutrophils after 45 min (Figure 11).

3.1.1 Adhesion is dose- and donor-dependent

The dose-dependency of adhesion in IC-stimulated neutrophils was confirmed by both microscopic appearance and impedance data of the reference IgG2 IC at 10 µg/mL antigen and 2 µg/mL antibody concentration.

Microscopic images of neutrophils were taken 45 min after IC-stimulation. As expected, IC-stimulated neutrophils showed evident spreading on surface as indicated by the uneven morphology, while unstimulated cells had an even, round shape (Figure 11). In addition, the number of adhered cells increased with the IC concentration.

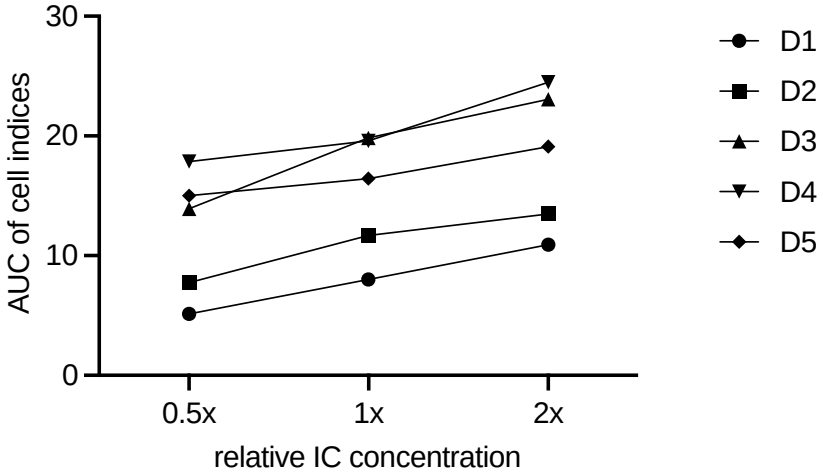

Figure 12. Adhesion of IC-stimulated neutrophils is dose- and donor-dependent. Freshly isolated human neutrophils were stimulated with IC consisting of reference IgG2 at 0.5x (5 µg/mL antigen and 1 µg/mL antibody), 1x (10 µg/mL antigen and 2 µg/mL antibody) and 2x (20 µg/mL antigen and 4 µg/mL antibody) concentrations for 1 h at 37 °C and 5 % CO_2. The impedance was measured by quantifying their spreading on a surface. These measurements were then converted by the xCELLigence RTCA system into unitless cell indices. The AUC of these indices was analysed for each concentration. The values are displayed as means of duplicate measurements. n = 5 independent experiments. AUC, area under the curve; D, donor; IC, immune complexes; IgG2, immunoglobulin γ 2.

These effects were further confirmed by real-time impedance measurement. All AUC values increased with the relative IC concentration, while the level of spreading

after IC-stimulation was different between the donors (Figure 12). Considering the heterogeneity of the obtained results, the data were normalised in further analysis.

3.1.2 Adhesion is significantly impacted by the differentially glycosylated IC

The adhesion kinetics of the impedance measurements expressed as cell indices showed an important difference between the various glycoforms (Figure 13). After the start of the experiment, neutrophils immediately adhered to the surface, reached a peak after approximately 15 min and returned to baseline levels after approximately 1 h. In this representative kinetic depiction from donor 1, the degalactosylated and galactosylated IgG2 IC showed nearly equally the highest adherence, followed by approximately one-third decrease for the reference and sialylated IgG2 IC. In addition, the latter showed a halt at approximately 30 min before decreasing its adherence. Of note, EndoS demonstrated the lowest adherence, with a reduction of about 50% when compared to reference IgG2 IC, and of two-thirds in comparison to degalactosylated and galactosylated IgG2 IC. With respect to the controls, the measured impedance was very low.

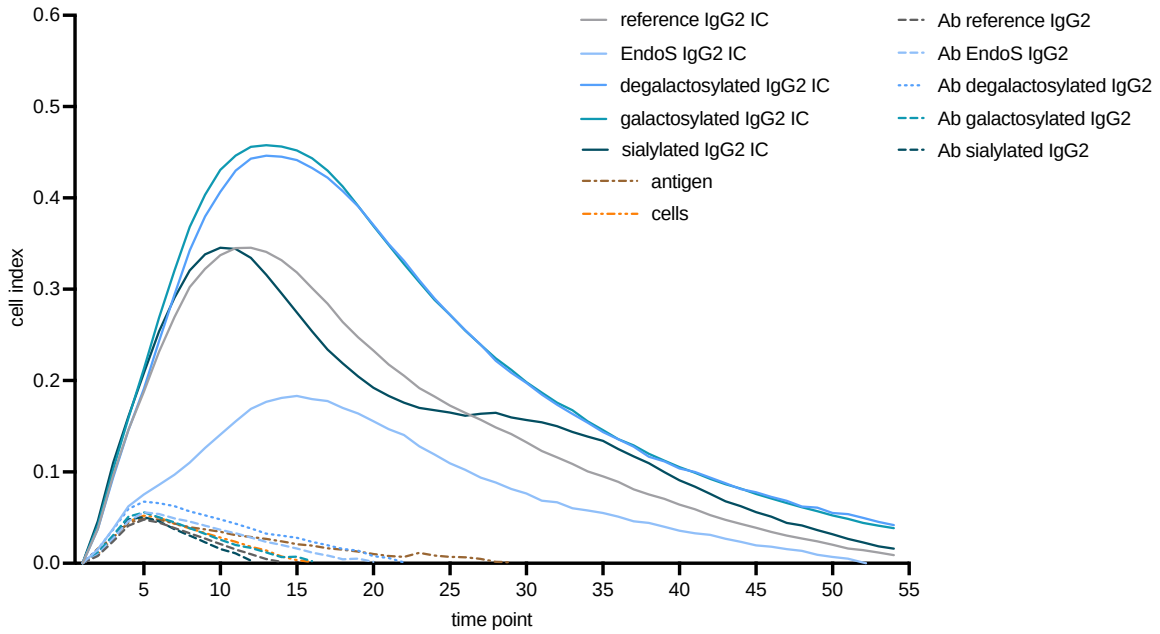

Figure 13. Representative adhesion kinetics of neutrophils stimulated with differentially glycosylated IgG2-containing IC. Freshly isolated human neutrophils were stimulated by immobilized IC containing different IgG2 glycoforms for 1 h at 37 °C and 5 % CO_2. The adhesion of neutrophils was further examined by real-time impedance measurement. The IC (reference IgG2, EndoS, degalactosylated, galactosylated and sialylated) were used each at 10 µg/mL antigen and 2 µg/mL antibody concentration. Unstimulated cells (cells), antigen and corresponding antibodies (Ab) served as negative controls. Representative data (n=1) from independent experiments (n=5). IC, immune complexes; IgG2, immunoglobulin γ 2.

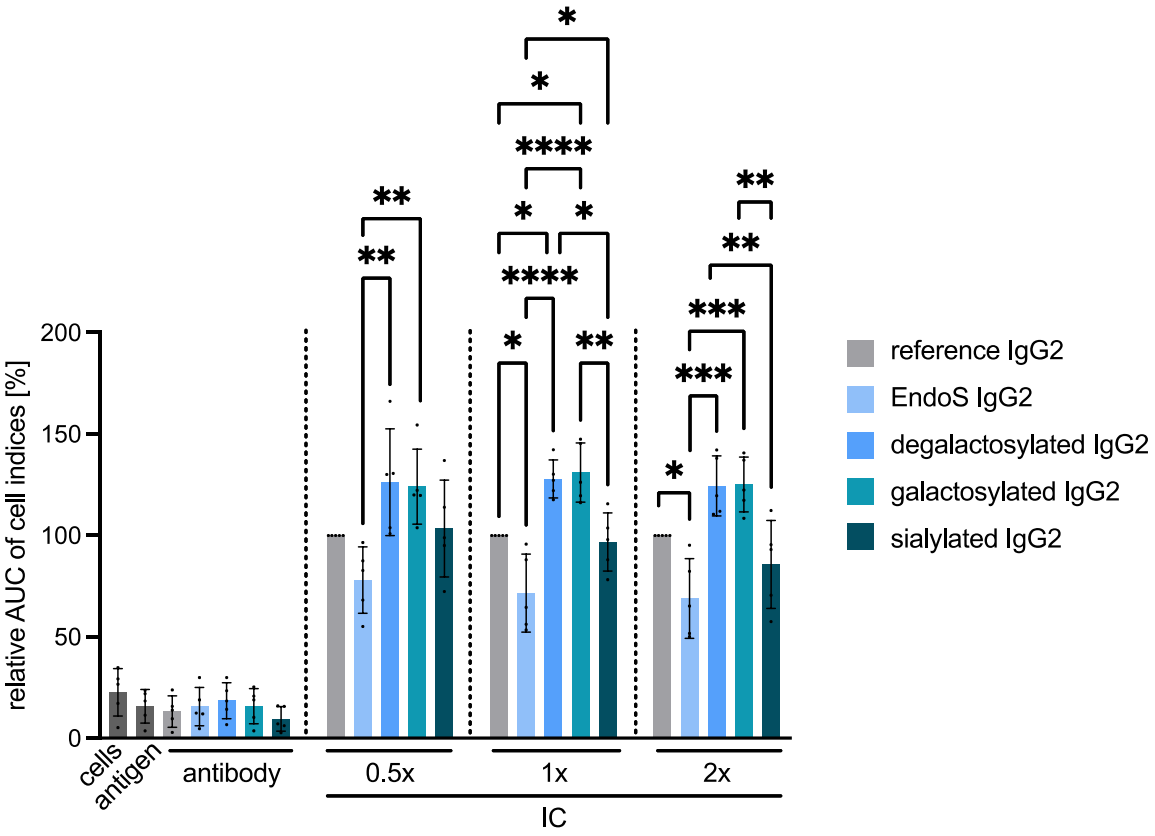

Figure 14. Effect of different glycoforms on the adhesion of IC-stimulated neutrophils. Freshly isolated human neutrophils were stimulated by immobilized IC containing different IgG2 glycoforms (reference IgG2, EndoS, degalactosylated, galactosylated and sialylated) for 1 h at 37 °C and 5 % CO_2. Meanwhile, the adhesion was measured by means of impedance. The AUC of cell indices was calculated and values were normalised to reference IgG2 for each concentration: 0.5x refers to 5 µg/mL antigen and 1 µg/mL antibody, 1x to 10 µg/mL antigen and 2 µg/mL antibody, and 2x refers to 20 µg/mL antigen and 4 µg/mL antibody concentrations. Cells, antigen and antibodies alone served as negative controls. n = 5 independent experiments. Results are shown as bar graphs denoting the mean ± standard deviation with the individual values represented as dots. ANOVA with Turkey post-test was performed for each individual IC concentration separately. * $p \leq 0.05$; ** $p \leq 0.01$; *** $p \leq 0.001$; **** $p \leq 0.0001$. AUC, area under the curve; IC, immune complexes; IgG2, immunoglobulin γ 2.

To further analyse the impact of differentially glycosylated IC on the adhesion of neutrophils, the AUC values were compared (Figure 14). EndoS showed a reduced adhesion in all three concentrations, which was highly significant compared to the degalactosylated and galactosylated IgG2 IC. In addition, at highest concentration this difference was significant also compared to the reference IgG2 IC. For the 1x concentration (10 µg/mL antigen and 2 µg/mL antibody concentration), the sialylated form demonstrated a significantly reduced adhesion in comparison to the galactosylated and degalactosylated IgG2 IC, while the latter showed a significant

increase when compared to reference IgG2 IC. This significant decrease of sialylated antibodies was found also at the highest concentration.

3.2 Activation of IC-stimulated neutrophils

Upregulation of CD18 and shedding of CD62L are hallmarks of neutrophil activation, facilitating firm adhesion to the endothelium and subsequent transmigration into tissues (143,144). Therefore, the activation of neutrophils upon IC stimulation was assessed by the expression of these two specific activating surface markers.

A flow cytometry assay (n=5) was carried out to evaluate the impact of the differentially glycosylated (reference IgG2, EndoS, degalactosylated, galactosylated, or sialylated) IgG2 IC at 0.5x (5 µg/mL antigen and 1 µg/mL antibody), 1x (10 µg/mL antigen and 2 µg/mL antibody) as well as 2x (20 µg/mL antigen and 4 µg/mL antibody) concentrations on the activation of neutrophils. The expression levels were quantified by the values of $CD18^{high}$ and $CD62L^{low}$ neutrophils, and AUC was calculated (Figure 15-17). Activation is characterized by an increase in CD18 and decrease in CD62. ANOVA with Turkey post-test was used for comparisons between the different glycosylated antibodies.

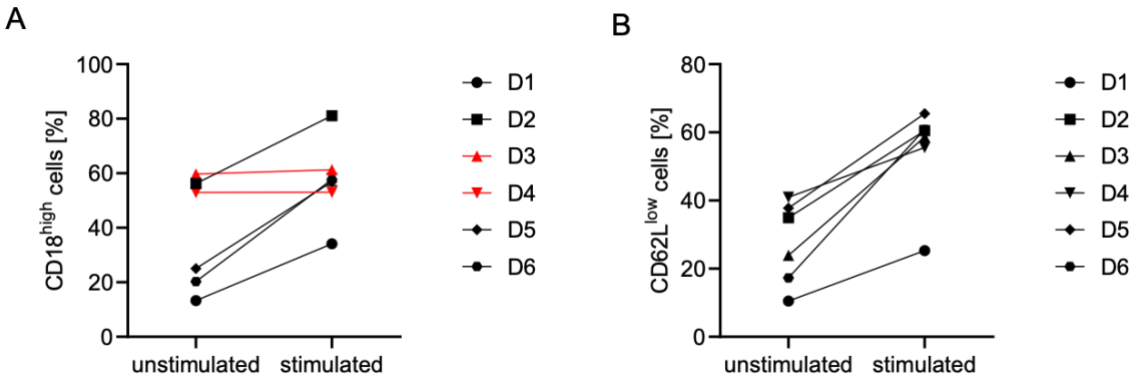

Figure 15. Increased CD18 expression and CD62L shedding after IC-stimulation of neutrophils. Freshly isolated human neutrophils were stimulated by immobilized IC containing reference IgG2 at 10 µg/mL antigen and 2 µg/mL antibody concentration and compared to unstimulated cells. Cells were stained for (**A**) CD18, and (**B**) CD62L by flow cytometry. Gating was performed according to Figure 8. The values are depicted as means of duplicate measurements. n = 6 independent experiments. CD, cluster of differentiation; D, donor; IC, immune complexes; IgG2, immunoglobulin γ 2.

3.2.1 CD18 expression and CD62L shedding is donor-dependent

Upon IC-mediated activation, neutrophils expressed higher levels of $CD18^{high}$ and increased CD62L shedding, except for donors 3 and 4 regarding $CD18^{high}$ (Figure 15). Therefore, these deviating values were excluded from further analysis. On the

other hand, the numeric values and degree of activation varied between donors, with a difference of up to 40% for both $CD18^{high}$ and $CD62L^{low}$. Since neutrophil activation was shown to be donor-dependent, data normalization was carried out for each donor and concentration for all further analyses.

3.2.2 The differentially glycosylated IC do not influence neutrophil activation

No significant differences were observed between the different IgG2-based glycoforms regarding CD18 expression (Figure 16). Most values were in the range of reference IgG2 IC, except for the 5 µg/mL antigen and 1 µg/mL antibody concentration, which was characterized by higher values of EndoS and sialylated forms. However, the differences were not statistically significant and the standard deviation was high.

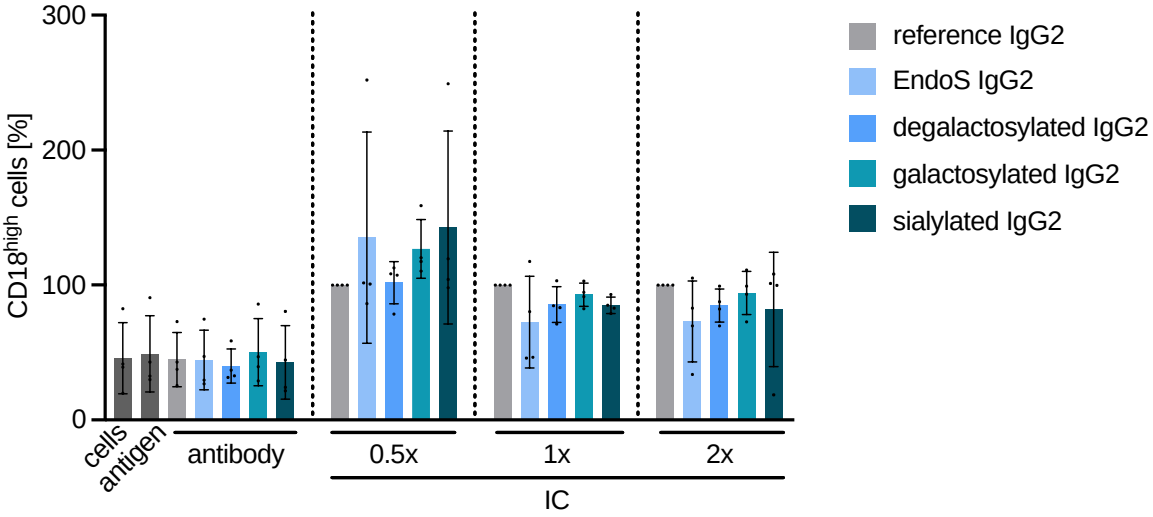

Figure 16. Differentially glycosylated IgG2-based IC have no significant effect on CD18 expression. Freshly isolated human neutrophils were stimulated by immobilized IC containing different IgG2 glycoforms (reference IgG2, EndoS, degalactosylated, galactosylated and sialylated) at 0.5x (5 µg/mL antigen and 1 µg/mL antibody), 1x (10 µg/mL antigen and 2 µg/mL antibody) and 2x (20 µg/mL antigen and 4 µg/mL antibody) concentrations, and stained for the activation marker CD18. The ratio of $CD18^{high}$ cells was used to assess the activation by flow cytometry. n = 4 independent experiments. Bars are means ± standard deviation and dots represent individual values. CD, cluster of differentiation; IC, immune complexes; IgG2, immunoglobulin γ 2.

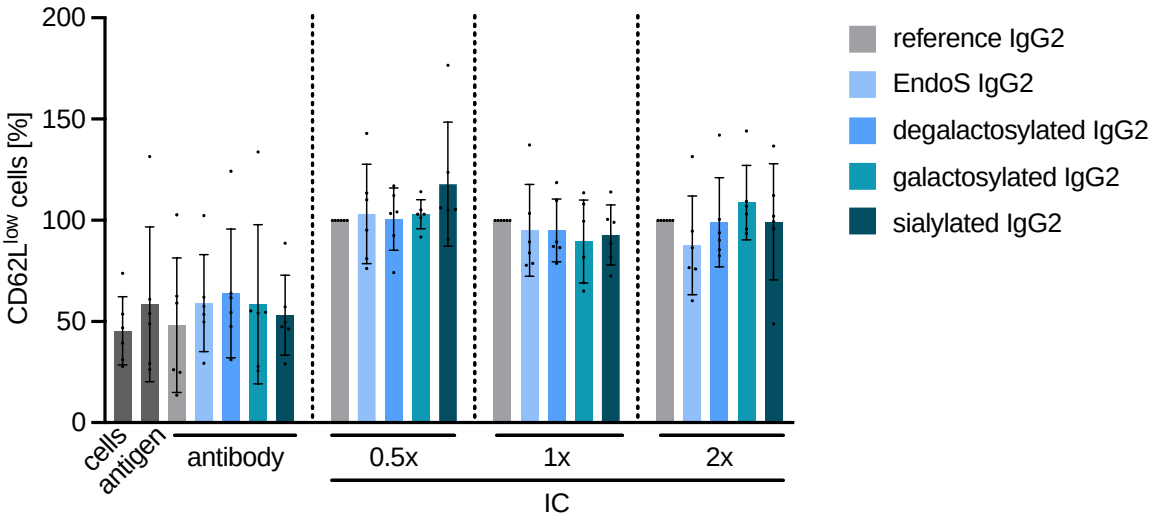

Figure 17. Differentially glycosylated IgG2-based IC have no significant effect on CD62L shedding. Human neutrophils were stained for flow cytometry after stimulation with immobilised IC comprised of differentially glycosylated IgG1 and human collagen 7 E-F at 0.5x (5 µg/mL antigen and 1 µg/mL antibody), 1x (10 µg/mL antigen and 2 µg/mL antibody) and 2x (20 µg/mL antigen and 4 µg/mL antibody) concentrations. The activity was determined by the share of $CD62L^{low}$ cells. n = 6 independent experiments. Bars are means ± standard deviation and dots represent individual values. CD, cluster of differentiation; IC, immune complexes; IgG2, immunoglobulin γ 2.

Likewise, CD62L shedding was also not influenced by the different glyco-based IC (Figure 17).

Overall, the differentially glycosylated IC did not have a significant influence on the activation of neutrophils assessed by CD18 expression and CD62L shedding.

3.3 ROS release by IC-stimulated neutrophils

Activated neutrophils cause tissue damage by releasing proteases and ROS (59). In EBA, neutrophils bind to skin-bound immune complexes via FcγR, activating pathways that release ROS and proteases, thus causing the characteristic subepidermal blisters (126–128).

A ROS release assay was conducted to determine whether differentially glycosylated IgG2 IC – including reference IgG2, EndoS, degalactosylated, galactosylated, and sialylated forms – at 5 µg/mL antigen and 1 µg/mL antibody, 10 µg/mL antigen and 2 µg/mL antibody, and 20 µg/mL antigen and 4 µg/mL antibody concentrations, exhibit an influence on the release of ROS in neutrophils from healthy donors (n=5) (Figure 18-21). PMA was used as a positive control (data not shown for clarity), while unstimulated cells, antigens, and each of all 4

gylcosylated antibodies alone served as negative controls. The AUC was analyzed for each glycoform and concentration, and ANOVA with Turkey post-test was employed to compare the different IC.

3.3.1 ROS release is dose- and donor-dependent

Upon activation, neutrophils release high levels of ROS, as indicated by the calculated AUC of the measured chemiluminescence (Figure 18). However, the extent of release and AUC values differed between the donors.

Overall, ROS release was directly proportional to relative IC concentration but different in all five donors (Figure 19). Thus, some donors showed a clear linear increase (D1 and D4), while others predominantly at the highest concentration (D2 and D3), or a slight overall increase in AUC values (D5), underlining the high donor-dependency of ROS release in IC-stimulated neutrophils. Therefore, all data were normalised to the reference IgG2 IC corresponding concentration in further analysis.

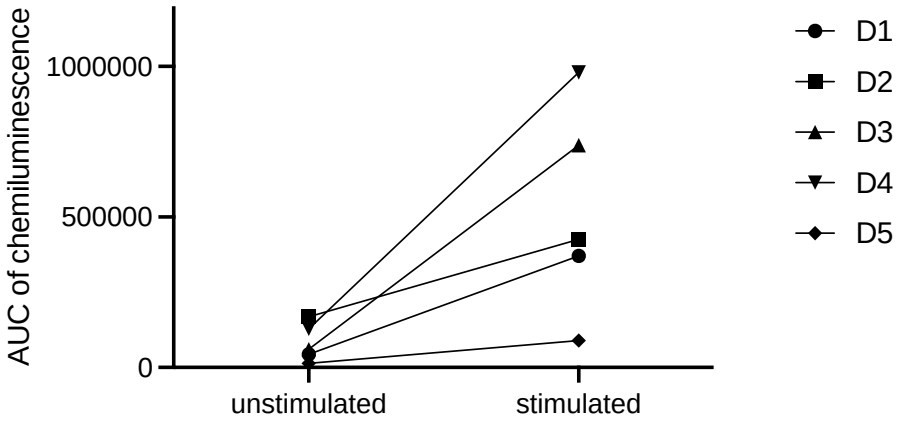

Figure 18. Increased ROS release after IC stimulation of neutrophils. Freshly isolated human neutrophils were stimulated by immobilized IC containing reference IgG2 at 10 µg/mL antigen and 2 µg/mL antibody concentration and compared to unstimulated cells. ROS release was detected indirectly via a luminol reaction, and the AUC was calculated. The values are depicted as means of duplicate measurements. n = 5 independent experiments. AUC, area under the curve; D, donor.; IC, immune complexes; IgG2, immunoglobulin γ 2.

3.3.2 ROS release is significantly influenced by the differentially glycosylated IC

The kinetics of ROS release as measured by the chemiluminescence signal was different between the various glycosylated IC. For the majority, a steep increase in ROS release that reached a peak after approximately 20-25 min and then abruptly decreased but without returning to the baseline, was observed (Figure 20). In this

representative analysis of donor 4, the degalactosylated form, followed by reference IgG2 IC demonstrated the highest ROS release. In contrast, EndoS showed a reduction of about half compared to reference IgG2 IC, while the controls exhibited insignificant levels of ROS release.

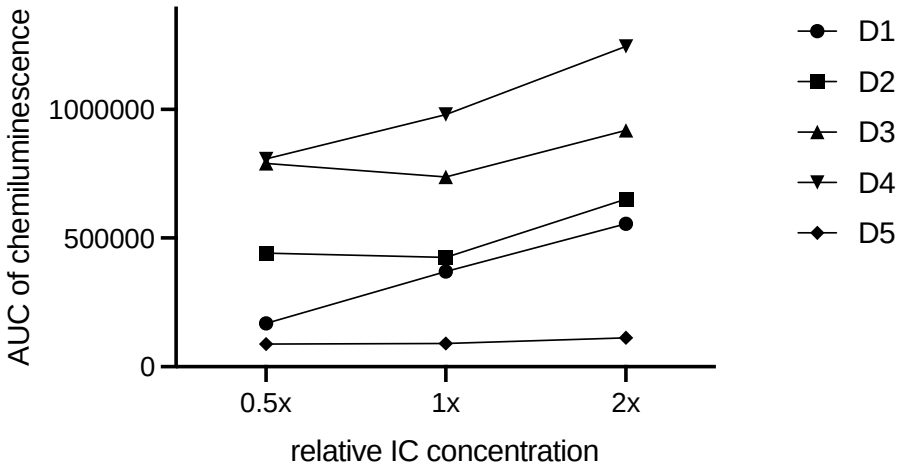

Figure 19. ROS release of IC-stimulated neutrophils is dose- and donor-dependent luminescence signal. Freshly isolated human neutrophils were stimulated with IgG2-containing IC at 0.5x (5 µg/mL antigen and 1 µg/mL antibody), 1x (10 µg/mL antigen and 2 µg/mL antibody) and 2x (20 µg/mL antigen and 4 µg/mL antibody) concentrations. ROS release was detected indirectly via a luminol reaction, and the AUC was calculated. The values are depicted as means of duplicate measurements. n = 5 independent experiments. AUC, area under the curve; D, donor; IC, immune complexes; IgG2, immunoglobulin γ 2.

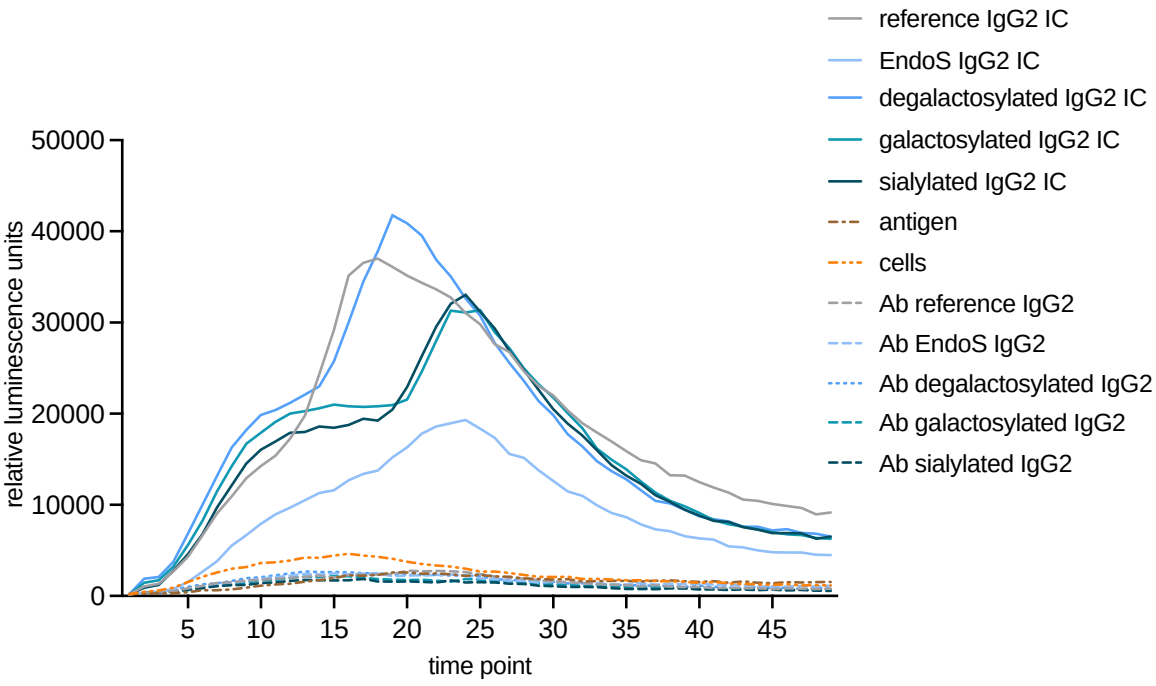

Figure 20. Representative kinetics of ROS release by IC-stimulated neutrophils. Freshly isolated human neutrophils were stimulated by immobilized IC containing reference IgG2 at 10 µg/mL antigen and 2 µg/mL antibody concentration. ROS release was detected indirectly via a luminol reaction over 2 h. Unstimulated cells (cells), antigen and corresponding antibodies (Ab) served as negative controls. Representative data (n=1) from independent experiments (n=5). IC, immune complexes; IgG2, immunoglobulin γ 2; ROS, reactive oxygen species.

After normalization of AUC values to corresponding reference IgG2 IC concentrations, significant differences in ROS release of up to 50% were observed between EndoS and reference IgG2 IC (Figure 21). The latter were statistically significant for the 1x (10 µg/mL antigen and 2 µg/mL antibody) and 2x (20 µg/mL antigen and 4 µg/mL antibody) concentrations ($p \leq 0.001$). This reduction in ROS release by EndoS was highly significant also in comparison to the other glycoforms, again for the 1x and 2x concentrations. In addition, the sialylated IgG2 IC demonstrated a decreasing tendency for ROS release with concentration, but this was not significant. All other glycoforms showed values in the range of reference IgG2 IC and were not significant.

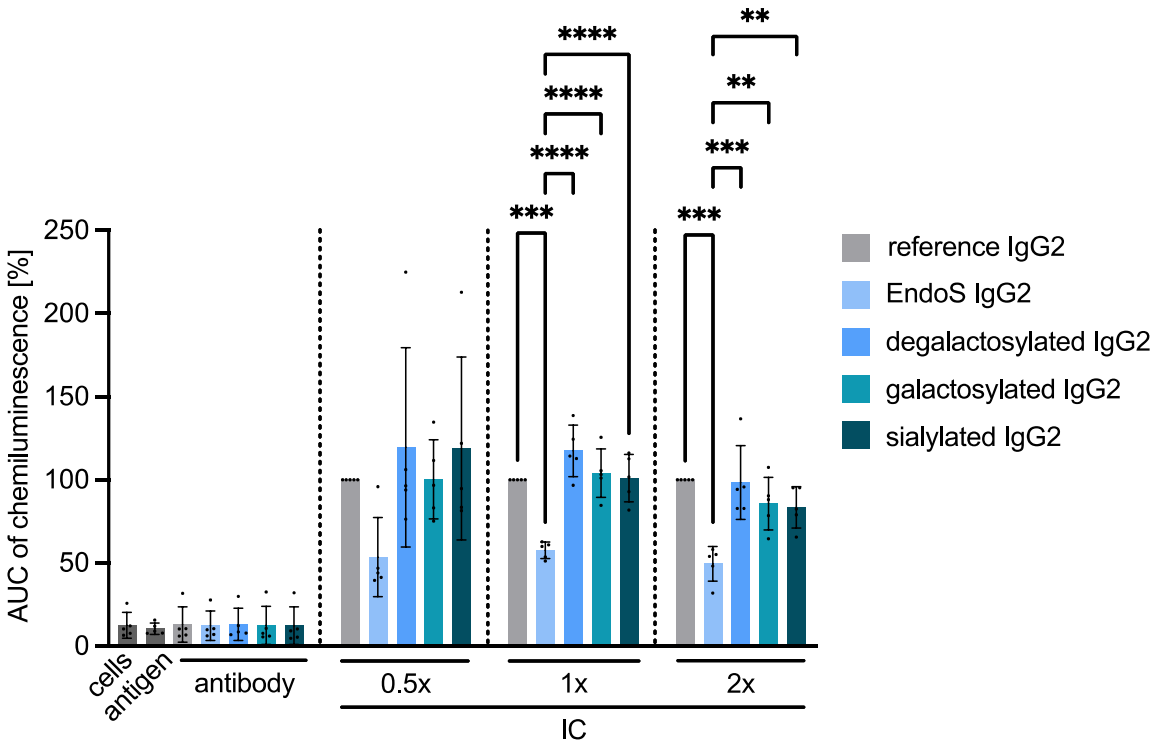

Figure 21. Effect of different glycoforms on the ROS release of IC-stimulated neutrophils. Freshly isolated human neutrophils were stimulated by immobilized IC containing different IgG2 glycoforms (reference IgG2, EndoS, degalactosylated, galactosylated and sialylated). ROS release was detected indirectly via a luminol reaction. The AUC was calculated and values were normalised to reference IgG2 for each

concentration: 0.5x refers to 5 µg/mL antigen and 1 µg/mL antibody, 1x to 10 µg/mL antigen and 2 µg/mL antibody, and 2x refers to 20 µg/mL antigen and 4 µg/mL antibody concentrations. n = 5 independent experiments. Results are shown as bar graphs denoting the mean ± standard deviation with the individual values represented as dots. ANOVA with Turkey post-test was performed for each individual IC concentration separately. * $p \leq 0.05$; ** $p \leq 0.01$; *** $p \leq 0.001$; **** $p \leq 0.0001$. AUC, area under the curve; IC, immune complexes; IgG2, immunoglobulin γ 2; ROS, reactive oxygen species.

3.4 Flow cytometric cytotoxicity assessment of the differentially glycosylated IC

The activation of neutrophils through their FcR by IC initiates a series of responses – ROS production, degranulation, and cytokine release, that not only promote inflammatory tissue destruction but also lead to apoptosis in neutrophils (63,147,148). To evaluate the potential influence of the differentially glycosylated IC on the neutrophil viability, a flow cytometry assay was performed (n=5). Freshly isolated human neutrophils were stimulated for 2 h with immobilised IC containing different IgG2-based glycoforms (reference IgG2, EndoS, degalactosylated, galactosylated and sialylated), and then stained with Zombie NIR™ and Annexin V. Thus, the viability of neutrophils was assessed by counting the Zombie$^-$ Annexin V$^-$ positive cells.

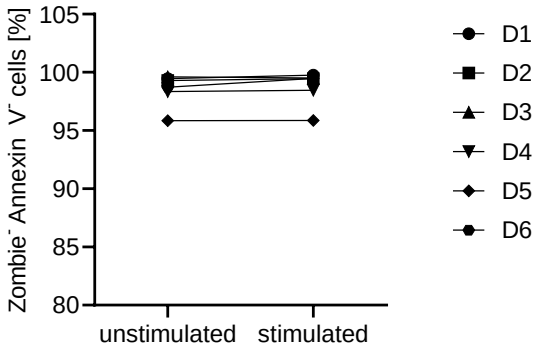

Figure 22. IC stimulation shows no toxicity on neutrophils. Freshly isolated human neutrophils were stimulated by immobilized IC containing reference IgG2 at 10 µg/mL antigen and 2 µg/mL antibody concentration and compared to unstimulated cells for 2 h. Cells were stained with Zombie NIR™ and Annexin V and the viability was determined by the share of Zombie$^-$ Annexin V$^-$ cells by flow cytometry. The values are depicted as means of duplicate measurements. Data were not normalised. n = 6 independent experiments. D, donor; IC, immune complexes; IgG2, immunoglobulin γ 2.

First, the comparison between IC-stimulated cells with reference IgG2 at 10 µg/mL antigen and 2 µg/mL antibody concentration and unstimulated cells showed no

difference in the number of viable cells in all five donors (Figure 22). Likewise, no significant differences in absolute values were observed between the differentially glycosylated IC-stimulated cells and controls (Figure 23). While all tested specimen including controls demonstrated at least 97% of viable cells count, glycoforms showed a rather higher viability of about 99% underlining that they do not exert any cytotoxic effects on stimulated neutrophils.

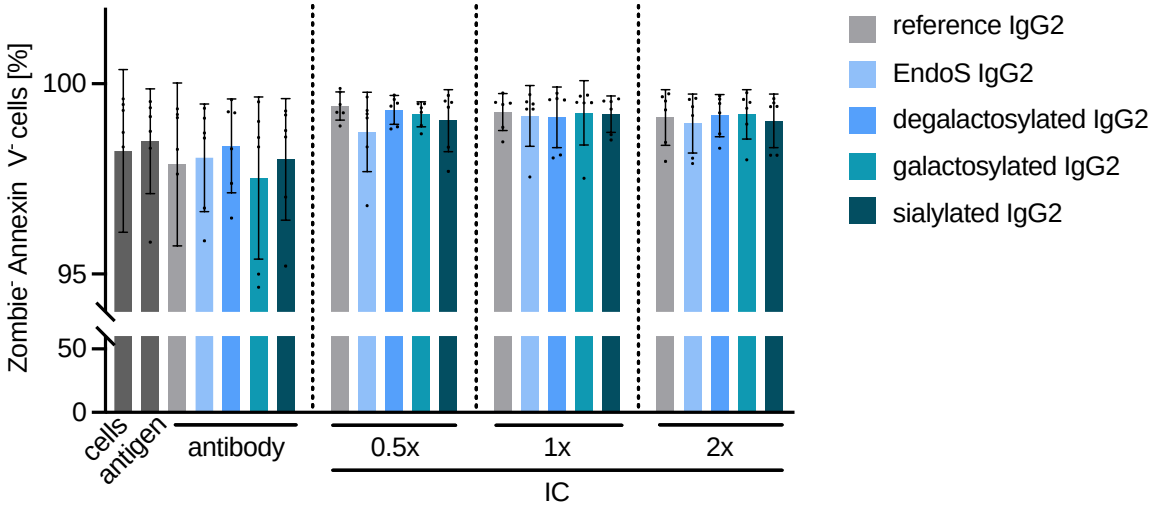

Figure 23. Differentially glycosylated IgG2-based IC do not influence neutrophil viability. Freshly isolated human neutrophils were stimulated by immobilized IC (reference IgG2, EndoS, degalactosylated, galactosylated, and sialylated) at 0.5x (5 µg/mL antigen and 1 µg/mL antibody), 1x (10 µg/mL antigen and 2 µg/mL antibody) and 2x (20 µg/mL antigen and 4 µg/mL antibody) concentrations for 2h and subsequently stained with Zombie NIR™ and Annexin V. The viability was determined by the share of Zombie⁻ Annexin V⁻ cells by flow cytometry. Data were not normalised. n = 6 independent experiments. Bars are means ± standard deviation and dots represent individual values. IC, immune complexes; IgG2, immunoglobulin γ 2.

3.5 Multiplex kinase activity profiling of IC-stimulated neutrophils

Accumulating data showed that depending on the nature of the stimulus, activation of each FcγR leads to a particular signal transduction pathway that, ultimately, renders distinct neutrophilic functions and predominant pro- or anti-inflammatory outcomes (73–75). To gain further insight into the intricate mechanisms of IC-induced signal transduction in neutrophils, a multiplex kinase activity profiling was conducted (n=3). Freshly isolated human neutrophils were stimulated with immobilized IC (reference IgG2, EndoS, degalactosylated, galactosylated and sialylated) at 10 µg/mL antigen and 2 µg/mL antibody concentration for 2, 8, or 15 min. Cells were subsequently lysed and the PTK and STK activity was measured by

PamGene. While unstimulated cells served as negative control, all differentially glycosylated IC were compared to the reference IgG2 IC for the corresponding timepoint. To ensure correct implementation, a ROS release assay was carried out in parallel (data not shown).

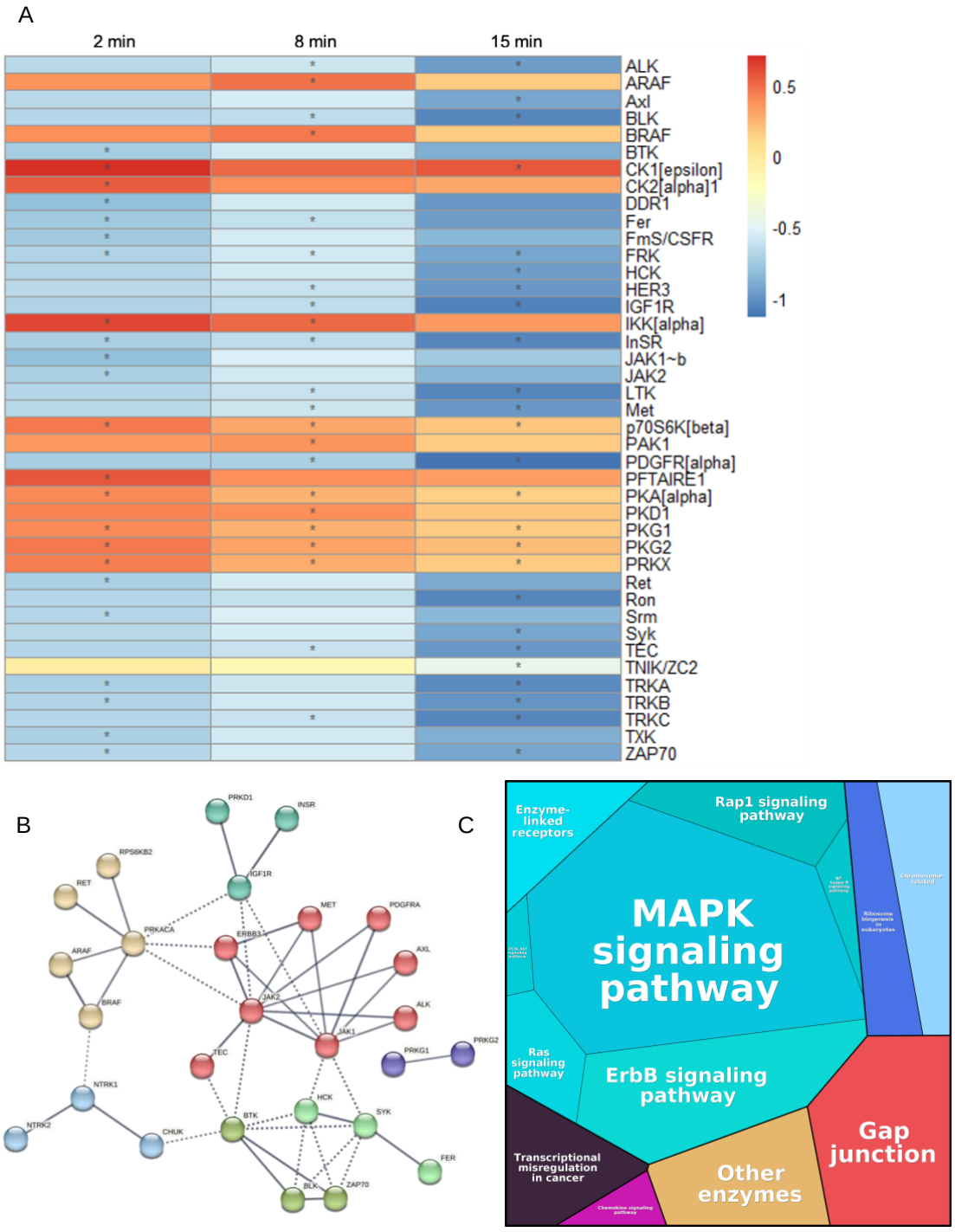

Figure 24. Kinase activity status over time in neutrophils stimulated with reference IgG2-containing IC. Freshly isolated human neutrophils were stimulated with immobilized IC containing reference IgG2 glycoform at 10 µg/mL antigen and 2 µg/mL

antibody concentration for 2, 8, or 15 min. Cells were subsequently lysed, and the PTK and STK activity was measured by PamGene. (**A**) The data are displayed as heatmaps of mean kinase statistic compared to unstimulated cells. Kinases were included if they exhibited a mean specificity score > 1 and a mean significance score > 0.5 for at least one time point. These kinases are indicated with an asterisk on the heatmap. Exact values can be found in the Appendix. (**B**) STRING database analysis of kinases modulated by reference IgG2, with interactions displayed at high confidence (thickness of the lines indicate the strength of the interaction); colours of modules are randomly chosen. n = 3 independent experiments for PTK and STK assays, respectively. (**C**) Proteomap illustrating the kinase signaling pathways involved in the reference IgG2-containing IC at the 8-minute time point, at 10 µg/mL antigen and 2 µg/mL antibody concentration, are presented. Proteomaps for the 2-minute and 15-minute time points are shown in Appendix. These proteomaps were generated using mean kinase statistics compared to unstimulated cells (149). Each tile represents a specific kinase signaling pathway, with different colors indicating various pathways; the colors were chosen according to the website's standards. Tile sizes represent the degree of involvement of kinase signaling pathways. IC, immune complexes; IgG2, immunoglobulin γ 2; PTK, protein tyrosine kinases; STK, serine/threonine kinases. All other abbreviations are listed in Abbreviations chapter.

Different PTK and STK kinases were up- or downregulated (data not shown). Their activation status over time in comparison to unstimulated cells was depicted as heatmaps, provided that they demonstrated a mean kinase specificity score of over 1 and a mean kinase significance score of more than 0.5 by at least one specific timepoint.

For reference IgG2 IC, the majority of kinases were downregulated, including tyrosine kinases JAK1b, JAK2, ZAP70, Syk and TRK A-C (Figure 24A-B). Kinases were primarily part of the Ras/ErbB/MAPK signaling pathway. (Figure 24C).

Regarding EndoS IC, fewer kinases were found to be involved, with a predominant activation at 2 minutes and subsequent decrease over time. The latter was demonstrated for CK1ε, ATR, GSK3β, IKKα and PFTAIRE1 (Figure 25). In contrast, the degalactosylated glycoform showed the highest number of involved kinases, with an increasing upregulation over time notably for GSK3β, PCTAIRE2, ROCK1, RSKL2, ANAF and BRAF. The galactosylated IgG2 IC led also to the activation of many kinases, in particular CK1ε at 2 and 8 min, and mTOR/FRAP at 8 min. Other upregulated kinases included CDK10, CaMK4, IKK, PFTAIRE1, PCTAIRE2, NuaK1 and DAPK3. On the other hand, sialylated glycoform showed a decreased activation of kinases, in particular at the last timepoint for CK1ε, IKKα and IKKβ, JNK1-3, p38Δ and RSKL2. Interestingly, CK1ε was found activated in all glycoforms. Moreover, certain kinases were activated only in one glycoform, such as MAPKAPK3 in EndoS,

ROCK1 in degalactosylated, CaMK4, CDK10 and mTOR/FRAP in galactosylated, and p38Δ and JNK1-2 in sialylated IgG2 IC (Figure 25).

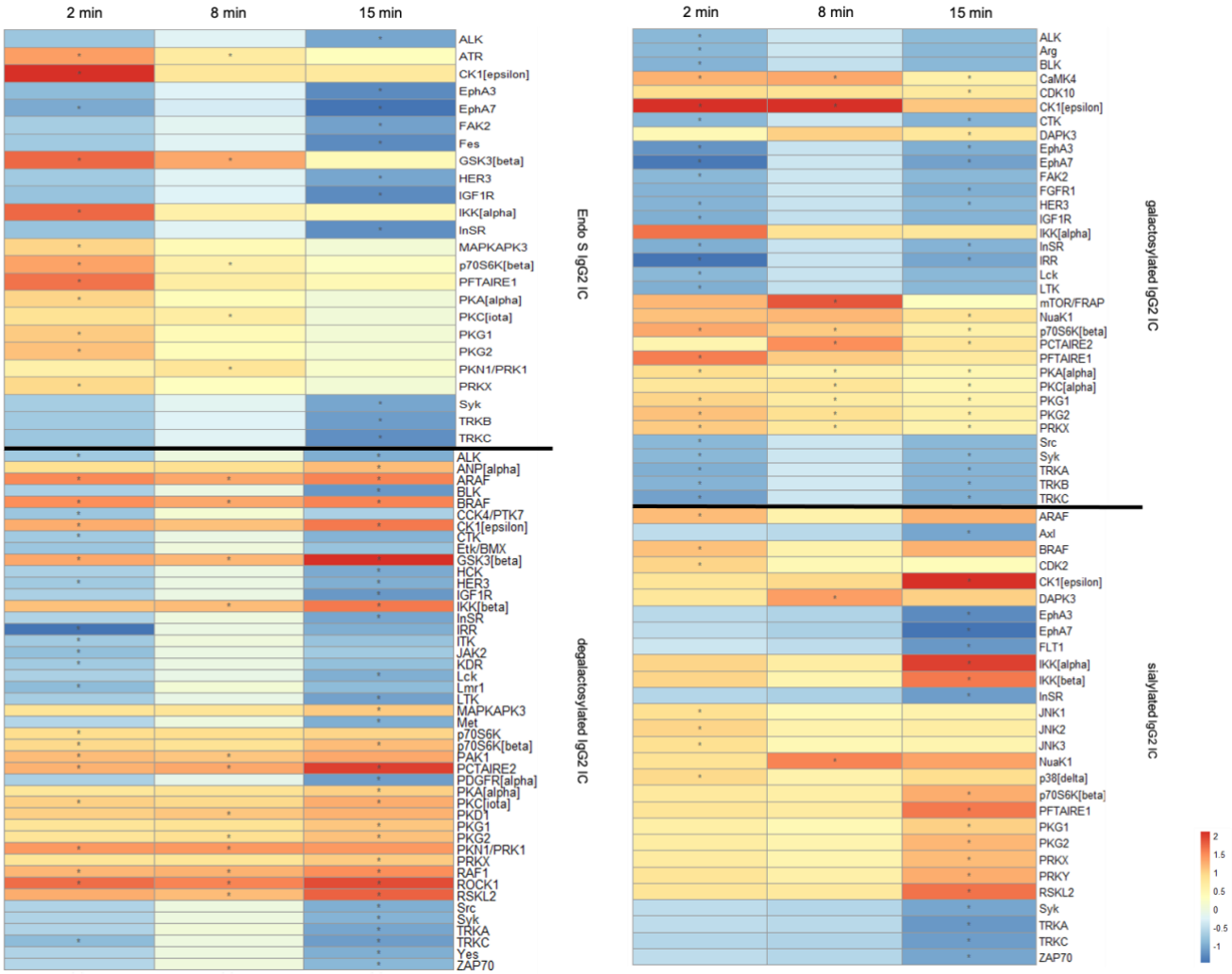

Figure 25. Kinase activity status over time in neutrophils stimulated with differentially glycosylated IgG2-containing IC. Freshly isolated human neutrophils were stimulated with immobilized IC containing different IgG2 glycoforms (EndoS, degalactosylated, galactosylated and sialylated) at 10 µg/mL antigen and 2 µg/mL antibody concentration for 2, 8, or 15 min. Cells were subsequently lysed, and the PTK and STK activity was measured by PamGene. The data are displayed as heatmaps of mean kinase statistic compared to unstimulated cells. Kinases were included if they exhibited a mean specificity score > 1 and a mean significance score > 0.5 for at least one time point. These kinases are indicated with an asterisk on the heatmap. Exact values can be found in the Appendix. n = 3 independent experiments for PTK and STK assays, respectively. IC, immune complexes; IgG2, immunoglobulin γ 2; PTK, protein tyrosine kinases; STK, serine/threonine kinases. All other abbreviations are listed in Abbreviations chapter.

4. DISCUSSION

Neutrophils have been shown to be the major culprit of the characteristic tissue destruction and subsequent dermal-epidermal separation in pemphigoid diseases, particularly EBA (112,126,150). In EBA, pathogenic autoantibodies pertaining mostly to the IgG class bind to hCOL7 at the basement membrane and form IC that recruit complement and immune effector cells by FcγR binding (151). These cells exert in turn their detrimental effects by characteristic FcγR-activated downstream signaling pathways (127). In relation to IgG subclass, IgG1 and IgG3 are mainly involved in the pathogenesis of EBA, while the role of IgG2 remains largely unknown (92,125). Their pathogenic effects are further modulated by the presence of their attached N-linked glycosylation site, the latter impacting the affinity of IgG antibodies for FcγR as well as the proportion of activatory and inhibitory FcγR on immune effector cells (65,92,152). Furthermore, immune cells recognize differences in glycosylation patterns through specific glycan-binding proteins, such as C-type lectin receptors, siglecs, and galectins (105). These glycoreceptors can modulate interactions by either activating or inhibiting inflammatory responses (99,106). For instance, galectin-1 dampens inflammation by blocking neutrophil recruitment and promoting apoptosis, while galectin-3-mediated ligand clustering activates neutrophils (109,110). As a result, IgG antibodies may trigger pro- or anti-inflammatory responses (96). Given all this, the purpose of this thesis was to determine the impact of differentially glycosylated IgG2-containing IC on the signaling (kinase activity) and effector functions of human neutrophils, i.e., adhesion, activation, toxicity and ROS release.

Spreading and adhesion of neutrophils to the surface of the IC bound to the skin basement membrane represents the initial step in the sequence of neutrophil-mediated tissue injury in EBA (112,127,151). It was previously demonstrated that blocking CD18, the subunit of β2-integrins, with specific antibodies or through genetic deficiency, abrogates the IC-induced neutrophil adhesion (139). This, in turn, significantly reduces characteristic tissue pathology in experimental models of EBA without affecting the subsequent release of ROS, thus underlining the crucial role of adhesion as a prerequisite for autoantibody-induced tissue destruction (139). In this work, neutrophils stimulated with EndoS IgG2 glycoforms showed significantly less adhesion by real-time impedance measurement as well as ROS

release when compared to all other antibodies. Indeed, the hydrolysis of the Fc glycan core by means of systemic administration of EndoS abrogated disease development and progression in mouse models of EBA (153). Moreover, it was linked to reduced lesional expression of activating FcγR and increased FcγRIIB. In line, Yu *et al.* showed that EndoS treatment in murine EBA impacts IC-induced neutrophil activation by altering the binding of IC to FcγR (154). Correspondingly, EndoS led to a decrease in activation of neutrophils as assessed by the ratio of $CD18^{high}$ (1x and 2x concentrations) and $CD62L^{low}$ cells by flow cytometry. However, these data did not reach statistical significance. Even though it was previously demonstrated that CD18 is crucial for neutrophil adhesion in experimental EBA, the contrasting results observed between adhesion and CD18 expression in relation to the differentially glycosylated IgG2 antibodies might be clarified by the presence of other relevant factors (139,155). For instance, neutrophil adhesion and migration is mainly mediated by Mac-1 integrin, the latter being composed of CD18 (β subunit) and CD11b (α subunit) (156). Traditionally, CD11b is known for its pro-inflammatory role in autoimmune diseases, yet in EBA, it appears to protect mice from severe disease progression (131,157,158). CD11b deficiency doesn't prevent disease development but reduces exacerbation, especially in the late phase, highlighting the initial role of other factors like pathogenic antibodies and complement. Therefore, further studies should assess also the other components of the CD18 integrins in a flow cytometry analysis.

Furthermore, sialylated IgG2 glycoforms showed reduced adhesion by impedance measurement compared to galactosylated and deglycosylated variants. Despite the activation and ROS release showed a decreasing tendency or at least comparable to reference IgG2 IC, the results were not significant. Indeed, sialylation is associated with anti-inflammatory responses, whereas autoimmune diseases are characterized by low levels of sialylated antibodies (96,101,102). Moreover, effective treatment restores the sialylation degree of antibodies in autoimmune diseases (98,103). In line, the therapeutic effect of intravenous immunoglobulin was shown to mainly rely on the sialylated antibody subfraction (101,104). On the other hand, the anti-inflammatory effect of sialylation may also be mediated through the engagement of glycoreceptors such as C-type lectins. Specifically, these include ICAM-3 Grabbing Non-Integrin-Related 1 in mice and Dendritic Cell-Specific ICAM-3 Grabbing Non-Integrin in humans, as well as the dendritic cell immunoreceptor

(159,160). However, the existence of a direct interaction between these entities remains under debate. Therefore, sialylation as an indicator of the inflammatory status may predict autoimmune disease development, while its immunosuppressive effect may be explained through FcγR-dependent or independent mechanisms (101,152).

Correspondingly, highly galactosylated antibodies in the form of IC exert anti-inflammatory responses by promoting the association between FcγRIIB and dectin-1 resulting in the phosphorylation of SHIP and Syk, respectively (99). As a result, ERK1/2 phosphorylation is blocked with subsequent abrogation of C5a-mediated neutrophil activation in both *in vitro* and *in vivo* in murine EBA (99). In current work, galactosylated antibodies showed similar levels to deglycosylated antibodies in matter of adhesion, while for the rest of effector functions, they were comparable to reference IgG2 and sialylated antibodies, respectively. Of note, the observed tendencies were not statistically significant. This was also observed when assessing the impact of different IgG1-containing glycoforms in human neutrophils, thus highlighting the possibility of different mechanisms and effects between human and mice regarding glycosylation and IgG subclass (161). On the other hand, galactosylated IgG antibodies strongly promote complement activation via complement component C1q, and galactosylated murine IgG3 autoantibodies, the correspondent of human IgG2 antibodies, were associated with the detrimental cryoglobulin activity in murine lupus-like model (162,163). Still, levels of agalactosylated antibodies were found to be increased in various autoimmune diseases, but again the underlining mechanisms via alternative and lectin complement activation pathways are controversial (96,97,99,107). While the anti-inflammatory effects of sialylated IgG antibodies are well-established, the roles and mechanisms of action of other IgG glycoforms, such as galactosylated and agalactosylated antibodies, are still debated. Therefore, future studies are needed to clarify the *in vivo* effects of these differentially glycosylated IgG antibodies, investigating potential concomitant factors that could drive disease development despite the presence of agalactosylated antibodies. This is crucial for developing targeted therapies and harnessing antibody glycoengineering for personalized treatments in autoimmune diseases.

In line with the presence of agalactosylated antibodies in rheumatic diseases, neutrophils stimulated with degalactosylated IgG2-containing glycoforms showed

significant differences in matters of adhesion and ROS releases when compared to putative anti-inflammatory glycosylated antibodies such as EndoS and sialylated. The pro-inflammatory effect may be due to their higher affinity towards activating FcγR (108). Another potential mechanism is through MBL and subsequent lectin complement pathway activation (107,164). Although initially thought not to fix complement, IgG2 could activate complement at high epitope densities by increasing affinity for C1q, which may occur with degalactosylated IgG2-containing IC (134).

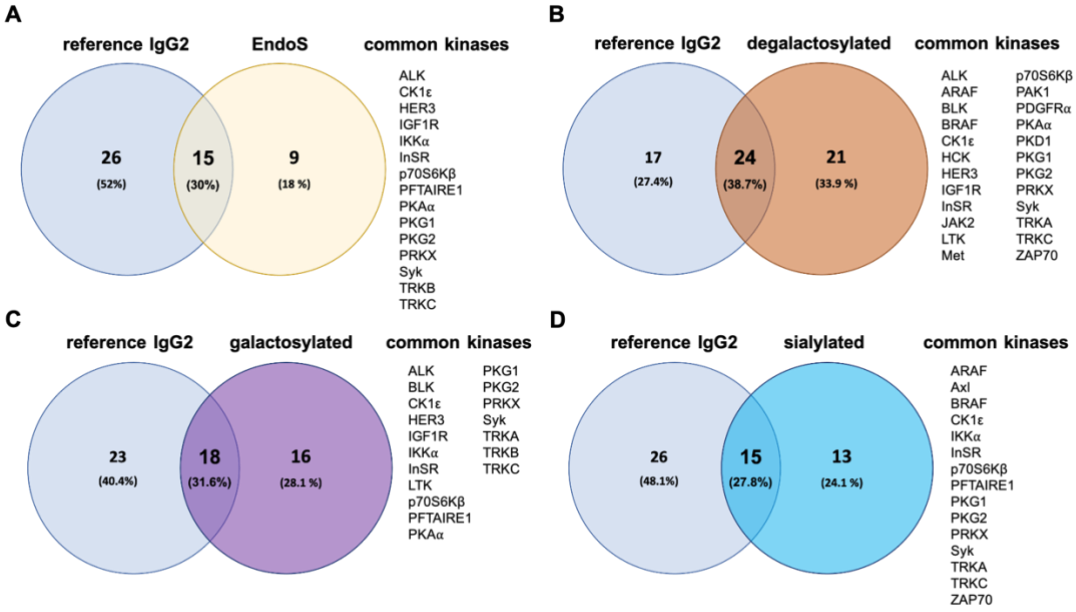

Figure 26. Venn diagrams illustrating upregulated kinases based on the observed differential glycosylation patterns, referencing Figures 24 and 25. The reference IgG2 IC is positioned on the left side, while the corresponding glycoforms are presented on the right side: (**A**) EndoS Ig2 IC, (**B**) degalactosylated Ig2 IC, (**C**) galactosylated Ig2 IC, and (**D**) sialylated Ig2 IC. Absolute numbers and relative values are indicated in the respective segments of the graphs. The diagrams were generated using Venny 2.1. IC, immune complexes; IgG2, immunoglobulin γ 2. For the rest of the abbreviations, please consult the Abbreviations chapter.

Analogously, the loss of sialic acid residues, which are characterized by reduced FcγR binding, and thus immunosuppressive responses, may further explain this effect (101). In line with the results of this work, higher levels of agalactosylated IgG antibodies were linked to an increased ROS release from neutrophils in murine EBA (165). However, complete deglycosylation of antibodies abrogates their binding to FcγR, and thus yield anti-inflammatory responses (95,153).

Taking into account that human IgG2 is traditionally known to barely interact with FcγR, the above-mentioned results underline that differentially glycosylated IgG2-containing IC do in fact impact the effector functions of human neutrophils, mainly the adhesion and ROS release, although to a lesser extent than IgG1-based glycoforms (65,67,161,166).

To better understand the underlying mechanisms behind IgG2-based IC-induced signal transduction in neutrophils, a multiplex kinase activity profiling of the different glycoforms was carried out by PamGene. Indeed, numerous kinases were involved and showed an altered activation status across the differentially glycosylated IgG2-containing IC.

In comparison to reference IgG1 as the major subclass involved in the pathogenesis of EBA, IgG2-based IC stimulation of neutrophils did not induce kinases of the pathogenetically relevant PI3K/AKT/mTOR, MAPK and cyclin-dependent kinases (CDKs) pathways (161,166).

In IgG1-based IC-stimulation, PMNs elicited the activation of JAK1 and JAK2 kinases, which are central components of the JAK/ signal transducer and activator of transcription (STAT) pathway (161,166). The latter plays a central role in cytokine signaling, and thus, is involved in many immune mediated disorders, including autoimmune blistering diseases (167,168). JAK inhibitors, notably Tofacitinib, a pan-JAK inhibitor, have already been approved for treating various rheumatological and dermatological conditions (169). Furthermore, off-label use of different JAK inhibitors has demonstrated promising outcomes in autoimmune blistering dermatoses (170). Accordingly, Fan *et al.* reported the successful deployment of tofacitinib in recurrent EBA, with notable disease improvement within a month and no adverse events or relapses (171). They also noted a reduction in circulating neutrophil counts, further stressing the pathogenetic role of the JAK signaling pathway in neutrophils in EBA.

Conversely, JAK kinases were not upregulated in IgG2-based IC-stimulation of neutrophils. This may indicate a lesser pathogenetic role of IgG2 in the pathogenesis of EBA or involvement of alternative mechanisms not mediated through the JAK/STAT signaling pathway.

Other kinases involved in autoantibody-induced neutrophil activation and tissue damage in murine models of bullous pemphigoid and EBA, including ERK1/2, p38 MAPK, and AKT, were not found to be upregulated in reference IgG2 IC. Inhibition

of these kinases, either directly through specific inhibitors or indirectly through methylprednisolone treatment, prevented IC-induced neutrophil activation *in vitro* and IC-induced dermal-epidermal separation in an *ex vivo* model (172).

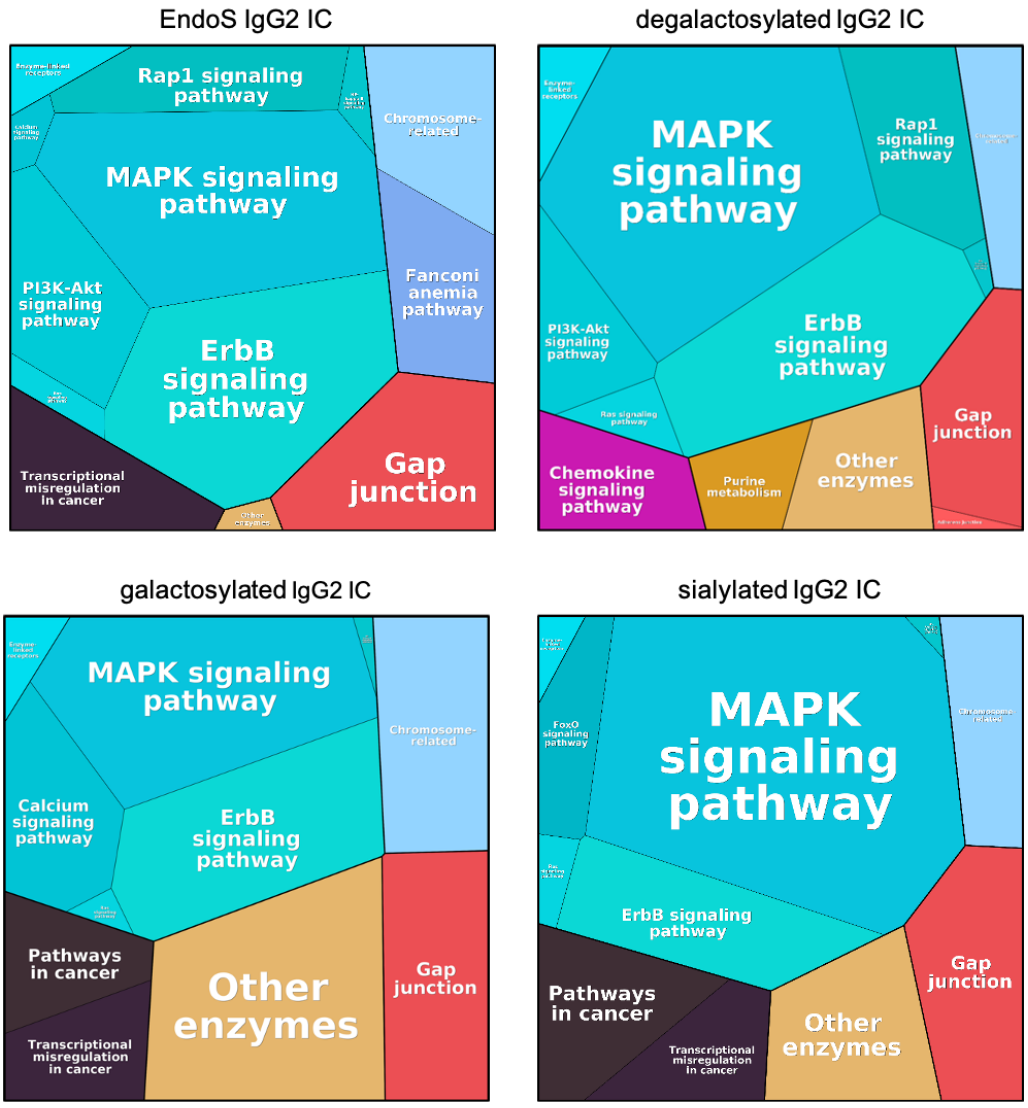

Figure 27. Proteomaps illustrating the kinase signaling pathways involved in differentially glycosylated IgG2-containing IC. Each tile represents a specific kinase signaling pathway, with different colors indicating various pathways; the colors were chosen according to the website's standards. Tile sizes represent the degree of involvement of kinase signaling pathways in the corresponding glycoform, i.e., EndoS, degalactosylated, galactosylated, and sialylated, at 10 µg/mL antigen and 2 µg/mL antibody concentration. These proteomaps refer to detected kinases at the 8-minute time point. Proteomaps for the 2-minute and 15-minute time points are shown in the Appendix. These proteomaps were generated using mean kinase statistics compared to unstimulated cells (149). See Figure 25. IC, immune complexes; IgG2, immunoglobulin γ 2. For other abbreviations, please refer to the Abbreviations chapter.

When comparing the upregulated kinases outlined in Figure 26 between reference IgG2 and each distinct glycoform, in comparison to unstimulated cells, many kinases were common across each comparison group. This finding underscores the particular relevance of their altered activation status. Furthermore, considering the glycoform composition of reference IgG2, about 65% are degalactosylated, explaining the highest number of common kinases. This is followed by approximately 30% galactosylated forms, which share the second highest number of kinases. In addition, the proinflammatory degalactosylated glycoform was associated with a higher number of activated kinases, whereas the anti-inflammatory, such as EndoS and sialylated showed less upregulated kinases.

Moreover, the depiction through Proteomaps of the specific pathways these kinases pertain to showed differences between the differentially glycosylated IgG2-based variants (Figure 27). While all glycoforms involved the ErbB/MAPK signaling pathway, sialylated IgG2 IC showed the highest proportion of involvement in the MAPK signaling pathway, yet with no involvement of the Rap pathway. In contrast, PI3K involvement was exclusively seen in EndoS and degalactosylated IgG2 IC. The inhibition of the latter showed promising therapeutic benefits *in vitro* as well as in mouse models of EBA (112,166).

Interestingly, in our study, all glycoforms, including the reference IgG2, led to an upregulation of CK1ε, but to a higher extent with the anti-inflammatory EndoS and galactosylated forms. CK1 has been identified as a crucial regulator that stabilizes β-catenin, subsequently promoting Wnt signaling (173). The Wnt/β-catenin signaling pathway plays an important role in regulating skin morphogenesis and homeostasis (174). Additionally, it was demonstrated that Wnt/β-catenin signaling stabilizes plectin and collagen XVII in hemidesmosomes, suggesting that activation of this pathway could serve as a potential therapy option in EBA or bullous pemphigoid by enhancing the stability of hemidesmosome components (175). In view of our findings, this indicates a potential anti-inflammatory function of IgG2 through the Wnt pathway. Nevertheless, additional research is necessary to investigate this therapeutic potential in greater depth.

Consistently, IgG2-based IC-stimulation of neutrophils did not induce the upregulation of Syk kinases. It was previously demonstrated that Syk-deficient PMNs protected against clinical disease in an EBA mouse model (176).

Nevertheless, the present study has some limitations to be acknowledged. First, human PMNs are subject to various factors including genetic predisposition, sex, age, and external factors such as temperature and physical activity. Indeed, in our study, all assessed effector functions of IC-stimulated PMNs displayed donor dependency. Moreover, it was previously demonstrated that the role of PMNs in the development of murine EBA is also genetically controlled (112,177). In addition, an age-dependent decline in PMNs activation by shedding CD62L was shown (23,53). Also, temperature changes can potentially elicit their activation, and physical activity could influence the cell state (178). Noteworthy as a potential limitation is that all centrifugations were performed at 4°C, except for the multiplex kinase activity profiling, which was done at 23 °C. Secondly, the *in vitro* experiments were conducted using five biological replicates. Due to the variability in donor-dependent reactivity observed in PMNs derived from blood sera, the obtained results require further validation in larger cohorts. Nonetheless, these findings are significant as they establish the foundation for subsequent, more comprehensive research. Another potential limitation pertains to the use of healthy human neutrophils, which may not be entirely applicable to EBA, as the latter PMNs are probably characterized by distinct signaling pathways and differently influenced by glycosylation patterns. Lastly, the identification of involved kinases relies on the analysis of phosphorylation patterns of substrate peptides rather than direct assessment, thus introducing the possibility for errors. Moreover, the detection of kinases is dependent on the accuracy of the BCA assay in determining overall protein concentration. In conclusion, it is imperative that further extensive *in vitro* and *in vivo* studies be conducted to corroborate the current findings.

It is noteworthy that the differentially glycosylated IgG2-based glycoforms did not exert any cytotoxic effects on stimulated neutrophils, further underlining their potential therapeutic applicability.

In conclusion, the findings of this thesis emphasize the pivotal role of IgG glycosylation in neutrophil signaling and function by defining the impact of five different IgG2-based glycoforms on the kinase activity and various effector functions of healthy human neutrophils. On one hand, antibody glycosylation engineering could enable the generation of anti-inflammatory glycoforms, which holds promise for treating various autoantibody-mediated diseases like EBA. As demonstrated, these anti-inflammatory glycoforms effectively inhibit crucial effector functions of

PMNs, including adhesion and ROS release. Conversely, the signaling pathways identified in this study suggest a potential protective role of IgG2-based IC stimulation in neutrophil-mediated inflammation and tissue damage. Ultimately, this research significantly enhances our understanding of the interplay between antibody glycosylation and neutrophil function across physiological and disease states. Specifically, the IgG2 subclass appears to play a potential protective role, while modulation of different sugar moieties leads to either activation or attenuation of PMNs functions.

5. SUMMARY

Epidermolysis bullosa acquisita (EBA) is a rare autoimmune blistering disease with significant therapeutic challenges due to its lack of steroid responsiveness and the absence of randomized clinical trials. This underscores the urgent need for both curative and targeted therapies. EBA is characterized by pathogenic autoantibodies targeting type VII collagen (COL7) in the skin's basement membrane, leading to complement activation, cytokine release, and leukocyte recruitment. Mainly, neutrophils activated by immune complexes (IC) via Fc gamma receptors release reactive oxygen species (ROS) and proteases, causing characteristic subepidermal blisters. While IgG1 and IgG3 antibodies are primarily involved in EBA, the role of IgG2 and its glycosylation in disease modulation is less understood.

In this body of work, experiments on differentially glycosylated anti-COL7 IgG2 IC demonstrated that EndoS-treated IgG2 IC significantly reduced neutrophil adhesion and ROS release. Correspondingly, pro-inflammatory degalactosylated IgG2 IC exhibited higher adhesion and ROS release compared to anti-inflammatory glycoforms. PamGene analysis revealed that, unlike IgG1, IgG2-based IC did not activate the pathogenic phosphoinositide 3-kinase (PI3K)/AK strain transforming (AKT)/mammalian target of rapamycin (mTOR) or the cyclin-dependent kinase (CDK) pathways. Pro-inflammatory degalactosylated glycoforms exhibited higher kinase activation, whereas anti-inflammatory forms showed fewer upregulated kinases. All IgG2-based glycoforms upregulated Casein kinase 1 epsilon, particularly EndoS and galactosylated forms, suggesting a potential anti-inflammatory role, possibly through Wnt signaling. IgG2 IC also did not upregulate Spleen tyrosine kinase (Syk), aligning with findings that Syk-deficient neutrophils protected against disease in murine EBA models.

In conclusion, these glycoforms effectively inhibited key neutrophil functions. The signaling pathways identified suggest a potential protective role of IgG2-based IC stimulation in neutrophil-mediated inflammation and tissue damage, presenting glycoengineering as a potential therapeutic future option in EBA.

6. KURZE ZUSAMMENFASSUNG

Epidermolysis bullosa acquisita (EBA) ist eine seltene blasenbildende Autoimmundermatose mit bedeutenden therapeutischen Herausforderungen aufgrund ihrer mangelnden Steroidansprechbarkeit und dem Fehlen randomisierter klinischer Studien. Dies unterstreicht das dringende Bedürfnis nach sowohl kurativen als auch zielgerichteten Therapien. EBA wird durch pathogene Autoantikörper charakterisiert, die Typ-VII-Kollagen (COL7) in der Basalmembran der Haut angreifen, was zu einer Aktivierung des Komplementsystems, Freisetzung von Zytokinen und Rekrutierung von Leukozyten führt. Hauptsächlich setzen Neutrophile, die durch Immunkomplexe aktiviert werden, reaktive Sauerstoffspezies (ROS) und Proteasen frei, die zu Blasenbildung führen. Die Rolle von IgG2 und seiner Glykosylierung bei EBA ist noch nicht ausreichend verstanden.

In dieser Arbeit zeigten Experimente an unterschiedlich glykosylierten anti-COL7 IgG2-IKs, dass EndoS-behandelte IgG2-IKs die Neutrophilenadhäsion und ROS-Freisetzung signifikant reduzierten. Entsprechend wiesen proinflammatorische degalaktosylierte IgG2-IKs eine höhere Adhäsion und ROS-Freisetzung im Vergleich zu antiinflammatorischen Glykoformen auf. PamGene-Analysen zeigten, dass im Gegensatz zu IgG1, IgG2-basierte IKs die pathogenen Phosphoinositid 3-Kinase (PI3K)/AK-Strain-Transforming (AKT)/mammaliane Ziel von Rapamycin (mTOR)- oder die cyclin-abhängigen Kinase (CDK)-Signalwege nicht aktivierten. Proinflammatorische degalaktosylierte Glykoformen wiesen eine höhere Kinaseaktivierung auf, während antiinflammatorische Formen weniger hochregulierte Kinasen zeigten. Alle IgG2-basierten Glykoformen regulierten die Casein-Kinase 1 epsilon hoch, insbesondere EndoS- und galaktosylierte Formen, was auf eine potenzielle antiinflammatorische Rolle, möglicherweise über das Wnt-Signalwegsystem, hinweist. IgG2-IKs regulierten auch nicht die Spleen-Tyrosinkinase (Syk) hoch, was mit Befunden übereinstimmt, dass Syk-defiziente Neutrophile in murinen EBA-Modellen vor der Krankheit schützen.

Zusammenfassend hemmten diese Glykoformen effektiv wichtige neutrophile Funktionen. Die identifizierten Signalwege deuten auf eine potenziell protektive Rolle der IgG2-IK-Stimulation bei neutrophilen-vermittelten Entzündungen und Gewebeschäden hin und machen Glykoengineering zu einer vielversprechenden Option für die EBA-Therapie.

7. AUSFÜHRLICHE ZUSAMMENFASSUNG

Einleitung

Epidermolysis bullosa acquisita (EBA) ist eine seltene Autoimmunblasenkrankheit mit vielfältigen klinischen Erscheinungsbildern, die in zwei Haupttypen unterteilt wird: mechano-bullös und nicht-mechano-bullös. Der mechano-bullöse Typ zeigt traumatisch bedingte Blasen und Erosionen an den Streckseiten, die Narben und Milien verursachen. Der nicht-mechano-bullöse Typ imitiert verschiedene andere Autoimmunblasenkrankheiten und verursacht eine erhebliche Krankheitslast. Da EBA nicht auf Steroidbehandlungen anspricht und zurzeit keine randomisierten klinischen Studien verfügbar sind, gestaltet sich die Behandlung der Erkrankung als herausfordernd. Daher besteht ein dringender Bedarf an maßgeschneiderten therapeutischen Ansätzen, um diesem ungedeckten medizinischen Bedarf gerecht zu werden.

Bei EBA richten zirkulierende pathogene Autoantikörper ihre Angriffe gegen Typ-VII-Kollagen (COL7) in der Basalmembran der Haut, was eine Aktivierung des Komplementsystems, die Freisetzung proinflammatorischer Zytokine und die Rekrutierung von Leukozyten auslöst. Neutrophile, die hauptsächlich über fragmentkristalline (Fc)-Gamma-Rezeptoren (FcγR) an hautgebundene Immunkomplexe (IK) binden, initiieren Signalwege, die zur Freisetzung reaktiver Sauerstoffspezies (ROS) und Proteasen führen und somit zur charakteristischen subepidermalen Blasenbildung beitragen. Während IgG1- und IgG3-Antikörper EBA hauptsächlich vorantreiben, ist die Rolle von IgG2 noch weitgehend unverstanden. Darüber hinaus beeinflusst die Antikörper-Glykosylierung kritisch ihre pro- und antiinflammatorischen Funktionen.

Vor diesem Hintergrund hatte diese Doktorarbeit zum Ziel, die Auswirkungen unterschiedlich glykosylierter anti-humaner COL7-IgG2-basierter IKs auf gesunde menschliche Neutrophile zu untersuchen. Fünf verschiedene IgG2-basierte Glykoformen - darunter EndoS, degalaktosyliert (G0), galaktosyliert (G1/G2) und sialyliert (G1S1/G2S1/G2S2) - wurden mit einem Referenz-IgG2 verglichen. Das Ziel dieser experimentellen Arbeit war es, die komplexen Pathomechanismen von EBA zu entschlüsseln, indem der durch IgG2 induzierte Signalweg in Neutrophilen untersucht wird, um potenzielle therapeutische Ziele zu identifizieren oder neue glykobasierte Behandlungsstrategien für EBA zu entwickeln.

Material und Methoden

Zur Beurteilung der Effekte von unterschiedlich glykosylierten IgG2-basierten IKs wurden zunächst neutrophile Granulozyten aus Vollblut gesunder Spender mittels des PolymorphPrep™-Gradienten gemäß den Anweisungen des Herstellers isoliert. Die Reinheit der neutrophilen Granulozyten wurde nach jeder Isolierung mittels Durchflusszytometrie (Miltenyi MacsQuant10® Analyzer) unter Verwendung fluoreszierender Färbung mit anti-CD14- und anti-CD16-Antikörpern bestätigt. Nur Isolate, die mindestens 85% polymorphonukleare neutrophile Granulozyten enthielten, wurden in weiteren Experimenten einbezogen.

Anschließend wurden humane neutrophile Granulozyten den immobilisierten IKs ausgesetzt, die verschiedene IgG2-basierte Glykoformen enthielten, um verschiedene Effektorfunktionen zu bewerten, einschließlich: (i) Adhäsion, quantifiziert durch Messung der elektrischen Impedanz nach Bindung an eine 96-Well-Gold beschichtete Platte unter Verwendung des xCELLigence RTCA Systems; (ii) Aktivierung der durch IK stimulierten neutrophilen Granulozyten, beurteilt mittels Durchflusszytometrie (Miltenyi MacsQuant10® Analyzer) unter Verwendung der Oberflächenmarker CD18 (Integrin β-Kette-2) und CD62L (L-Selektin); (iii) Überleben der durch IK stimulierten neutrophilen Granulozyten, bestimmt mittels Durchflusszytometrie (Miltenyi MacsQuant10® Analyzer) unter Verwendung der Annexin V- und Zombie NIR™-Färbungen als Marker für Apoptose bzw. Nekrose; (iv) Messung der Freisetzung von ROS aus unterschiedlich glykosylierten durch IK stimulierten neutrophilen Granulozyten unter Verwendung einer Chemilumineszenzmethode und des GloMax® Discover-Geräts; (v) Multiplex-Kinaseaktivitätsprofilierung mittels PamGene®-Technologie zur direkten Bestimmung der Kinaseaktivität in Zelllysat mit Hilfe von PamChips®. Zur genauen Bestimmung der Proteinkonzentration in den Zelllysaten wurde das Pierce™ BCA Protein Assay Kit gemäß den Anweisungen des Herstellers verwendet.

Die aus den Experimenten gewonnenen Daten wurden auf die Referenz-IgG2-Konzentration von 10 µg/mL Antigen und 2 µg/mL Antikörper normalisiert, wobei jede der drei Konzentrationen der unterschiedlich glykosylierten IKs (1, 2 oder 4 µg/mL) auf diesen Standard normalisiert wurde, der auf 100% festgelegt war. Die statistische Analyse erfolgte mit GraphPad Prism (Version 9.3.1) und präsentierte die Ergebnisse als Balkendiagramme mit Mittelwert ± Standardabweichung und individuellen Werten als Punkten. Die gewöhnliche einwegige Varianzanalyse

(ANOVA) mit Tukey-Post-Test verglich jede Konzentrationsgruppe der Referenz-IgG2-IKs mit allen entsprechenden Glykoformen und bewertete den Einfluss jeder Glykoform auf verschiedene Funktionen der durch IK stimulierten neutrophilen Granulozyten. Eine statistische Signifikanz wurde definiert als p-Wert < 0,05.

Ergebnisse

Die Ergebnisse dieser Doktorarbeit zeigten, dass neutrophile Granulozyten, die mit EndoS-basierten IgG2-Glykoformen stimuliert wurden, im Vergleich zu allen anderen Antikörpern eine signifikant verringerte Adhäsion aufwiesen, wie durch Impedanzmessungen in Echtzeit gemessen wurde, sowie eine verminderte ROS-Freisetzung. Ebenso führte EndoS zu einer Abnahme der Aktivierung der Neutrophilen, wie durch das Verhältnis von CD18high/CD62Llow-Zellen gemessen mittels Durchflusszytometrie. Diese Beobachtungen erreichten jedoch keine statistische Signifikanz. Darüber hinaus zeigten sialylierte IgG2-Glykoformen im Vergleich zu galaktosylierten und deglykosylierten Varianten eine verringerte Adhäsion, obwohl die Unterschiede in der Aktivierung und der ROS-Freisetzung, während sie einen abnehmenden Trend aufwiesen, nicht statistisch signifikant waren im Vergleich zu den Referenz-IgG2-IK. Galaktosylierte Antikörper wiesen Adhäsionsniveaus auf, die denen deglykosylierter Antikörper ähnlich waren. Beachtenswert ist, dass neutrophile Granulozyten, die mit degalaktosylierten IgG2-haltigen Glykoformen stimuliert wurden, signifikante Unterschiede in der Adhäsion und der ROS-Freisetzung im Vergleich zu vermeintlich entzündungshemmenden glykosylierten Antikörpern wie EndoS und sialylierten IgG2-haltigen IKs zeigten.

Pamgene-Analysen zeigten die Beteiligung zahlreicher Kinasen, wobei ein veränderter Aktivierungsstatus über die unterschiedlich glykosylierten IgG2-haltigen IK beobachtet wurde. Im Vergleich zu Referenz-IgG1, das als Hauptunterklasse in die Pathogenese von EBA involviert ist, führte die Stimulation von Neutrophilen mit IgG2-haltigen IK nicht zur Induktion von Kinasen aus pathogenetisch relevanten Signalwegen wie Phosphoinositid 3-Kinase (PI3K)/AK-Strain-Transforming (AKT)/mammalianes Ziel von Rapamycin (mTOR) oder cyclin-abhängige Kinasen (CDK). Beim Vergleich der hochregulierten Kinasen zwischen Referenz-IgG2 und jeder einzelnen glykosylierten Form wurden viele Kinasen festgestellt, die in allen Vergleichsgruppen gemeinsam aktiviert waren. Zusätzlich wurde die proinflammatorische deglykosylierte Glykoform mit einer höheren Anzahl von

aktivierten Kinasen assoziiert, während die entzündungshemmenden Glykoformen wie EndoS und sialyliert weniger hochregulierte Kinasen zeigten.

Diskussion

Diese Dissertation hatte zum Ziel, die Auswirkungen verschieden glykosylierter IgG2-haltiger IK auf gesunde menschliche Neutrophile zu bewerten und ihre Wirkung auf Effektorfunktionen und Kinase-Signalwege zu untersuchen. Neutrophile, die mit den entzündungshemmenden EndoS-basierten IgG2-haltigen IKs stimuliert wurden, zeigten im Vergleich zu anderen Antikörpern eine signifikant verringerte Adhäsion und ROS-Freisetzung. Sialylierte IgG2-Glykoformen wiesen ebenfalls eine verringerte Adhäsion im Vergleich zu proinflammatorischen Varianten auf. Im Gegensatz dazu zeigten Neutrophile, die mit degalaktosylierten IgG2-haltigen IK stimuliert wurden, signifikante Unterschiede in Adhäsion und ROS-Freisetzung im Vergleich zu potenziell entzündungshemmenden Varianten. Multiplex-Kinaseaktivitätsprofilierung ergab, dass proinflammatorische degalaktosylierte Glykoformen mit einer höheren Kinaseaktivierung assoziiert waren, während entzündungshemmende Formen wie EndoS und sialylierte weniger Hochregulation zeigten. Proteomaps zeigten Unterschiede in den Signalwegen zwischen glycosylierten IgG2-Varianten. Alle waren am ErbB/MAPK-Signalweg beteiligt. Sialylierte IgG2-IK wiesen die höchste Beteiligung am MAPK-Signalweg auf, ohne Beteiligung am Rap-Signalweg, während PI3K ausschließlich bei EndoS und degalaktosylierten IgG2-IK vorkam. Interessanterweise führten alle Glykoformen, einschließlich des Referenz-IgG2, zu einer Hochregulation von Casein-Kinase 1 (CK1) epsilon. CK1 wurde als Regulator identifiziert, der die Wnt-Signalgebung fördert und somit eine entzündungshemmende Rolle von IgG2 andeutet. Entsprechend führte die Stimulation von Neutrophilen mit IgG2-haltigen IKs nicht zu einer Hochregulation von Spleen-Tyrosinkinase, die zuvor als schützend gegen klinische Erkrankungen in einem EBA-Mausmodell gezeigt wurden. Zusammenfassend inhibieren unterschiedlich glykosylierte IgG2-Glykoformen effektiv neutrophile Funktionen und weisen auf eine schützende Rolle bei neutrophilen-vermittelten Entzündungen hin. Diese Forschung betont die Bedeutung der Antikörperglykosylierung für die Immunantwort und das therapeutische Potenzial von IgG2. Sie bietet Einblicke in die Mechanismen der Neutrophilenregulation und stellt mögliche therapeutische Strategien zur gezielten Beeinflussung der Glykosylierung vor.

8 REFERENCES

1. Bieber K, Hundt JE, Yu X, Ehlers M, Petersen F, Karsten CM, Köhl J, Kridin K, Kalies K, Kasprick A, Goletz S, Humrich JY, Manz RA, Künstner A, Hammers CM, Akbarzadeh R, Busch H, Sadik CD, Lange T, Grasshoff H, Ludwig RJ (2023). Autoimmune pre-disease. *Autoimmun Rev*. 22(2): 103236.
2. Eaton WW, Rose NR, Kalaydjian A, Pedersen MG, Mortensen PB (2007). Epidemiology of autoimmune diseases in Denmark. *J Autoimmun*. 29(1): 1–9.
3. Wang L, Wang FS, Gershwin ME (2015). Human autoimmune diseases: a comprehensive update. *J Intern Med*. 278(4): 369–95.
4. Miller FW (2022). The increasing prevalence of autoimmunity and autoimmune diseases: an urgent call to action for improved understanding, diagnosis, treatment, and prevention. *Curr Opin Immunol*. 80: 102266.
5. Mayadas TN, Cullere X, Lowell CA (2014). The multifaceted functions of neutrophils. *Annu Rev Pathol*. 9: 181–218.
6. Rosales C (2018). Neutrophil: A Cell with Many Roles in Inflammation or Several Cell Types? *Front Physiol*. 9: 113.
7. Boxer LA (2012). How to approach neutropenia. *Hematology Am Soc Hematol Educ Program*. 2012: 174–82.
8. Silvestre-Roig C, Braster Q, Ortega-Gomez A, Soehnlein O (2020). Neutrophils as regulators of cardiovascular inflammation. *Nat Rev Cardiol*. 17(6): 327–40.
9. Wang X, Qiu L, Li Z, Wang XY, Yi H (2018). Understanding the Multifaceted Role of Neutrophils in Cancer and Autoimmune Diseases. *Front Immunol*. 9: 2456.
10. Hampton HR, Chtanova T (2019). Lymphatic Migration of Immune Cells. *Front Immunol*. 10: 1168.
11. Chen F, Wu W, Millman A, Craft JF, Chen E, Patel N, Boucher JL, Urban JF Jr, Kim CC, Gause WC (2014). Neutrophils prime a long-lived effector macrophage phenotype that mediates accelerated helminth expulsion. *Nat Immunol*. 15(10): 938–46.

12. Vono M, Lin A, Norrby-Teglund A, Koup RA, Liang F, Loré K (2017). Neutrophils acquire the capacity for antigen presentation to memory CD4+ T cells in vitro and ex vivo. *Blood*. 129(14): 1991–2001.
13. Hampton HR, Bailey J, Tomura M, Brink R, Chtanova T (2015). Microbe-dependent lymphatic migration of neutrophils modulates lymphocyte proliferation in lymph nodes. *Nat Commun*. 6: 7139.
14. Beauvillain C, Delneste Y, Scotet M, Peres A, Gascan H, Guermonprez P, Barnaba V, Jeannin P (2007). Neutrophils efficiently cross-prime naive T cells in vivo. *Blood*. 110(8): 2965–73.
15. Tillack K, Breiden P, Martin R, Sospedra M (2012). T lymphocyte priming by neutrophil extracellular traps links innate and adaptive immune responses. *J Immunol*. 188(7): 3150–9.
16. Puga I, Cols M, Barra CM, He B, Cassis L, Gentile M, Comerma L, Chorny A, Shan M, Xu W, Magri G, Knowles DM, Tam W, Chiu A, Bussel JB, Serrano S, Lorente JA, Bellosillo B, Lloreta J, Juanpere N, Alameda F, Baró T, de Heredia CD, Torán N, Català A, Torrebadell M, Fortuny C, Cusí V, Carreras C, Diaz GA, Blander JM, Farber CM, Silvestri G, Cunningham-Rundles C, Calvillo M, Dufour C, Notarangelo LD, Lougaris V, Plebani A, Casanova JL, Ganal SC, Diefenbach A, Aróstegui JI, Juan M, Yagüe J, Mahlaoui N, Donadieu J, Chen K, Cerutti A (2011). B cell-helper neutrophils stimulate the diversification and production of immunoglobulin in the marginal zone of the spleen. *Nat Immunol*. 13(2): 170–80.
17. Costa S, Bevilacqua D, Cassatella MA, Scapini P (2019). Recent advances on the crosstalk between neutrophils and B or T lymphocytes. *Immunology*. 156(1): 23–32.
18. Tecchio C, Cassatella MA (2016). Neutrophil-derived chemokines on the road to immunity. *Semin Immunol*. 28(2): 119–28.
19. Ericson JA, Duffau P, Yasuda K, Ortiz-Lopez A, Rothamel K, Rifkin IR, Monach PA; ImmGen Consortium (2014). Gene expression during the generation and activation of mouse neutrophils: implication of novel functional and regulatory pathways. *PLoS One*. 9(10): e108553.
20. Netea MG, Joosten LA, Latz E, Mills KH, Natoli G, Stunnenberg HG, O'Neill LA, Xavier RJ (2016). Trained immunity: A program of innate immune memory in health and disease. *Science*. 352(6284): aaf1098.

21. Evrard M, Kwok IWH, Chong SZ, Teng KWW, Becht E, Chen J, Sieow JL, Penny HL, Ching GC, Devi S, Adrover JM, Li JLY, Liong KH, Tan L, Poon Z, Foo S, Chua JW, Su IH, Balabanian K, Bachelerie F, Biswas SK, Larbi A, Hwang WYK, Madan V, Koeffler HP, Wong SC, Newell EW, Hidalgo A, Ginhoux F, Ng LG (2018). Developmental Analysis of Bone Marrow Neutrophils Reveals Populations Specialized in Expansion, Trafficking, and Effector Functions. *Immunity*. 48(2): 364-379.e8.
22. Ng LG, Ostuni R, Hidalgo A (2019). Heterogeneity of neutrophils. *Nat Rev Immunol*. 19(4): 255–65.
23. Adrover JM, Nicolás-Ávila JA, Hidalgo A (2016). Aging: A Temporal Dimension for Neutrophils. *Trends Immunol*. 37(5): 334–45.
24. Silvestre-Roig C, Fridlender ZG, Glogauer M, Scapini P (2019). Neutrophil Diversity in Health and Disease. *Trends Immunol*. 40(7): 565–83.
25. Xie X, Shi Q, Wu P, Zhang X, Kambara H, Su J, Yu H, Park SY, Guo R, Ren Q, Zhang S, Xu Y, Silberstein LE, Cheng T, Ma F, Li C, Luo HR (2020). Single-cell transcriptome profiling reveals neutrophil heterogeneity in homeostasis and infection. *Nat Immunol*. 21(9): 1119–33.
26. Navarini AA, Lang KS, Verschoor A, Recher M, Zinkernagel AS, Nizet V, Odermatt B, Hengartner H, Zinkernagel RM (2009). Innate immune-induced depletion of bone marrow neutrophils aggravates systemic bacterial infections. *Proc Natl Acad Sci U S A*. 106(17): 7107–12.
27. Summers C, Rankin SM, Condliffe AM, Singh N, Peters AM, Chilvers ER (2010). Neutrophil kinetics in health and disease. *Trends Immunol*. 31(8): 318–24.
28. von Vietinghoff S, Ley K (2008). Homeostatic regulation of blood neutrophil counts. *J Immunol*. 181(8): 5183–8.
29. Boettcher S, Manz MG (2017). Regulation of Inflammation- and Infection-Driven Hematopoiesis. *Trends Immunol*. 38(5): 345–57.
30. Adrover JM, Del Fresno C, Crainiciuc G, Cuartero MI, Casanova-Acebes M, Weiss LA, Huerga-Encabo H, Silvestre-Roig C, Rossaint J, Cossío I, Lechuga-Vieco AV, García-Prieto J, Gómez-Parrizas M, Quintana JA, Ballesteros I, Martin-Salamanca S, Aroca-Crevillen A, Chong SZ, Evrard M, Balabanian K, López J, Bidzhekov K, Bachelerie F, Abad-Santos F, Muñoz-Calleja C, Zarbock A, Soehnlein O, Weber C, Ng LG, Lopez-Rodriguez C,

Sancho D, Moro MA, Ibáñez B, Hidalgo A (2019). A Neutrophil Timer Coordinates Immune Defense and Vascular Protection. *Immunity*. 50(2): 390-402.e10.

31. Casanova-Acebes M, Pitaval C, Weiss LA, Nombela-Arrieta C, Chèvre R, Gonzalez NA, Kunisaki Y, Zhang D, van Rooijen N, Silberstein LE, Weber C, Nagasawa T, Frenette PS, Hidalgo A (2013). Rhythmic modulation of the hematopoietic niche through neutrophil clearance. *Cell*. 153(5): 1025–35.
32. Moses K, Brandau S (2016). Human neutrophils: Their role in cancer and relation to myeloid-derived suppressor cells. *Semin Immunol*. 28(2): 187–96.
33. Carmona-Rivera C, Kaplan MJ (2013). Low-density granulocytes: a distinct class of neutrophils in systemic autoimmunity. *Semin Immunopathol*. 35(4): 455–63.
34. Görgens A, Radtke S, Möllmann M, Cross M, Dürig J, Horn PA, Giebel B (2013). Revision of the human hematopoietic tree: granulocyte subtypes derive from distinct hematopoietic lineages. *Cell Rep*. 3(5): 1539–52.
35. Borregaard N (2010). Neutrophils, from marrow to microbes. *Immunity*. 33(5): 657–70.
36. Lacy P (2006). Mechanisms of degranulation in neutrophils. *Allergy Asthma Clin Immunol*. 2(3): 98–108.
37. Dancey JT, Deubelbeiss KA, Harker LA, Finch CA (1976). Neutrophil kinetics in man. *J Clin Invest*. 58(3): 705–15.
38. Semerad CL, Liu F, Gregory AD, Stumpf K, Link DC (2002). G-CSF is an essential regulator of neutrophil trafficking from the bone marrow to the blood. *Immunity*. 17(4): 413–23.
39. Demetri GD, Griffin JD (1991). Granulocyte colony-stimulating factor and its receptor. *Blood*. 78(11): 2791–808.
40. Eash KJ, Greenbaum AM, Gopalan PK, Link DC (2010). CXCR2 and CXCR4 antagonistically regulate neutrophil trafficking from murine bone marrow. *J Clin Invest*. 120(7): 2423–31.
41. Martin C, Burdon PCE, Bridger G, Gutierrez-Ramos JC, Williams TJ, Rankin SM (2003). Chemokines acting via CXCR2 and CXCR4 control the release of neutrophils from the bone marrow and their return following senescence. *Immunity*. 19(4): 583–93.

42. Petit I, Szyper-Kravitz M, Nagler A, Lahav M, Peled A, Habler L, Ponomaryov T, Taichman RS, Arenzana-Seisdedos F, Fujii N, Sandbank J, Zipori D, Lapidot T (2002). G-CSF induces stem cell mobilization by decreasing bone marrow SDF-1 and up-regulating CXCR4. *Nat Immunol*. 3(7): 687–94.
43. Kim HK, De La Luz Sierra M, Williams CK, Gulino AV, Tosato G (2006). G-CSF down-regulation of CXCR4 expression identified as a mechanism for mobilization of myeloid cells. *Blood*. 108(3): 812–20.
44. Köhler A, De Filippo K, Hasenberg M, van den Brandt C, Nye E, Hosking MP, Lane TE, Männ L, Ransohoff RM, Hauser AE, Winter O, Schraven B, Geiger H, Hogg N, Gunzer M (2011). G-CSF-mediated thrombopoietin release triggers neutrophil motility and mobilization from bone marrow via induction of Cxcr2 ligands. *Blood*. 117(16): 4349–57.
45. von Vietinghoff S, Ley K (2009). IL-17A controls IL-17F production and maintains blood neutrophil counts in mice. *J Immunol*. 183(2): 865–73.
46. Ley K, Smith E, Stark MA (2006). IL-17A-producing neutrophil-regulatory Tn lymphocytes. *Immunol Res*. 34(3): 229–42.
47. Pelletier M, Maggi L, Micheletti A, Lazzeri E, Tamassia N, Costantini C, Cosmi L, Lunardi C, Annunziato F, Romagnani S, Cassatella MA (2010). Evidence for a cross-talk between human neutrophils and Th17 cells. *Blood*. 115(2): 335–43.
48. Weaver CT, Elson CO, Fouser LA, Kolls JK (2013). The Th17 pathway and inflammatory diseases of the intestines, lungs, and skin. *Annu Rev Pathol*. 8: 477–512.
49. Stark MA, Huo Y, Burcin TL, Morris MA, Olson TS, Ley K (2005). Phagocytosis of apoptotic neutrophils regulates granulopoiesis via IL-23 and IL-17. *Immunity*. 22(3): 285–94.
50. Pillay J, den Braber I, Vrisekoop N, Kwast LM, de Boer RJ, Borghans JAM, Tesselaar K, Koenderman L (2010). In vivo labeling with 2H2O reveals a human neutrophil lifespan of 5.4 days. *Blood*. 116(4): 625–7.
51. Deniset JF, Kubes P (2018). Neutrophil heterogeneity: Bona fide subsets or polarization states? *J Leukoc Biol*. 103(5): 829–38.
52. Casanova-Acebes M, Nicolás-Ávila JA, Li JL, García-Silva S, Balachander A, Rubio-Ponce A, Weiss LA, Adrover JM, Burrows K, A-González N, Ballesteros I, Devi S, Quintana JA, Crainiciuc G, Leiva M, Gunzer M, Weber

C, Nagasawa T, Soehnlein O, Merad M, Mortha A, Ng LG, Peinado H, Hidalgo A (2018). Neutrophils instruct homeostatic and pathological states in naive tissues. *J Exp Med*. 215(11): 2778–95.

53. Martin C, Burdon PCE, Bridger G, Gutierrez-Ramos JC, Williams TJ, Rankin SM (2003). Chemokines acting via CXCR2 and CXCR4 control the release of neutrophils from the bone marrow and their return following senescence. *Immunity*. 19(4): 583–93.
54. Ley K, Laudanna C, Cybulsky MI, Nourshargh S (2007). Getting to the site of inflammation: the leukocyte adhesion cascade updated. *Nat Rev Immunol*. 7(9): 678–89.
55. Mócsai A, Walzog B, Lowell CA (2015). Intracellular signalling during neutrophil recruitment. *Cardiovasc Res*. 107(3): 373–85.
56. Futosi K, Fodor S, Mócsai A (2013). Neutrophil cell surface receptors and their intracellular signal transduction pathways. *Int Immunopharmacol*. 17(3): 638–50.
57. Kolaczkowska E, Kubes P (2013). Neutrophil recruitment and function in health and inflammation. *Nat Rev Immunol*. 13(3): 159–75.
58. Sheshachalam A, Srivastava N, Mitchell T, Lacy P, Eitzen G (2014). Granule protein processing and regulated secretion in neutrophils. *Front Immunol*. 5: 448.
59. Zeng MY, Miralda I, Armstrong CL, Uriarte SM, Bagaitkar J (2019). The roles of NADPH oxidase in modulating neutrophil effector responses. *Mol Oral Microbiol*. 34(2): 27–38.
60. Yipp BG, Petri B, Salina D, Jenne CN, Scott BN V, Zbytnuik LD, Pittman K, Asaduzzaman M, Wu K, Meijndert HC, Malawista SE, de Boisfleury Chevance A, Zhang K, Conly J, Kubes P (2012). Infection-induced NETosis is a dynamic process involving neutrophil multitasking in vivo. *Nat Med*. 18(9): 1386–93.
61. Sollberger G, Tilley DO, Zychlinsky A (2018). Neutrophil Extracellular Traps: The Biology of Chromatin Externalization. *Dev Cell*. 44(5): 542–53.
62. Wigerblad G, Kaplan MJ (2023). Neutrophil extracellular traps in systemic autoimmune and autoinflammatory diseases. *Nat Rev Immunol*. 23(5):274-288.

63. Greenlee-Wacker MC (2016). Clearance of apoptotic neutrophils and resolution of inflammation. *Immunol Rev*. 273(1): 357–70.
64. Pérez-Figueroa E, Álvarez-Carrasco P, Ortega E, Maldonado-Bernal C (2021). Neutrophils: Many Ways to Die. *Front Immunol*. 12: 631821.
65. Nimmerjahn F, Ravetch JV (2008). Fcgamma receptors as regulators of immune responses. *Nat Rev Immunol*. 8(1): 34–47.
66. Daëron M (1997). Fc receptor biology. *Annu Rev Immunol*. 15: 203–34.
67. Bruhns P, Iannascoli B, England P, Mancardi DA, Fernandez N, Jorieux S, Daëron M (2009). Specificity and affinity of human Fcgamma receptors and their polymorphic variants for human IgG subclasses. *Blood*. 113(16): 3716–25.
68. Vidarsson G, Dekkers G, Rispens T (2014). IgG subclasses and allotypes: from structure to effector functions. *Front Immunol*. 5: 520.
69. Wang Y, Jönsson F (2019). Expression, Role, and Regulation of Neutrophil Fcγ Receptors. *Front Immunol*. 10: 1958.
70. Jakus Z, Németh T, Verbeek JS, Mócsai A (2008). Critical but overlapping role of FcgammaRIII and FcgammaRIV in activation of murine neutrophils by immobilized immune complexes. *J Immunol*. 180(1): 618–29.
71. Guyre PM, Campbell AS, Kniffin WD, Fanger MW (1990). Monocytes and polymorphonuclear neutrophils of patients with streptococcal pharyngitis express increased numbers of type I IgG Fc receptors. *J Clin Invest*. 86(6): 1892–6.
72. Repp R, Valerius T, Sendler A, Gramatzki M, Iro H, Kalden JR, Platzer E (1991). Neutrophils express the high affinity receptor for IgG (Fc gamma RI, CD64) after in vivo application of recombinant human granulocyte colony-stimulating factor. *Blood*. 78(4): 885–9.
73. van Rees DJ, Szilagyi K, Kuijpers TW, Matlung HL, van den Berg TK (2016). Immunoreceptors on neutrophils. *Semin Immunol*. 28(2): 94–108.
74. Alemán OR, Mora N, Cortes-Vieyra R, Uribe-Querol E, Rosales C (2016). Transforming Growth Factor-β-Activated Kinase 1 Is Required for Human FcγRIIIb-Induced Neutrophil Extracellular Trap Formation. *Front Immunol*. 7: 277.

75. Alemán OR, Mora N, Cortes-Vieyra R, Uribe-Querol E, Rosales C (2016). Differential Use of Human Neutrophil Fcγ Receptors for Inducing Neutrophil Extracellular Trap Formation. *J Immunol Res*. 2016: 2908034.
76. Reth M (1989). Antigen receptor tail clue. *Nature*. 338(6214): 383–4.
77. Daëron M, Latour S, Malbec O, Espinosa E, Pina P, Pasmans S, Fridman WH (1995). The same tyrosine-based inhibition motif, in the intracytoplasmic domain of Fc gamma RIIB, regulates negatively BCR-, TCR-, and FcR-dependent cell activation. *Immunity*. 3(5): 635–46.
78. Lowell CA (2011). Src-family and Syk kinases in activating and inhibitory pathways in innate immune cells: signaling cross talk. *Cold Spring Harb Perspect Biol*. 3(3):a002352.
79. Hawkins PT, Stephens LR, Suire S, Wilson M (2010). PI3K signaling in neutrophils. *Curr Top Microbiol Immunol*. 346: 183–202.
80. Kim C, Dinauer MC (2001). Rac2 is an essential regulator of neutrophil nicotinamide adenine dinucleotide phosphate oxidase activation in response to specific signaling pathways. *J Immunol*. 166(2): 1223–32.
81. Mócsai A, Walzog B, Lowell CA (2015). Intracellular signalling during neutrophil recruitment. *Cardiovasc Res*. 107(3): 373–85.
82. Ferris CD, Huganir RL, Supattapone S, Snyder SH (1989). Purified inositol 1,4,5-trisphosphate receptor mediates calcium flux in reconstituted lipid vesicles. *Nature*. 342(6245): 87–9.
83. Bertram A, Ley K (2011). Protein kinase C isoforms in neutrophil adhesion and activation. *Arch Immunol Ther Exp (Warsz)*. 59(2): 79–87.
84. Ortiz-Stern A, Rosales C (2005). FcγRIIIB stimulation promotes β1 integrin activation in human neutrophils. *J Leukoc Biol*. 77(5): 787–99.
85. Löfgren R, Serrander L, Forsberg M, Wilsson A, Wasteson A, Stendahl O (1999). CR3, FcgammaRIIA and FcgammaRIIIB induce activation of the respiratory burst in human neutrophils: the role of intracellular Ca(2+), phospholipase D and tyrosine phosphorylation. *Biochim Biophys Acta*. 1452(1): 46–59.
86. Tamir I, Dal Porto JM, Cambier JC (2000). Cytoplasmic protein tyrosine phosphatases SHP-1 and SHP-2: regulators of B cell signal transduction. *Curr Opin Immunol*. 12(3): 307–15.

87. Rohrschneider LR, Fuller JF, Wolf I, Liu Y, Lucas DM (2000). Structure, function, and biology of SHIP proteins. *Genes Dev*. 14(5): 505–20.
88. Mata-Martínez P, Bergón-Gutiérrez M, del Fresno C (2022). Dectin-1 Signaling Update: New Perspectives for Trained Immunity. *Front Immunol*. 13:812148.
89. Papara C, Karsten CM, Ujiie H, Schmidt E, Schmidt-Jiménez LF, Baican A, Freire PC, Izumi K, Bieber K, Peipp M, Verschoor A, Ludwig RJ, Köhl J, Zillikens D, Hammers CM (2022). The relevance of complement in pemphigoid diseases: A critical appraisal. *Front Immunol*. 13: 973702.
90. Jefferis R, Lund J, Mizutani H, Nakagawa H, Kawazoe Y, Arata Y, Takahashi N (1990). A comparative study of the N-linked oligosaccharide structures of human IgG subclass proteins. *Biochem J*. 268(3): 529–37.
91. Stanley P, Schachter H, Taniguchi N (2009). N-Glycans. In: Varki A, Cummings RD, Esko JD, Freeze HH, Stanley P, Bertozzi CR, Hart GW, Etzler ME (Eds.): Essentials of Glycobiology. 2nd ed., Chapter 8, Cold Spring Harbor Laboratory Press, New York.
92. Jennewein MF, Alter G (2017). The Immunoregulatory Roles of Antibody Glycosylation. *Trends Immunol*. 38(5): 358–72.
93. Biermann MH, Griffante G, Podolska MJ, Boeltz S, Stürmer J, Muñoz LE, Bilyy R, Herrmann M (2016). Sweet but dangerous - the role of immunoglobulin G glycosylation in autoimmunity and inflammation. *Lupus*. 25(8): 934–42.
94. Collin M, Olsén A (2001). EndoS, a novel secreted protein from Streptococcus pyogenes with endoglycosidase activity on human IgG. *EMBO J*. 20(12): 3046–55.
95. Albert H, Collin M, Dudziak D, Ravetch JV, Nimmerjahn F (2008). In vivo enzymatic modulation of IgG glycosylation inhibits autoimmune disease in an IgG subclass-dependent manner. *Proc Natl Acad Sci U S A*. 105(39): 15005–9.
96. Seeling M, Brückner C, Nimmerjahn F (2017). Differential antibody glycosylation in autoimmunity: sweet biomarker or modulator of disease activity? *Nat Rev Rheumatol*. 13(10): 621–30.
97. Parekh RB, Roitt IM, Isenberg DA, Dwek RA, Ansell BM, Rademacher TW (1988). Galactosylation of IgG associated oligosaccharides: reduction in

patients with adult and juvenile onset rheumatoid arthritis and relation to disease activity. *Lancet*. 1(8592): 966–9.

98. Gińdzieńska-Sieśkiewicz E, Radziejewska I, Domysławska I, Klimiuk PA, Sulik A, Rojewska J, Gabryel-Porowska H, Sierakowski S (2016). Changes of glycosylation of IgG in rheumatoid arthritis patients treated with methotrexate. *Adv Med Sci*. 61(2): 193–7.
99. Karsten CM, Pandey MK, Figge J, Kilchenstein R, Taylor PR, Rosas M, McDonald JU, Orr SJ, Berger M, Petzold D, Blanchard V, Winkler A, Hess C, Reid DM, Majoul IV, Strait RT, Harris NL, Köhl G, Wex E, Ludwig R, Zillikens D, Nimmerjahn F, Finkelman FD, Brown GD, Ehlers M, Köhl J (2012). Anti-inflammatory activity of IgG1 mediated by Fc galactosylation and association of FcγRIIB and dectin-1. *Nat Med*. 18(9): 1401–6.
100. Shields RL, Lai J, Keck R, O'Connell LY, Hong K, Meng YG, Weikert SHA, Presta LG (2002). Lack of fucose on human IgG1 N-linked oligosaccharide improves binding to human Fcgamma RIII and antibody-dependent cellular toxicity. *J Biol Chem*. 277(30): 26733–40.
101. Kaneko Y, Nimmerjahn F, Ravetch JV (2006). Anti-inflammatory activity of immunoglobulin G resulting from Fc sialylation. *Science*. 313(5787): 670–3.
102. Kemna MJ, Plomp R, van Paassen P, Koeleman CAM, Jansen BC, Damoiseaux JGMC, Cohen Tervaert JW, Wuhrer M (2017). Galactosylation and Sialylation Levels of IgG Predict Relapse in Patients With PR3-ANCA Associated Vasculitis. *EBioMedicine*. 17: 108–18.
103. Ogata S, Shimizu C, Franco A, Touma R, Kanegaye JT, Choudhury BP, Naidu NN, Kanda Y, Hoang LT, Hibberd ML, Tremoulet AH, Varki A, Burns JC (2013). Treatment response in Kawasaki disease is associated with sialylation levels of endogenous but not therapeutic intravenous immunoglobulin G. *PLoS One*. 8(12): e81448.
104. Washburn N, Schwab I, Ortiz D, Bhatnagar N, Lansing JC, Medeiros A, Tyler S, Mekala D, Cochran E, Sarvaiya H, Garofalo K, Meccariello R, Meador JW 3rd, Rutitzky L, Schultes BC, Ling L, Avery W, Nimmerjahn F, Manning AM, Kaundinya GV, Bosques CJ (2015). Controlled tetra-Fc sialylation of IVIg results in a drug candidate with consistent enhanced anti-inflammatory activity. *Proc Natl Acad Sci U S A*. 112(11): E1297-306.

105. Pinho SS, Alves I, Gaifem J, Rabinovich GA (2023). Immune regulatory networks coordinated by glycans and glycan-binding proteins in autoimmunity and infection. *Cell Mol Immunol*. 20(10): 1101–13.
106. Heyl KA, Karsten CM, Slevogt H (2016). Galectin-3 binds highly galactosylated IgG1 and is crucial for the IgG1 complex mediated inhibition of C5aReceptor induced immune responses. *Biochem Biophys Res Commun*. 479(1): 86–90.
107. Malhotra R, Wormald MR, Rudd PM, Fischer PB, Dwek RA, Sim RB (1995). Glycosylation changes of IgG associated with rheumatoid arthritis can activate complement via the mannose-binding protein. *Nat Med*. 1(3): 237–43.
108. Nimmerjahn F, Anthony RM, Ravetch JV (2007). Agalactosylated IgG antibodies depend on cellular Fc receptors for in vivo activity. *Proc Natl Acad Sci U S A*. 104(20): 8433–7.
109. Rabinovich GA, Sotomayor CE, Riera CM, Bianco I, Correa SG (2000). Evidence of a role for galectin-1 in acute inflammation. *Eur J Immunol*. 30(5): 1331–9.
110. Nieminen J, St-Pierre C, Sato S (2005). Galectin-3 interacts with naïve and primed neutrophils, inducing innate immune responses. *J Leukoc Biol*. 78(5): 1127–35.
111. van de Bovenkamp FS, Hafkenscheid L, Rispens T, Rombouts Y (2016). The Emerging Importance of IgG Fab Glycosylation in Immunity. *J Immunol*. 196(4): 1435–41.
112. Koga H, Prost-Squarcioni C, Iwata H, Jonkman MF, Ludwig RJ, Bieber K (2019). Epidermolysis Bullosa Acquisita: The 2019 Update. *Front Med (Lausanne)*. 5: 362.
113. Hübner F, Recke A, Zillikens D, Linder R, Schmidt E (2016). Prevalence and Age Distribution of Pemphigus and Pemphigoid Diseases in Germany. *J Invest Dermatol*. 136(12): 2495–8.
114. Prost-Squarcioni C, Caux F, Schmidt E, Jonkman MF, Vassileva S, Kim SC, Iranzo P, Daneshpazhooh M, Terra J, Bauer J, Fairley J, Hall R, Hertl M, Lehman JS, Marinovic B, Patsatsi A, Zillikens D; International Bullous Diseases Group; Werth V, Woodley DT, Murrell DF (2018). International

Bullous Diseases Group: consensus on diagnostic criteria for epidermolysis bullosa acquisita. *Br J Dermatol*. 179(1): 30–41.

115. Kridin K, Vorobyev A, Papara C, De Luca DA, Bieber K, Ludwig RJ (2023). Risk factors and sequelae of epidermolysis bullosa acquisita: A propensity-matched global study in 1,344 patients. *Front Immunol*. 13:1103533.
116. Gupta R, Woodley DT, Chen M (2012). Epidermolysis bullosa acquisita. *Clin Dermatol*. 30(1): 60–9.
117. Bieber K, Sun S, Ishii N, Kasperkiewicz M, Schmidt E, Hirose M, Westermann J, Yu X, Zillikens D, Ludwig RJ (2010). Animal models for autoimmune bullous dermatoses. *Exp Dermatol*. 19(1): 2–11.
118. Woodley DT, Burgeson RE, Lunstrum G, Bruckner-Tuderman L, Reese MJ, Briggaman RA (1988). Epidermolysis bullosa acquisita antigen is the globular carboxyl terminus of type VII procollagen. *J Clin Invest*. 81(3): 683–7.
119. Goletz S, Zillikens D, Schmidt E (2017). Structural proteins of the dermal-epidermal junction targeted by autoantibodies in pemphigoid diseases. *Exp Dermatol*. 26(12): 1154–62.
120. Bieber K, Ernst AL, Tukaj S, Holtsche MM, Schmidt E, Zillikens D, Ludwig RJ, Kasperkiewicz M (2017). Analysis of serum markers of cellular immune activation in patients with bullous pemphigoid. *Exp Dermatol*. 26(12): 1248–52.
121. Bieber K, Koga H, Nishie W (2017). In vitro and in vivo models to investigate the pathomechanisms and novel treatments for pemphigoid diseases. *Exp Dermatol*. 26(12): 1163–70.
122. Gammon WR, Murrell DF, Jenison MW, Padilla KM, Prisayanh PS, Jones DA, Briggaman RA, Hunt SW 3rd (1993). Autoantibodies to type VII collagen recognize epitopes in a fibronectin-like region of the noncollagenous (NC1) domain. *J Invest Dermatol*. 100(5): 618–22.
123. Vorobyev A, Ujiie H, Recke A, Buijsrogge JJA, Jonkman MF, Pas HH, Iwata H, Hashimoto T, Kim SC, Hoon Kim J, Groves R, Samavedam U, Gupta Y, Schmidt E, Zillikens D, Shimizu H, Ludwig RJ (2015). Autoantibodies to Multiple Epitopes on the Non-Collagenous-1 Domain of Type VII Collagen Induce Blisters. *J Invest Dermatol*. 135(6): 1565–73.
124. Iwata H, Vorobyev A, Koga H, Recke A, Zillikens D, Prost-Squarcioni C, Ishii N, Hashimoto T, Ludwig RJ (2018). Meta-analysis of the clinical and

immunopathological characteristics and treatment outcomes in epidermolysis bullosa acquisita patients. *Orphanet J Rare Dis*. 13(1): 153.

125. Recke A, Sitaru C, Vidarsson G, Evensen M, Chiriac MT, Ludwig RJ, Zillikens D (2010). Pathogenicity of IgG subclass autoantibodies to type VII collagen: Induction of dermal–epidermal separation. *J Autoimmun*. 34(4): 435–44.
126. Sitaru C, Kromminga A, Hashimoto T, Bröcker EB, Zillikens D (2002). Autoantibodies to Type VII Collagen Mediate Fcγ-Dependent Neutrophil Activation and Induce Dermal-Epidermal Separation in Cryosections of Human Skin. *Am J Pathol*. 161(1): 301–11.
127. Ludwig RJ (2017). Signalling and targeted therapy of inflammatory cells in epidermolysis bullosa acquisita. *Exp Dermatol*. 26(12): 1179–86.
128. Sezin T, Krajewski M, Wutkowski A, Mousavi S, Chakievska L, Bieber K, Ludwig RJ, Dahlke M, Rades D, Schulze FS, Schmidt E, Kalies K, Gupta Y, Schilf P, Ibrahim SM, König P, Schwudke D, Zillikens D, Sadik CD (2017). The Leukotriene B4 and its Receptor BLT1 Act as Critical Drivers of Neutrophil Recruitment in Murine Bullous Pemphigoid-Like Epidermolysis Bullosa Acquisita. *J Invest Dermatol*. 137(5): 1104–13.
129. Kopecki Z, Ludwig RJ, Cowin AJ (2016). Cytoskeletal Regulation of Inflammation and Its Impact on Skin Blistering Disease Epidermolysis Bullosa Acquisita. *Int J Mol Sci*. 17(7):1116.
130. Kulkarni U, Karsten CM, Kohler T, Hammerschmidt S, Bommert K, Tiburzy B, Meng L, Thieme L, Recke A, Ludwig RJ, Pollok K, Kalies K, Bogen B, Boettcher M, Kamradt T, Hauser AE, Langer C, Huber-Lang M, Finkelman FD, Köhl J, Wong DM, Manz RA (2016). IL-10 mediates plasmacytosis-associated immunodeficiency by inhibiting complement-mediated neutrophil migration. *J Allergy Clin Immunol*. 137(5): 1487-1497.e6.
131. Deng F, Chen Y, Zheng J, Huang Q, Cao X, Zillikens D, Petersen F, Yu X (2017). CD11b-deficient mice exhibit an increased severity in the late phase of antibody transfer-induced experimental epidermolysis bullosa acquisita. *Exp Dermatol*. 26(12): 1175–8.
132. Kuijpers TW, Weening RS, Out TA (1992). IgG subclass deficiencies and recurrent pyogenic infections, unresponsiveness against bacterial polysaccharide antigens. *Allergol Immunopathol (Madr)*. 20(1): 28–34.

133. Latiff AHA, Kerr MA (2007). The clinical significance of immunoglobulin A deficiency. *Ann Clin Biochem*. 44(Pt 2): 131–9.
134. Diebolder CA, Beurskens FJ, de Jong RN, Koning RI, Strumane K, Lindorfer MA, Voorhorst M, Ugurlar D, Rosati S, Heck AJ, van de Winkel JG, Wilson IA, Koster AJ, Taylor RP, Saphire EO, Burton DR, Schuurman J, Gros P, Parren PW (2014). Complement is activated by IgG hexamers assembled at the cell surface. *Science*. 343(6176): 1260–3.
135. Kappler K, Hennet T (2020). Emergence and significance of carbohydrate-specific antibodies. *Genes Immun*. 21(4): 224–39.
136. Khil'chenko S, Boch K, van Beek N, Vorobyev A, Zillikens D, Schmidt E, Ludwig RJ (2020). Alterations of Total Serum Immunoglobulin Concentrations in Pemphigus and Pemphigoid: Selected IgG2 Deficiency in Bullous Pemphigoid. *Front Med (Lausanne)*. 7:472.
137. Hammarström L, Carbonara AO, DeMarchi M, Lefranc G, Möller G, Smith CI, Zegers BJ (1987). Subclass restriction pattern of antigen-specific antibodies in donors with defective expression of IgG or IgA subclass heavy chain constant region genes. *Clin Immunol Immunopathol*. 45(3): 461–70.
138. Bignold LP, Ferrante A (1987). Mechanism of separation of polymorphonuclear leukocytes from whole blood by the one-step Hypaque-Ficoll method. *J Immunol Methods*. 96(1): 29–33.
139. Yu X, Akbarzadeh R, Pieper M, Scholzen T, Gehrig S, Schultz C, Zillikens D, König P, Petersen F (2018). Neutrophil Adhesion Is a Prerequisite for Antibody-Mediated Proteolytic Tissue Damage in Experimental Models of Epidermolysis Bullosa Acquisita. *J Invest Dermatol*. 138(9): 1990–8.
140. Scrace S, O'Neill E, Hammond EM, Pires IM (2013). Use of the xCELLigence system for real-time analysis of changes in cellular motility and adhesion in physiological conditions. *Methods Mol Biol*. 1046: 295–306.
141. van Engeland M, Nieland LJ, Ramaekers FC, Schutte B, Reutelingsperger CP (1998). Annexin V-affinity assay: a review on an apoptosis detection system based on phosphatidylserine exposure. *Cytometry*. 31(1): 1–9.
142. Bergamaschi D, Vossenkamper A, Lee WYJ, Wang P, Bochukova E, Warnes G (2019). Simultaneous polychromatic flow cytometric detection of multiple forms of regulated cell death. *Apoptosis*. 24(5–6): 453–64.

143. Vega A, El Bekay R, Chacón P, Ventura I, Monteseirín J (2010). Angiotensin II induces CD62L shedding in human neutrophils. *Atherosclerosis*. 209(2): 344–51.
144. Kishimoto TK, Jutila MA, Berg EL, Butcher EC (1989). Neutrophil Mac-1 and MEL-14 adhesion proteins inversely regulated by chemotactic factors. *Science*. 245(4923): 1238–41.
145. Hilhorst R, Houkes L, Mommersteeg M, Musch J, van den Berg A, Ruijtenbeek R (2013). Peptide Microarrays for Profiling of Serine/Threonine Kinase Activity of Recombinant Kinases and Lysates of Cells and Tissue Samples. In: Peptide Microarrays for Profiling of Serine/Threonine Kinase Activity of Recombinant Kinases and Lysates of Cells and Tissue Samples. 977:259-71.
146. Smith PK, Krohn RI, Hermanson GT, Mallia AK, Gartner FH, Provenzano MD, Fujimoto EK, Goeke NM, Olson BJ, Klenk DC (1985). Measurement of protein using bicinchoninic acid. *Anal Biochem*. 150(1): 76–85.
147. Ottonello L, Frumento G, Arduino N, Dapino P, Tortolina G, Dallegri F (2001). Immune complex stimulation of neutrophil apoptosis: investigating the involvement of oxidative and nonoxidative pathways. *Free Radic Biol Med*. 30(2): 161–9.
148. Karmakar U, Chu JY, Sundaram K, Astier AL, Garside H, Hansen CG, Dransfield I, Vermeren S (2021). Immune complex-induced apoptosis and concurrent immune complex clearance are anti-inflammatory neutrophil functions. *Cell Death Dis*. 12(4): 296.
149. Liebermeister W, Noor E, Flamholz A, Davidi D, Bernhardt J, Milo R (2014). Visual account of protein investment in cellular functions. *Proc Natl Acad Sci U S A*. 111(23): 8488–93.
150. Shimanovich I, Mihai S, Oostingh GJ, Ilenchuk TT, Bröcker EB, Opdenakker G, Zillikens D, Sitaru C (2004). Granulocyte-derived elastase and gelatinase B are required for dermal–epidermal separation induced by autoantibodies from patients with epidermolysis bullosa acquisita and bullous pemphigoid. *J Pathol*. 204(5): 519–27.
151. Ludwig RJ, Vanhoorelbeke K, Leypoldt F, Kaya Z, Bieber K, McLachlan SM, Komorowski L, Luo J, Cabral-Marques O, Hammers CM, Lindstrom JM, Lamprecht P, Fischer A, Riemekasten G, Tersteeg C, Sondermann P,

Rapoport B, Wandinger KP, Probst C, El Beidaq A, Schmidt E, Verkman A, Manz RA, Nimmerjahn F (2017). Mechanisms of Autoantibody-Induced Pathology. *Front Immunol*. 8: 603.

152. Collin M, Ehlers M (2013). The carbohydrate switch between pathogenic and immunosuppressive antigen-specific antibodies. *Exp Dermatol*. 22(8): 511–4.
153. Hirose M, Vafia K, Kalies K, Groth S, Westermann J, Zillikens D, Ludwig RJ, Collin M, Schmidt E (2012). Enzymatic autoantibody glycan hydrolysis alleviates autoimmunity against type VII collagen. *J Autoimmun*. 39(4): 304–14.
154. Yu X, Zheng J, Collin M, Schmidt E, Zillikens D, Petersen F (2014). EndoS reduces the pathogenicity of anti-mCOL7 IgG through reduced binding of immune complexes to neutrophils. *PLoS One*. 9(2): e85317.
155. Kelm M, Lehoux S, Azcutia V, Cummings RD, Nusrat A, Parkos CA, Brazil JC (2020). Regulation of neutrophil function by selective targeting of glycan epitopes expressed on the integrin CD11b/CD18. *FASEB J*. 34(2): 2326–43.
156. Krautter F, Iqbal AJ (2021). Glycans and Glycan-Binding Proteins as Regulators and Potential Targets in Leukocyte Recruitment. *Front Cell Dev Biol*. 9:624082.
157. Saggu G, Okubo K, Chen Y, Vattepu R, Tsuboi N, Rosetti F, Cullere X, Washburn N, Tahir S, Rosado AM, Holland SM, Anthony RM, Sen M, Zhu C, Mayadas TN (2018). Cis interaction between sialylated FcγRIIA and the αI-domain of Mac-1 limits antibody-mediated neutrophil recruitment. *Nat Commun*. 9(1): 5058.
158. Tang T, Rosenkranz A, Assmann KJM, Goodman MJ, Gutierrez-Ramos JC, Carroll MC, Cotran RS, Mayadas TN (1997). A Role for Mac-1 (CDIIb/CD18) in Immune Complex–stimulated Neutrophil Function In Vivo: Mac-1 Deficiency Abrogates Sustained Fcγ Receptor–dependent Neutrophil Adhesion and Complement-dependent Proteinuria in Acute Glomerulonephritis. *J Exp Med*. 186(11): 1853–63.
159. Schwab I, Nimmerjahn F (2014). Role of sialylation in the anti-inflammatory activity of intravenous immunoglobulin - F(ab′) 2 versus Fc sialylation. *Clin Exp Immunol*. 178: 97–9.

160. Vattepu R, Sneed SL, Anthony RM (2022). Sialylation as an Important Regulator of Antibody Function. *Front Immunol*. 13:818736.
161. Schlotfeldt M. Impact of glycosylation on IgG1-induced signalling in neutrophils (Einfluss der Glykosylierung auf IgG1-induzierte Signalübertragung in Neutrophilen). Master's thesis. Lübeck, 2022.
162. van Osch TLJ, Nouta J, Derksen NIL, van Mierlo G, van der Schoot CE, Wuhrer M, Rispens T, Vidarsson G (2021). Fc Galactosylation Promotes Hexamerization of Human IgG1, Leading to Enhanced Classical Complement Activation. *J Immunol*. 207(6): 1545–54.
163. Kuroki A, Kuroda Y, Kikuchi S, Lajaunias F, Fulpius T, Pastore Y, Fossati-Jimack L, Reininger L, Toda T, Nakata M, Kojima N, Mizuochi T, Izui S (2002). Level of galactosylation determines cryoglobulin activity of murine IgG3 monoclonal rheumatoid factor. *Blood*. 99(8): 2922–8.
164. Dong X, Storkus WJ, Salter RD (1999). Binding and uptake of agalactosyl IgG by mannose receptor on macrophages and dendritic cells. *J Immunol*. 163(10): 5427–34.
165. Clauder AK, Kordowski A, Bartsch YC, Köhl G, Lilienthal GM, Almeida LN, Lindemann T, Petry J, Rau CN, Gramalla-Schmitz A, Dühring L, Elbracht C, Kenno S, Tillmann J, Wuhrer M, Ludwig RJ, Ibrahim SM, Bieber K, Köhl J, Ehlers M, Manz RA (2021). IgG Fc N-Glycosylation Translates MHCII Haplotype into Autoimmune Skin Disease. *J Invest Dermatol*. 141(2): 285–94.
166. Zillikens H, Kasprick A, Osterloh C, Gross N, Radziewitz M, Hass C, Hartmann V, Behnen-Härer M, Ernst N, Boch K, Vidarsson G, Visser R, Laskay T, Yu X, Petersen F, Ludwig RJ, Bieber K (2021). Topical Application of the PI3Kβ-Selective Small Molecule Inhibitor TGX-221 Is an Effective Treatment Option for Experimental Epidermolysis Bullosa Acquisita. *Front Med (Lausanne)*. 8:713312.
167. Szilveszter KP, Németh T, Mócsai A (2019). Tyrosine Kinases in Autoimmune and Inflammatory Skin Diseases. *Front Immunol*. 10:1862.
168. Samavedam U, Scheuber J, Seavey M, Koga H, Witte M, Schulze F, Matsumoto, K, Zillikens D, Ludwig RJ (2014). Therapeutic efficacy of a novel selective JAK2 inhibitor (CEP-33779) in organ-specific, autoantibody-induced tissue injury. *J Invest Dermatol*. 134: S1–17.

169. Sadeghi S, Goodarzi A (2022). Various Applications of Tofacitinib and Ruxolitinib (Janus Kinase Inhibitors) in Dermatology and Rheumatology: A Review of Current Evidence and Future Perspective. *Dermatol Pract Concept*. 12(4):e2022178.
170. Huang D, Zhang Y, Kong L, Lu J, Shi Y (2023). Janus kinase inhibitors in autoimmune bullous diseases. *Front Immunol*. 14:1220887.
171. Fan B, Wang M (2023). Treatment of Recurrent Epidermolysis Bullosa Acquisita With Tofacitinib. *JAMA Dermatol*. 159(3): 342.
172. Hellberg L, Samavedam UKSRL, Holdorf K, Hänsel M, Recke A, Beckmann T, Steinhorst K, Boehncke WH, Kirchner T, Möckel N, Solbach W, Zillikens D, Schmidt E, Ludwig RJ, Laskay T (2013). Methylprednisolone blocks autoantibody-induced tissue damage in experimental models of bullous pemphigoid and epidermolysis bullosa acquisita through inhibition of neutrophil activation. *J Invest Dermatol*. 133(10): 2390–9.
173. Gao ZH, Seeling JM, Hill V, Yochum A, Virshup DM (2002). Casein kinase I phosphorylates and destabilizes the β-catenin degradation complex. *Proc Natl Acad Sci U S A*. 99(3): 1182–7.
174. Veltri A, Lang C, Lien WH (2018). Concise Review: Wnt Signaling Pathways in Skin Development and Epidermal Stem Cells. *Stem Cells*. 36(1): 22–35.
175. Kosumi H, Watanabe M, Shinkuma S, Nohara T, Fujimura Y, Tsukiyama T, Donati G, Iwata H, Nakamura H, Ujiie H, Natsuga K (2022). Wnt/β-Catenin Signaling Stabilizes Hemidesmosomes in Keratinocytes. *J Invest Dermatol*. 142(6): 1576-1586.e2.
176. Németh T, Virtic O, Sitaru C, Mócsai A (2017). The Syk Tyrosine Kinase Is Required for Skin Inflammation in an In Vivo Mouse Model of Epidermolysis Bullosa Acquisita. *J Invest Dermatol*. 137(10): 2131–9.
177. Kulkarni S, Sitaru C, Jakus Z, Anderson KE, Damoulakis G, Davidson K, Hirose M, Juss J, Oxley D, Chessa TA, Ramadani F, Guillou H, Segonds-Pichon A, Fritsch A, Jarvis GE, Okkenhaug K, Ludwig R, Zillikens D, Mocsai A, Vanhaesebroeck B, Stephens LR, Hawkins PT (2011). PI3Kβ Plays a Critical Role in Neutrophil Activation by Immune Complexes. *Sci Signal*. 4(168):ra23.
178. Peake J, Peiffer JJ, Abbiss CR, Nosaka K, Okutsu M, Laursen PB, Suzuki K (2008). Body temperature and its effect on leukocyte mobilization, cytokines

and markers of neutrophil activation during and after exercise. *Eur J Appl Physiol*. 102(4): 391–401.

9 APPENDIX

9.1 Ethics approval for the procurement of blood samples from healthy donors to study the pathogenesis and therapy of autoantibody-induced tissue damage; file number: 20-338

UNIVERSITÄT ZU LÜBECK

Universität zu Lübeck · Ratzeburger Allee 160 · 23538 Lübeck

Herrn
Prof. Dr. med. Ralf Ludwig
Direktor des Institutes für Experimentelle Dermatologie

im Hause

Ralf.ludwig@uksh.de

Ethik-Kommission
Vorsitzender:
Herr Prof. Dr. med. Alexander Katalinic
Universität zu Lübeck
Stellv. Vorsitzender:
Herr Prof. Dr. med. Frank Gieseler

Geschäftsstelle:
Dr. Angelike Hüppe
Dr. Inga Kaufhold
Janine Kurzaj-Erdmann
Doris Seuthe

E-Mail: ethikkomission@uni-luebeck.de
Website: www.uni-luebeck.de/forschung/kommissionen/ethikkommission

Aktenzeichen: 20-338
Datum: 17. November 2020 DS

Sitzung der Ethik-Kommission am 01. Oktober 2020
Antragsteller: Herr Prof. Dr. Ralf Ludwig
Titel: Pathogenese und Therapie Autoantikörper-induzierter Gewebeschädigung Blutentnahmen bei gesunden Proband*innen

Sehr geehrter Herr Prof. Ludwig,

vielen Dank für Ihr Schreiben vom 11. November 2020, in dem Sie den Hinweisen aus unserem Votum vom 22. Oktober 2020 nachkommen.

Folgende Unterlagen lagen vor:

- Ihre E-Mail vom 13. November 2020
- Geändertes Basisformular vom 11. November 2020
- Pathogenese und Therapie Version vom 04. November 2020
- Synopsis Version vom 04. November 2020
- Probandeninformation und Einwilligung Version vom 04. November 2020

Die Kommission hat gegen die Durchführung der Studien keine Bedenken.

Bitte überprüfen Sie nochmals die Verwendung der Begriffe „anonymisiert" und „pseudonymisiert", hier sind weiterhin Diskrepanzen in den Texten zu finden.

Bei Änderung des Studiendesigns sollte der Antrag erneut vorgelegt werden.
Datenschutzrechtliche Aspekte von Forschungsvorhaben werden durch die Ethikkommission grundsätzlich nur kursorisch geprüft. Dieses Votum / diese Bewertung ersetzt mithin nicht die Konsultation des zuständigen Datenschutzbeauftragten.

Mit freundlichen Grüßen

Prof. Dr. med. Alexander Katalinic
Vorsitzender

9.2 *p*-values

9.2.1 *p*-values adhesion test for IgG2-based IC at 10 µg/mL antigen and 2 µg/mL antibody concentration

Tukey's multiple comparisons test	Mean Diff.	95,00% CI of diff.	Summary	Adjusted P Value
Reference IgG2 IC vs. EndoS IgG2 IC	28.44	3.430 to 53.45	*	0.0211
Reference IgG2 IC vs. degalactosylated IgG2 IC	-27.83	-52.84 to -2.820	*	0.0246
Reference IgG2 IC vs. galactosylated IgG2 IC	-30.91	-55.93 to -5.902	*	0.0110
Reference IgG2 IC 1x vs. sialylated IgG2 IC	3.303	-21.71 to 28.31	ns	0.9944
EndoS IgG2 IC vs. degalactosylated IgG2 IC	-56.27	-81.29 to -31.26	****	<0.0001
EndoS IgG2 IC vs. galactosylated IgG2 IC	-59.36	-84.37 to -34.34	****	<0.0001
EndoS IgG2 IC vs. sialylated IgG2 IC	-25.14	-50.15 to -0.1274	*	0.0485
Degalactosylated IgG2 IC vs. galactosylated IgG2 IC	-3.082	-28.09 to 21.93	ns	0.9957
Degalactosylated IgG2 IC vs. sialylated IgG2 IC	31.13	6.123 to 56.15	*	0.0104
Galactosylated IgG2 IC vs. sialylated IgG2 IC	34.22	9.205 to 59.23	**	0.0046

CI, confidence interval; Diff, different; IC, immune complexes; IgG2, immunoglobulin γ 2; ns, non-significant.

9.2.2 *p*-values flow cytometry for IgG2-based IC at 10 µg/mL antigen and 2 µg/mL antibody concentration

Tukey's multiple comparisons test	Mean Diff.	95,00% CI of diff.	Summary	Adjusted P Value
CD18				
Reference IgG2 IC vs. EndoS IgG2 IC	27.55	-9.555 to 64.65	ns	0.2007
Reference IgG2 IC vs. degalactosylated IgG2 IC	14.45	-22.65 to 51.55	ns	0.7499
Reference IgG2 IC vs. galactosylated IgG2 IC	7.172	-29.93 to 44.27	ns	0.9734
Reference IgG2 IC 1x vs. sialylated IgG2 IC	15.07	-22.04 to 52.17	ns	0.7215
EndoS IgG2 IC vs. degalactosylated IgG2 IC	-13.09	-50.20 to 24.01	ns	0.8090
EndoS IgG2 IC vs. galactosylated IgG2 IC	-20.38	-57.48 to 16.73	ns	0.4651
EndoS IgG2 IC vs. sialylated IgG2 IC	-12.48	-49.58 to 24.62	ns	0.8337
Degalactosylated IgG2 IC vs. galactosylated IgG2 IC	-7.281	-44.38 to 29.82	ns	0.9720
Degalactosylated IgG2 IC vs. sialylated IgG2 IC	0.6146	-36.49 to 37.72	ns	>0.9999
Galactosylated IgG2 IC vs. sialylated IgG2 IC	7.895	-29.21 to 45.00	ns	0.9626
CD62L				
Reference IgG2 IC vs. EndoS IgG2 IC	4.972	-23.34 to 33.28	ns	0.9850
Reference IgG2 IC vs. degalactosylated IgG2 IC	4.969	-23.34 to 33.28	ns	0.9850
Reference IgG2 IC vs. galactosylated IgG2 IC	10.46	-17.86 to 38.77	ns	0.8127
Reference IgG2 IC 1x vs. sialylated IgG2 IC	7.248	-21.06 to 35.56	ns	0.9418
EndoS IgG2 IC vs. degalactosylated IgG2 IC	-0.002822	-28.32 to 28.31	ns	>0.9999
EndoS IgG2 IC vs. galactosylated IgG2 IC	5.484	-22.83 to 33.80	ns	0.9784
EndoS IgG2 IC vs. sialylated IgG2 IC	2.276	-26.04 to 30.59	ns	0.9993
Degalactosylated IgG2 IC vs. galactosylated IgG2 IC	5.487	-22.83 to 33.80	ns	0.9784
Degalactosylated IgG2 IC vs. sialylated IgG2 IC	2.279	-26.03 to 30.59	ns	0.9993
Galactosylated IgG2 IC vs. sialylated IgG2 IC	-3.208	-31.52 to 25.11	ns	0.9972
Zombie NIR™ and Annexin V				
Reference IgG2 IC vs. EndoS IgG2 IC	0.1025	-1.087 to 1.292	ns	0.9990
Reference IgG2 IC vs. degalactosylated IgG2 IC	0.1417	-1.047 to 1.331	ns	0.9966
Reference IgG2 IC vs. galactosylated IgG2 IC	0.02417	-1.165 to 1.213	ns	>0.9999
Reference IgG2 IC 1x vs. sialylated IgG2 IC	0.05750	-1.132 to 1.247	ns	>0.9999
EndoS IgG2 IC vs. degalactosylated IgG2 IC	0.03917	-1.150 to 1.228	ns	>0.9999
EndoS IgG2 IC vs. galactosylated IgG2 IC	-0.07833	-1.267 to 1.111	ns	0.9997
EndoS IgG2 IC vs. sialylated IgG2 IC	-0.04500	-1.234 to 1.144	ns	>0.9999
Degalactosylated IgG2 IC vs. galactosylated IgG2 IC	-0.1175	-1.307 to 1.072	ns	0.9983
Degalactosylated IgG2 IC vs. sialylated IgG2 IC	-0.08417	-1.273 to 1.105	ns	0.9996
Galactosylated IgG2 IC vs. sialylated IgG2 IC	0.03333	-1.156 to 1.222	ns	>0.9999

CI, confidence interval; Diff, different; IC, immune complexes; IgG2, immunoglobulin γ 2; ns, non-significant.

9.2.3 *p*-values ROS release assay for IgG2-based IC at 10 µg/mL antigen and 2 µg/mL antibody concentration

Tukey's multiple comparisons test	Mean Diff.	95,00% CI of diff.	Summary	Adjusted P Value
Reference IgG2 IC vs. EndoS IgG2 IC	42.32	20.29 to 64.36	***	0.0001
Reference IgG2 IC vs. degalactosylated IgG2 IC	-17.40	-39.43 to 4.639	ns	0.1669
Reference IgG2 IC vs. galactosylated IgG2 IC	-4.015	-26.05 to 18.02	ns	0.9813
Reference IgG2 IC 1x vs. sialylated IgG2 IC	-1.045	-23.08 to 20.99	ns	0.9999
EndoS IgG2 IC vs. degalactosylated IgG2 IC	-59.72	-81.76 to -37.68	****	<0.0001
EndoS IgG2 IC vs. galactosylated IgG2 IC	-46.34	-68.37 to -24.30	****	<0.0001
EndoS IgG2 IC vs. sialylated IgG2 IC	-43.37	-65.40 to -21.33	****	<0.0001
Degalactosylated IgG2 IC vs. galactosylated IgG2 IC	13.38	-8.654 to 35.42	ns	0.3917
Degalactosylated IgG2 IC vs. sialylated IgG2 IC	16.35	-5.684 to 38.39	ns	0.2127
Galactosylated IgG2 IC vs. sialylated IgG2 IC	2.970	-19.07 to 25.01	ns	0.9940

CI, confidence interval; Diff, different; IC, immune complexes; IgG2, immunoglobulin γ 2; ns, non-significant.

9.3 Mean kinase statistics used for the heatmaps in Figures 24 and 25

9.3.1 Mean kinase statistic of reference IgG2 IC

Kinase	2 min	8 min	15 min
ALK	-0.671	-0.591	-0.955
ARAF	0.365	0.463	0.154
Axl	-0.676	-0.552	-0.923
BLK	-0.691	-0.650	-1.052
BRAF	0.374	0.461	0.160
BTK	-0.733	-0.567	-0.884
CK1[epsilon]	0.700	0.506	0.568
CK2[alpha]1	0.544	0.383	0.295
DDR1	-0.813	-0.566	-0.982
Fer	-0.761	-0.635	-0.966
FmS/CSFR	-0.749	-0.565	-0.849
FRK	-0.695	-0.567	-0.921
HCK	-0.676	-0.580	-0.955
HER3	-0.675	-0.608	-0.977
IGF1R	-0.704	-0.653	-1.063
IKK[alpha]	0.618	0.500	0.336
InSR	-0.718	-0.642	-1.044
JAK1~b	-0.811	-0.536	-0.762
JAK2	-0.729	-0.575	-0.850
LTK	-0.691	-0.620	-1.061
Met	-0.669	-0.587	-0.976
p70S6K[beta]	0.449	0.291	0.178
PAK1	0.348	0.352	0.152
PDGFR[alpha]	-0.736	-0.726	-1.135
PFTAIRE1	0.563	0.383	0.325
PKA[alpha]	0.398	0.244	0.139
PKD1	0.415	0.370	0.168
PKG1	0.406	0.259	0.167
PKG2	0.447	0.306	0.215
PRKX	0.431	0.261	0.161
Ret	-0.713	-0.562	-0.902
Ron	-0.692	-0.625	-1.045
Srm	-0.693	-0.541	-0.859
Syk	-0.668	-0.563	-0.933
TEC	-0.692	-0.607	-0.982
TNIK/ZC2	-0.038	-0.148	-0.451
TRKA	-0.730	-0.600	-1.034
TRKB	-0.707	-0.579	-0.994

TRKC	-0.686	-0.614	-1.057
TXK	-0.719	-0.570	-0.887
ZAP70	-0.687	-0.565	-0.928

* The green-marked colored cells in the tables represent kinases that are significant, i.e., they exhibited a mean specificity score > 1 and a mean significance score > 0.5.

9.3.2 Mean kinase statistic of EndoS IgG2 IC

Kinase	2 min	8 min	15 min
ALK	-0.422	0.038	-0.696
ATR	1.491	0.885	0.556
CK1[epsilon]	2.138	0.939	0.902
EphA3	-0.544	0.018	-0.887
EphA7	-0.659	-0.039	-1.061
FAK2	-0.389	0.073	-0.734
Fes	-0.408	0.030	-0.884
GSK3[beta]	1.786	1.410	0.633
HER3	-0.419	0.038	-0.688
IGF1R	-0.461	0.014	-0.885
IKK[alpha]	1.817	0.774	0.650
InSR	-0.469	0.042	-0.868
MAPKAPK3	1.124	0.618	0.319
p70S6K[beta]	1.453	0.779	0.498
PFTAIRE1	1.726	0.839	0.654
PKA[alpha]	1.134	0.584	0.303
PKC[iota]	0.992	0.843	0.294
PKG1	1.192	0.631	0.322
PKG2	1.259	0.601	0.347
PKN1/PRK1	0.780	0.977	0.436
PRKX	1.113	0.512	0.344
Syk	-0.380	0.073	-0.691
TRKB	-0.407	0.016	-0.751
TRKC	-0.449	0.044	-0.842

* The green-marked colored cells in the tables represent kinases that are significant, i.e., they exhibited a mean specificity score > 1 and a mean significance score > 0.5.

9.3.3 Mean kinase statistic of degalactosylated IgG2 IC

Kinase	2 min	8 min	15 min
ALK	-0.732	-0.040	-0.978
ANP[alpha]	0.875	0.868	1.159
ARAF	1.487	1.279	1.549
BLK	-0.657	-0.082	-1.165
BRAF	1.467	1.278	1.540
CCK4/PTK7	-0.787	0.105	-0.667
CK1[epsilon]	1.266	1.104	1.611
CTK	-0.737	-0.061	-0.940
Etk/BMX	-0.785	0.010	-0.818
GSK3[beta]	1.301	1.184	2.088
HCK	-0.667	-0.070	-1.023
HER3	-0.733	-0.061	-0.974
IGF1R	-0.661	-0.068	-1.158
IKK[beta]	1.093	1.136	1.604
InSR	-0.652	-0.016	-1.076
IRR	-1.472	-0.078	-0.994
ITK	-0.742	-0.011	-0.805
JAK2	-0.837	-0.059	-0.742
KDR	-0.748	-0.078	-0.840
Lck	-0.660	-0.092	-0.977
Lmr1	-0.873	0.063	-0.880
LTK	-0.703	-0.095	-1.085
MAPKAPK3	0.787	0.805	1.052
Met	-0.617	-0.031	-0.986
p70S6K	0.908	0.892	0.980
p70S6K[beta]	0.915	0.829	1.157
PAK1	1.152	1.063	1.285
PCTAIRE2	1.217	1.300	1.954
PDGFR[alpha]	-0.678	-0.139	-1.124
PKA[alpha]	0.744	0.809	1.015
PKC[iota]	1.007	0.922	1.245
PKD1	1.008	1.073	1.215
PKG1	0.788	0.827	1.073
PKG2	0.799	0.849	1.117
PKN1/PRK1	1.402	1.385	1.408
PRKX	0.796	0.803	1.028
RAF1	1.167	1.207	1.464
ROCK1	1.664	1.530	1.886
RSKL2	1.252	1.140	1.736
Src	-0.639	-0.045	-0.998

Syk	-0.641	-0.023	-0.945
TRKA	-0.645	0.043	-1.045
TRKC	-0.882	-0.015	-1.116
Yes	-0.638	-0.027	-0.998
ZAP70	-0.617	0.012	-0.922

* The green-marked colored cells in the tables represent kinases that are significant, i.e., they exhibited a mean specificity score > 1 and a mean significance score > 0.5.

9.3.4 Mean kinase statistic of galactosylated IgG2 IC

Kinase	2 min	8 min	15 min
ALK	-0.752	-0.222	-0.712
Arg	-0.736	-0.210	-0.721
BLK	-0.762	-0.275	-0.745
CaMK4	1.516	1.609	0.843
CDK10	1.185	1.119	0.999
CK1[epsilon]	2.444	2.426	1.362
CTK	-0.747	-0.189	-0.755
DAPK3	0.698	1.307	1.024
EphA3	-1.047	-0.226	-0.816
EphA7	-1.249	-0.192	-0.905
FAK2	-0.730	-0.215	-0.718
FGFR1	-0.756	-0.213	-0.795
HER3	-0.764	-0.261	-0.737
IGF1R	-0.812	-0.294	-0.764
IKK[alpha]	1.990	1.108	1.042
InSR	-0.813	-0.233	-0.783
IRR	-1.316	-0.246	-0.894
Lck	-0.745	-0.260	-0.731
LTK	-0.797	-0.282	-0.740
mTOR/FRAP	1.477	2.163	0.556
NuaK1	1.407	1.490	1.115
p70S6K[beta]	1.589	1.328	0.839
PCTAIRE2	0.756	1.769	1.066
PFTAIRE1	1.906	1.334	1.004
PKA[alpha]	1.176	0.860	0.746
PKC[alpha]	1.044	1.053	0.744
PKG1	1.255	0.967	0.797
PKG2	1.418	1.136	0.885
PRKX	1.338	1.018	0.818
Src	-0.737	-0.190	-0.730
Syk	-0.725	-0.199	-0.729
TRKA	-0.794	-0.159	-0.785
TRKB	-0.785	-0.175	-0.780
TRKC	-0.914	-0.214	-0.825

* The green-marked colored cells in the tables represent kinases that are significant, i.e., they exhibited a mean specificity score > 1 and a mean significance score > 0.5.

9.3.5 Mean kinase statistic of sialylated IgG2 IC

Kinase	2 min	8 min	15 min
ARAF	0.765	0.344	0.815
Axl	-0.430	-0.469	-0.825
BRAF	0.753	0.342	0.815
CDK2	0.639	0.253	0.211
CK1[epsilon]	0.521	0.606	1.453
DAPK3	0.474	0.923	0.669
EphA3	-0.464	-0.518	-0.987
EphA7	-0.435	-0.552	-1.123
FLT1	-0.373	-0.440	-0.892
IKK[alpha]	0.630	0.396	1.372
IKK[beta]	0.640	0.297	1.096
InSR	-0.480	-0.542	-0.871
JNK1	0.561	0.258	0.323
JNK2	0.629	0.322	0.419
JNK3	0.564	0.259	0.317
NuaK1	0.534	1.041	0.898
p38[delta]	0.614	0.326	0.582
p70S6K[beta]	0.456	0.379	0.836
PFTAIRE1	0.507	0.445	1.099
PKG1	0.395	0.244	0.676
PKG2	0.421	0.311	0.788
PRKX	0.433	0.308	0.774
PRKY	0.509	0.365	0.858
RSKL2	0.524	0.468	1.131
Syk	-0.445	-0.493	-0.820
TRKA	-0.446	-0.475	-0.893
TRKC	-0.479	-0.509	-0.877
ZAP70	-0.451	-0.488	-0.833

* The green-marked colored cells in the tables represent kinases that are significant, i.e., they exhibited a mean specificity score > 1 and a mean significance score > 0.5.

9.4 Kinome trees

9.4.1 Kinome tree for reference IgG2 IC

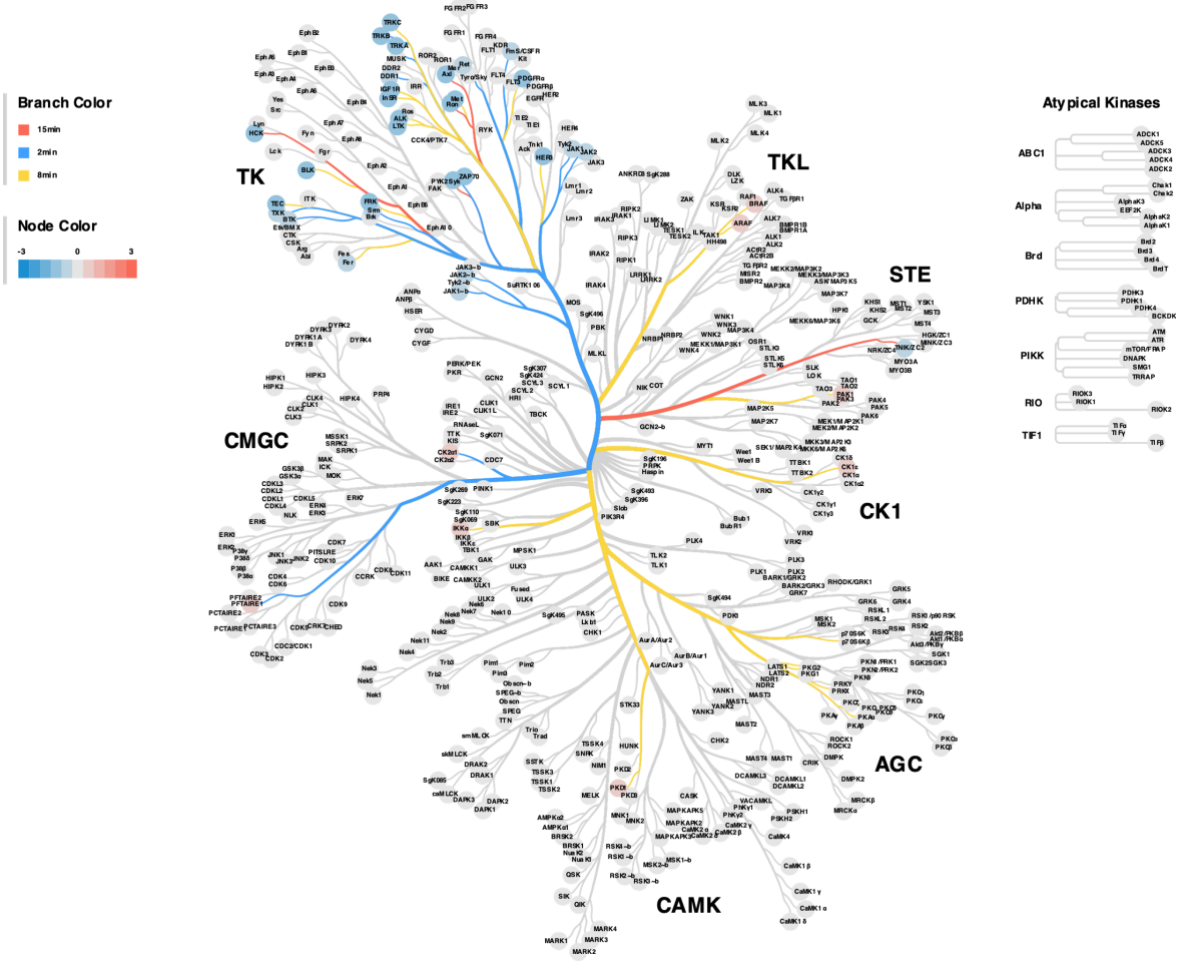

9.4.2 Kinome tree for EndoS IgG2 IC

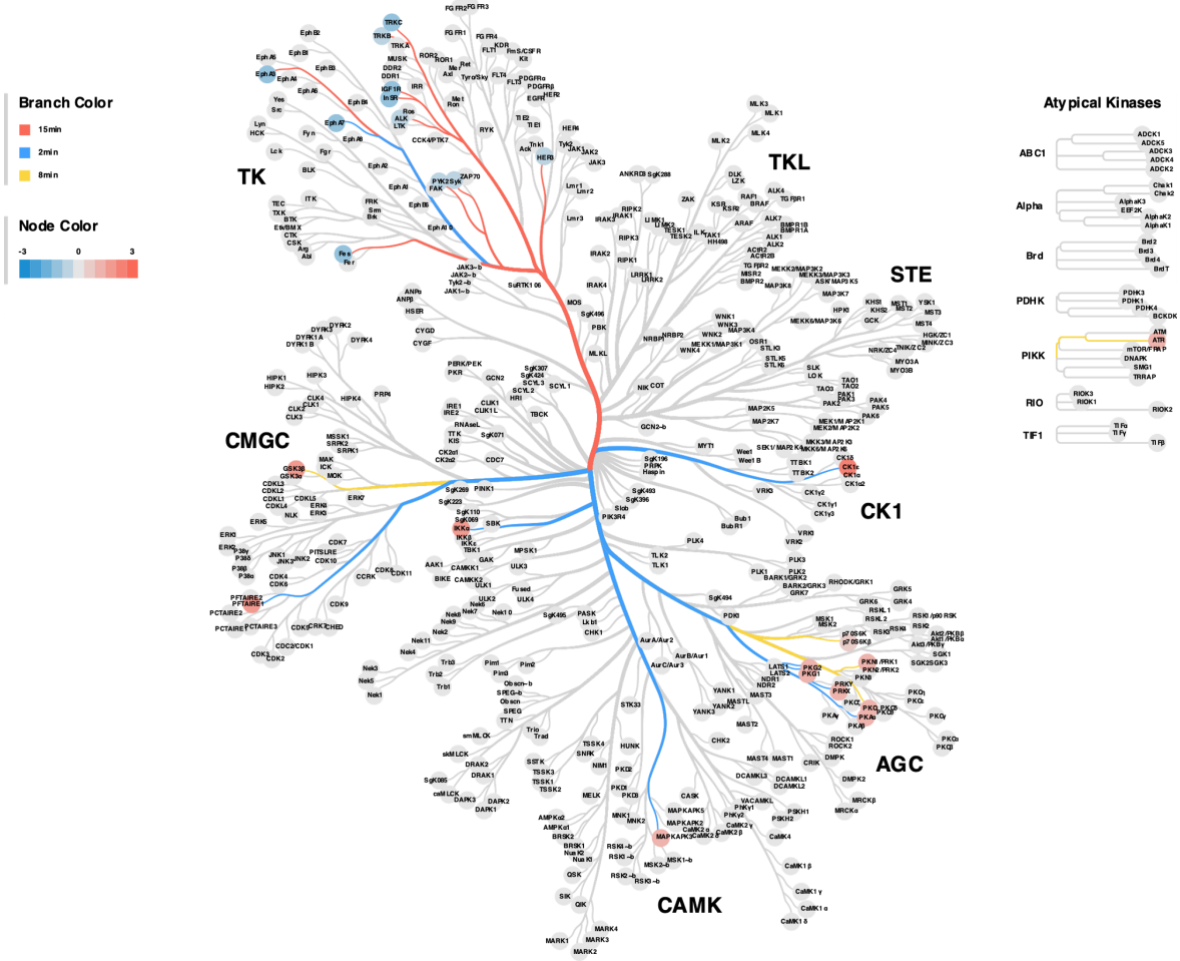

9.4.3 Kinome tree for degalactosylated IgG2 IC

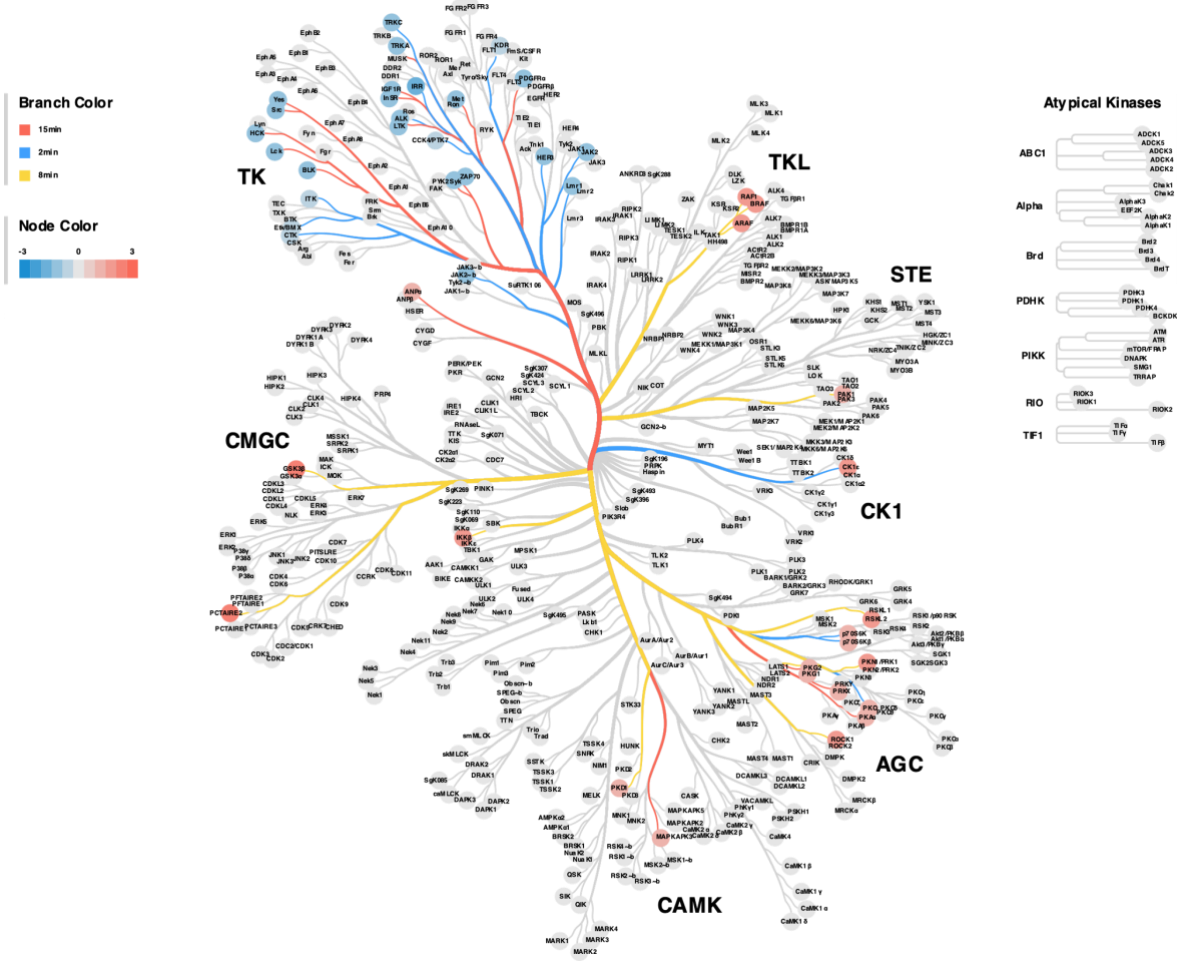

9.4.4 Kinome tree for galactosylated IgG2 IC

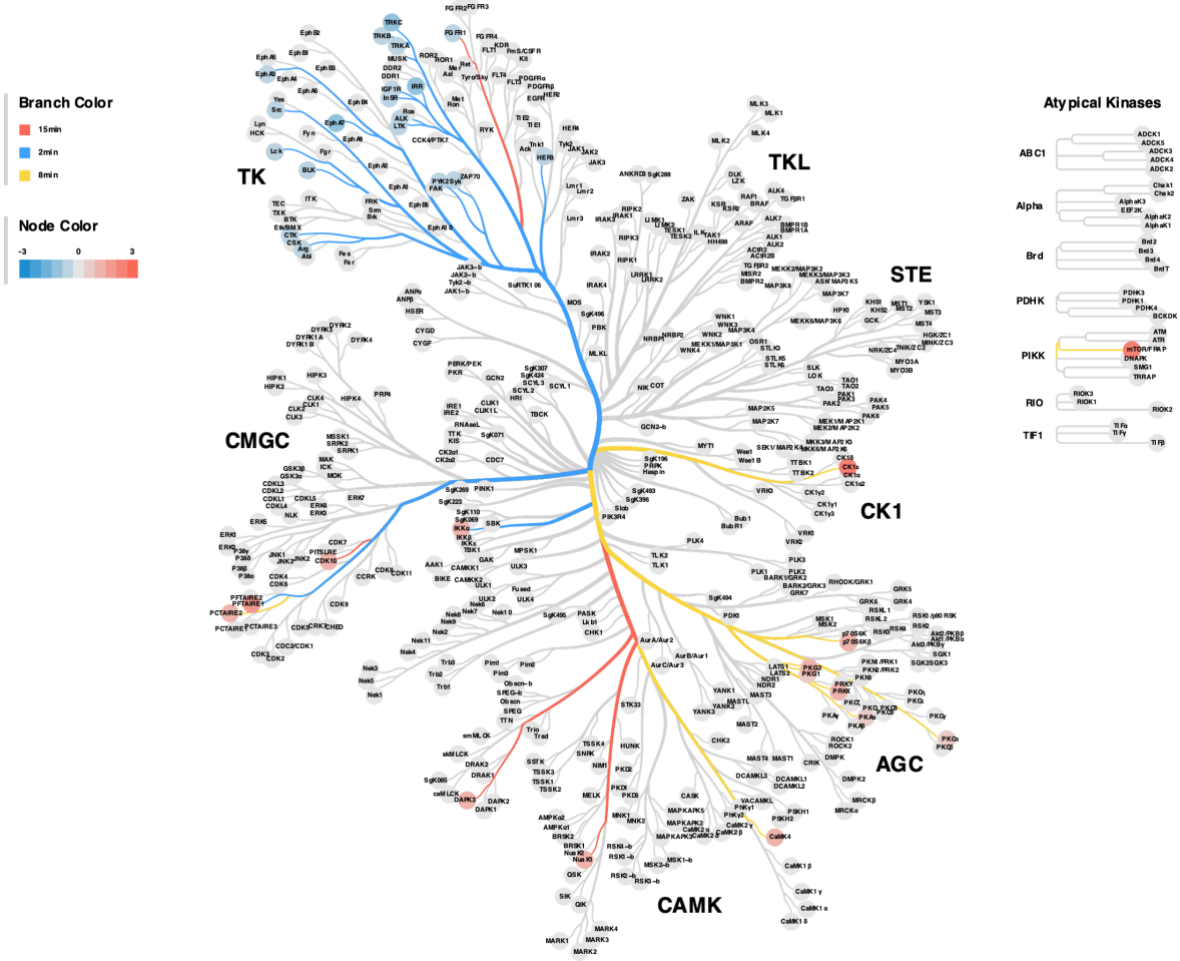

9.4.5 Kinome tree for sialylated IgG2 IC

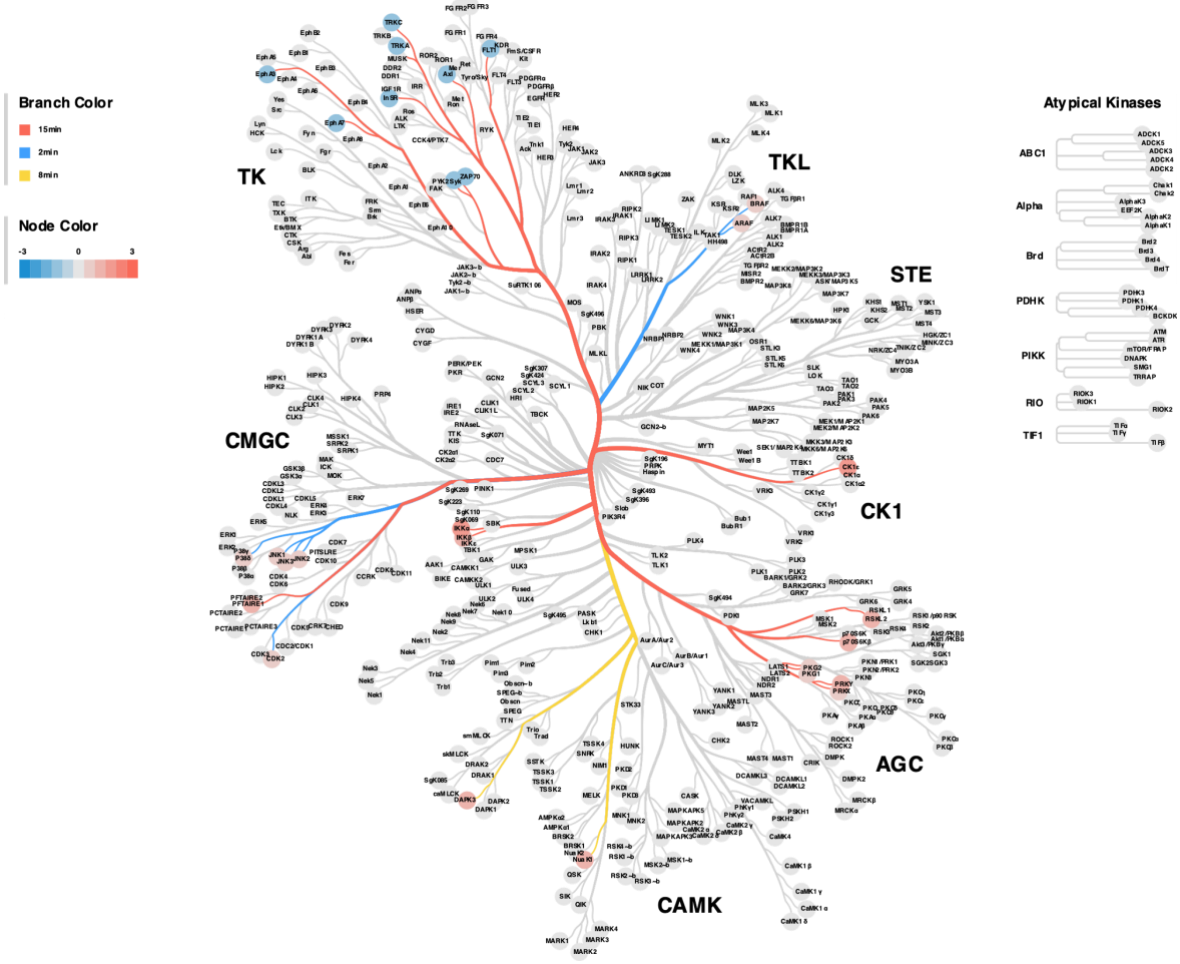

9.5 Proteomaps illustrating the kinase signaling pathways involved in differentially glycosylated IgG2-containing IC at 10 µg/mL antigen and 2 µg/mL antibody concentration, at the 2-minute and 15-minute timepoints

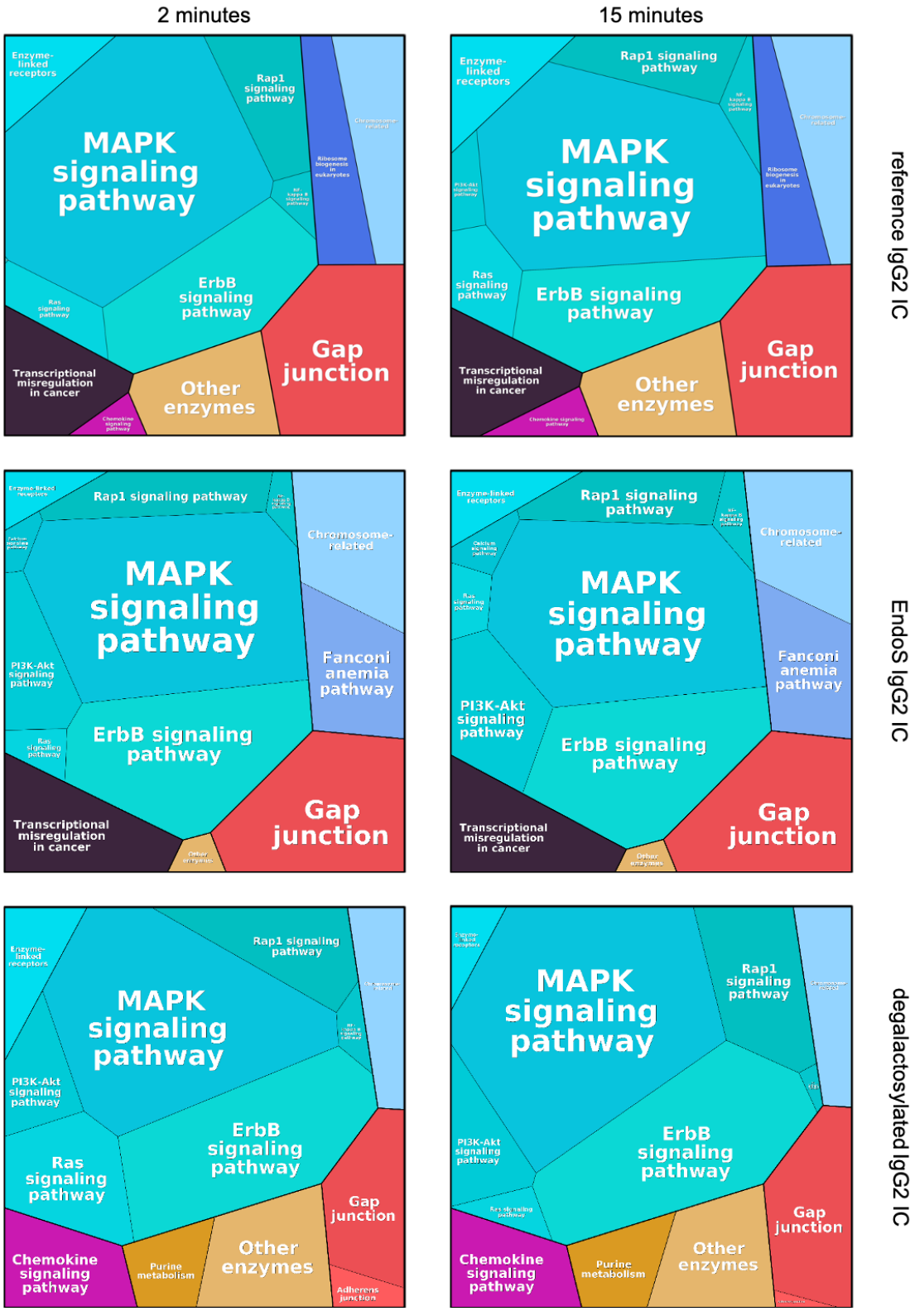

2 minutes

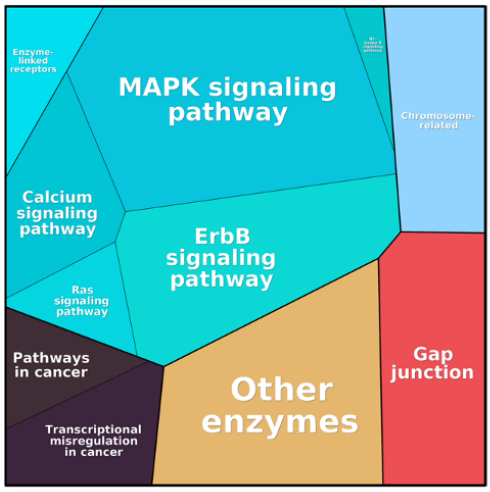

15 minutes

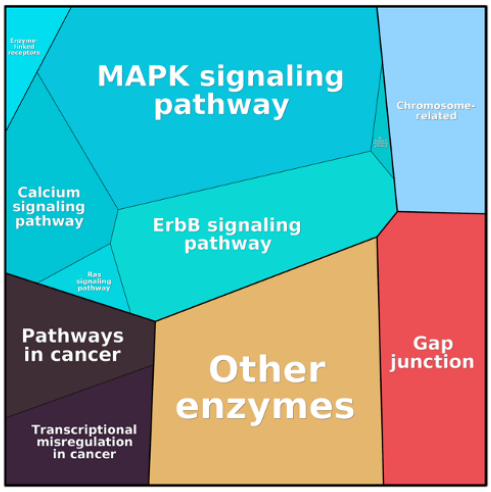

galactosylated IgG2 IC

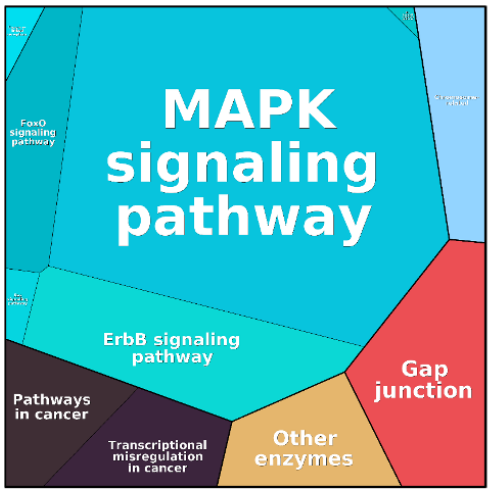

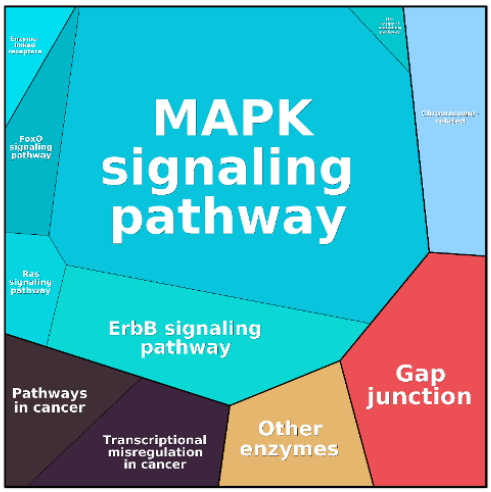

sialylated IgG2 IC

10 ACKNOWLEDGEMENTS

First and foremost, I would like to express my deepest gratitude to Prof. Dr. Zillikens. Without his chance, guidance, and support, I wouldn't be here today in Germany as a researcher and dermatologist. May he rest in peace.

I am also immensely grateful to Prof. Dr. Ludwig for welcoming me into his wonderful working group, where I found my place, expanded my research skills, learned so many things, and had the opportunity to meet exceptional individuals, some of whom became friends. It was here that I met my doctoral supervisor, PD Dr. Katja Bieber, the best supervisor one could have: kind, helpful, meticulous, funny, and always inspiring me to improve myself and my work. I extend my heartfelt thanks to her for standing by me every step of the way during my thesis journey. I also extend my sincere thanks to my co-supervisor, Dr. Kathrin Kalies.

From the lab, I am indebted to my mentor, Dr. Nancy Ernst, and colleagues Dr. Anika Kasprick, Dr. Natalie Groß, Colin Osterloh, Leon Schmidt-Jiménez, Claudia Kauderer, Astrid Fischer, Alexandra Wobig, and the staff at the research centre Borstel. Special appreciation goes to my lab partner, Mareile Schlotfeldt, for her unwavering support.

I am also deeply grateful to all my friends, both from Germany and Romania, in particular David, Megi, Amalia, Irina, Alex, and Andrada, whose emotional support and optimism sustained me throughout so that today I can successfully complete my thesis. I thank them for their friendship, love, and encouragement.

Last but certainly not least, I owe a debt of gratitude to my wonderful family, including Monica, Margareta, and Dorin in heaven, whose love, patience, and support have been my rock. Without them, I wouldn't be where I am today.